Star-Structured Polyethylene Nanoparticles via Pd-Catalyzed Living Polymerization: Synthesis, Characterization, and Catalytic Applications

by

Eric D. Landry

A thesis submitted in partial fulfillment
of the requirements for the degree of
Master of Applied Science (MASc) in Natural Resources Engineering

The Faculty of Graduate Studies,
Laurentian University
Sudbury, Ontario, Canada

THESIS DEFENCE COMMITTEE/COMITÉ DE SOUTENANCE DE THÈSE
Laurentian Université/Université Laurentienne
Faculty of Graduate Studies/Faculté des études supérieures

Title of Thesis Titre de la thèse	Star-Structured Polyethylene Nanoparticles via Pd-Catalyzed Living Polymerization: Synthesis, Characterization, and Catalytic Applications
Name of Candidate Nom du candidat	Landry, Eric
Degree Diplôme	Master of Applied Science

Department/Program Département/Programme	Natural Resources Engineering	Date of Defence Date de la soutenance	October 30, 2014

APPROVED/APPROUVÉ

Thesis Examiners/Examinateurs de thèse:

Dr. Zhibin Ye
(Supervisor/Directeur de thèse)

Dr. Ramesh Subramanian
(Committee member/Membre du comité)

Dr. M'hamed Chahma
(Committee member/Membre du comité)

Dr. Huining Xiao
(External Examiner/Examinateur externe)

Approved for the Faculty of Graduate Studies
Approuvé pour la Faculté des études supérieures
Dr. David Lesbarrères
M. David Lesbarrères
Acting Dean, Faculty of Graduate Studies
Doyen intérimaire, Faculté des études supérieures

ACCESSIBILITY CLAUSE AND PERMISSION TO USE

Abstract

The arm-first synthesis of large unimolecular star-structured polyethylene nanoparticles or SPE-NPs (M_W > 1,000 kg/mol, PDI ≈ 1.1) joined by a cross-linked polynorbornadiene (PNBD) core is described in this thesis. SPE-NPs having high arm number (f_n > 100) and tunable arm topologies (hyperbranched HBPE or linear-but-branched LBPE) are conveniently synthesized in a single reactor following four consecutive steps.

In step 1, living ethylene polymerization is catalyzed by 0.1 mmol of Pd-diimine catalyst **1** to grow HBPE arms (1 atm C_2H_4/15 °C) or LBPE arms (27 atm C_2H_4/5 °C) of tunable lengths (t_E = 1-5 h, M_n = 11-40 kg/mol). In step 2, the norbornadiene (NBD) cross-linker is added into the ethylene reactor for several hours (t_{NBD} = 1-4 h) yielding PE-b-PNBD block copolymers with a short PNBD segment bearing cross-linkable pendant double bonds. SPEs are then formed in step 3 during precipitation in acidified methanol (H^+/MeOH) and the final SPE-NPs are formed in step 4 after several hours of drying *in vacuo* at 120 °C.

A thorough systematic investigation of the reaction parameters indicates that to produce increasingly larger SPE-NPs, it is essential to add a significant molar excess of NBD to **1** ($[NBD]_0/[\mathbf{1}]_0$ > 50) and synthesize short LBPE arms but large HBPE arms. When synthesized with LBPE arms, the SPE-NPs have higher M_W compared to those synthesized with HBPE arms due to the lower steric hindrance of the linear arms which enables a high number of arms to be joined at the PNBD core.

Furthermore, the Pd-diimine catalyst used in the synthesis of the SPE-NPs was encapsulated within the cross-linked PNBD core. These encapsulated Pd(II) species were tested for their activity in hydrogenation reactions of terminal alkenes and alkynes (1-octene, 1-hexene, and 1-hexyne) and Heck coupling reactions of iodobenzene and n-butyl acrylate. Preliminary data suggests that these SPE-NPs may be used as models for the design of more advanced recyclable nanovessel for Pd(II) catalysts.

Acknowledgements

I would first like to express my deepest gratitude to my supervisor, Dr. Zhibin Ye, for giving me the exceptional opportunity to undertake graduate studies in polymer chemistry research, a field in which I had no prior knowledge or experience. Because of his outstanding dedication, passion, and mentorship, it helped me gain exceptional technical skills, research abilities, and work ethics, which have built a foundation of principles that I will carry with me throughout my professional career.

I have the upmost appreciation for all the helpful support, insights, and contributions of each of my colleagues, especially Peng Xiang, Zhongmin Dong, Pingwei Liu, and Lixin Xu. It has been a joy to collaborate with you and to learn from your research expertise, and I wish you all the best in your future endeavors.

I also thank Dr. Gerardo Ulibarri for his assistance and operational training of the 500 MHz nuclear magnetic resonance (NMR) spectrometer; Dr. Helen Joly for her expertise and training of the 200 MHz NMR spectrometer and gas chromatography analysis; and Mauricio Melo Jr. for his training of the atomic absorption spectrometer and friendly support. Also, this research project would not have been possible without the financial assistance from the National Sciences and Engineering Research Council of Canada (NSERC).

Lastly, I want to thank my parents François and Rachel Landry, my sister Julie Landry, my daughter Mackenzie Landry, and my soul mate Kelly Mann for their endless support and encouragement throughout my studies. You are the driving force behind my quest for success.

Table of Contents

List of Abbreviations

[ethylene]	Ethylene Concentration
$[\eta]_w$	Weight-Average Intrinsic Viscosity
°C	Degree Celsius
µg	Microgram
µg/mL	Microgram per Milliliter
µL	Microliter
µm	Micrometer
µmol	Micromole
Å	Ångtröm
A_{BrBz}	Gas Chromatography Elution Peak Area of Bromobenzene
ACS	American Chemical Society
AFM	Atomic Force Microscope
A_{NBD}	Gas Chromatography Elution Peak Area of Norbornadiene
atm	Atmospheric Pressure
ATRP	Atom Transfer Radical Polymerization
BA	Butyl Acrylate
BDA	1,4-Butanediol Diacrylate
BHT	Butylated Hydroxytoluene
BIEA	2-(2-Bromoisobutyryloxy)ethyl Acrylate
BrBz	Bromobenzene
CAS No	Chemical Abstracts Service Registry Number
$CDCl_3$	Deuterated Chloroform
CH_2Cl_2	Dichloromethane

ClBz	Chlorobenzene
cm	Centimeter
D	Deuterium
D_h	Hydrodynamic Diameter
DLS	Dynamic Light Scattering
DNA	Deoxyribonucleic Acid
d*n*/d*c*	Differential Refractive Index Increment Value
DRI	Differential Refractive Index
DVB	Divinylbenzene
E66	Wavelength Energy of Pd Hollow Cathode Lamp
FAAS	Flame Atomic Absorption Spectroscopy
FID	Flame Ionization Detector
f_n	Number-Average Arm Number
g	Gram
GC	Gas Chromatography
GPC	Gel Permeation Chromatography
GPC-LS	Gel Permeation Chromatography-Light Scattering
h	Hour
H^+ MeOH	2% (v/v) Hydrochloride Methanol Solution
H_2	Hydrogen Gas
H_2O_2	Hydrogen Peroxide
HBPE(s)	Hyperbranched Polyethylene(s)
HCl	Hydrochloric Acid
HDPE(s)	High Density Polyethylene(s)

HPLC	High Performance Liquid Chromatography
Hz	Hertz
I_a	^{1}H NMR Integration of Resonance Peak a
Inc.	Incorporated
K	Mark-Houwink Constant
kg/mol	Kilogram per Mole
KHz	Kilohertz
k_p	Rate Constant of Chain Propagation
k_w	Rate Constant of Chain Walking
LBPE(s)	Linear-but-Branched Polyethylene(s)
LDPE(s)	Low Density Polyethylene(s)
LLDPE(s)	Linear Low Density Polyethylene(s)
LS	Light Scattering
m	Meter
mA	Milliamp
MAO	Methylaluminoxane
MeOH	Methanol
mg/mL	Milligram per Milliliter
MHz	Megahertz
MI(s)	Macroinitiator(s)
min	Minute
mL	Milliliter
mL/g	Milliliter per Gram
mL/min	Milliliter per Minute

mm	Millimeter
MMA	Methyl Methacrylate
mm Hg	Millimeter of Mercury
mmol	Millimole
M_n	Number-Average Molecular Weight
mV	Millivolt
M_w	Weight-Average Molecular Weight
MWCNT(s)	Multi-Walled Carbon Nanotube(s)
N	Normality
NB	Norbornene
NBD	Norbornadiene
nm	Nanometer
NP(s)	Nanoparticle(s)
PDI(s)	Polydispersity Index(es)
PDVB	Poly(divinylbenzene)
PE(s)	Polyethylene(s)
PE-*b*-PNB	Ethylene-Norbornene Block Copolymer
PE-*b*-PNBD	Ethylene-Norbornadiene Block Copolymer
PE-*c*-PNB	Ethylene-Norbornene Copolymer
PMMA	Poly(methyl methacrylate)
PNBD	Poly(norbornadiene)
PPA(s)	Polymer Processing Aid(s)
PPT	Precipitation/Precipitated
R_g	Gyration Radius

R_g/ R_h	Chain Compactness Factor
R_h	Hydrodynamic Radius
R_p	Rate of Chain Propagation
R_w	Rate of Catalyst Chain Walking
SDBS	Spectral Database for Organic Compounds
SEC-MALS	Size Exclusion Chromatography-Multi-Angle Light Scattering
Si-NP(s)	Silica Nanoparticle(s)
siRNA	small interfering Ribonucleic Acid
SPE-NP(s)	Star Polyethylene Nanoparticle(s)
SPE(s)	Star Polyethylene(s)
STEM	Scanning Tunneling Electron Microscopy
t	Polymerization Time
TEM	Transmission Electron Microscopy
THF	Tetrahydrofuran
t_{NBD}	Norbornadiene Polymerization Time
t_E	Ethylene Polymerization Time
v/v	Volume per Volume
VI	Viscosity Index
x_{NBD}	Norbornadiene Conversion
α	Mark-Houwink Exponent
^{1}H NMR	Proton Nuclear Magnetic Resonance
2D	Two Dimensional
3D	Three Dimensional
^{13}C NMR	^{13}Carbon Nuclear Magnetic Resonance

List of Figures

Chapter 1: Introduction, Background, and Objectives

Chapter 2: Experimental Methodology

Chapter 3: Arm-First Pd-Diimine–Catalyzed Synthesis of Star Polyethylene Nanoparticles

Chapter 4: Catalytic Applications of Star Polyethylene Nanoparticles as Recyclable Vessels for Encapsulated Pd(II) Catalysts

List of Tables

Chapter 3: Arm-First Pd-Diimine–Catalyzed Synthesis of Star Polyethylene Nanoparticles

CHAPTER 1: Introduction, Background, and Objectives

1.1 Introduction to Polyethylenes

In today's technologically driven world, polymers have become a vital and integral part of everyday life. Polymeric materials are found in virtually all consumer products from electronics to cosmetics, clothing to household furnishings, pharmaceuticals to medical implants, etc., which makes them crucial to the global economy.

Polyethylene (PE) accounts for the world's largest volume of commercial synthetic polymers with about 77 million metric tons produced annually.[1] Commercially produced PEs are cheap and versatile thermoplastics used in the manufacturing of countless products due to their valuable material properties including good tensile strength and flexibility, chemical resistance, etc. These properties can be tailored for specific material applications by manipulating the polymer chain parameters, such as molecular weight (M) and molecular weight distribution, comonomer content and distribution, chain architecture/topology, etc.[2]

Conventionally, PEs have been classified into the following three traditional categories according to their manufacturing methods and properties: low density polyethylene (LDPE), linear low density polyethylene (LLDPE), and high density polyethylene (HDPE).[1, 3] Figure 1.1 illustrates schematically the chain structures of the three traditional PE grades.

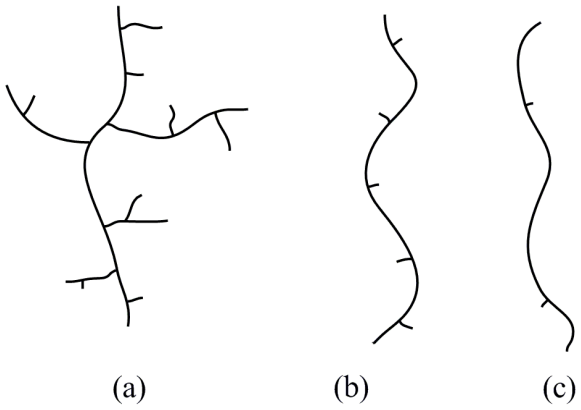

Figure 1.1 Schematic representation of the three conventional polyethylene grades: (a) low-density polyethylene; (b) linear low-density polyethylene; and (c) high-density polyethylene.

LDPE was the first commercially available PE grade. It is produced by free-radical polymerization of ethylene at high pressure (1,000 - 3,000 atm) and high temperature (150 - 350 °C).[1, 4-5] The free-radical polymerization process produces LDPE with chain structures consisting of a PE backbone with randomly distributed short chain branches and long chain branches generated by intra-chain transfer (also known as backbiting) and inter-chain transfer, respectively.[3] At the molecular level, the branching structures of LDPE hinder the formation of crystal frameworks, which reduces the material's crystallinity, melting point (105 - 115 °C), and density (0.90 - 0.94 g/mL). [3] As a result, LDPEs are tough, flexible, tear resistant, and easily processed materials. They are widely used in the manufacturing of flexible plastic goods like plastic bags and bottles, computer hardware, etc.,[4, 6] but their main uses are in film applications and packaging. LDPEs are now competing with LLDPEs for higher shares of the PE film market because the latter have superior material properties and they are produced at lower costs.[7]

LLDPE and HDPE were first developed in the 1950's and they are produced via transition metal catalysed coordination polymerization technology. LLDPE are synthesized by copolymerizing ethylene with a small percentage of α-olefin (e.g. 1-butene, 1-hexene, and 1-octene) at low pressure (20 - 70 atm) and low temperature (80 - 250 °C).[5-6, 8] The LLDPE polymer chain structure contains short chain branches, obtained by the

copolymerization of α-olefins, randomly distributed along the linear PE backbone. Compared to LDPE, the average chain length of LLDPE is longer and the linear chain topology allows chains to be packed closer together. However, the crystallinity and density (0.91 - 0.94 g/mL) remain low due to the presence of short chain branches.[3, 6, 8] Furthermore, the material properties of LLDPE, including flexibility, tear resistance, and impact strength, can be tuned for desired applications simply by controlling the amount of short chain branching.[9] LLDPE is used to make plastic bags, plastic wrap, flexible tubing, and films.[3, 10]

Since its commercialization in the 1950's, HDPE now accounts for nearly half (45 %) of the PE market.[7, 10] Using ethylene as the sole monomer source, HDPE synthesis is facilitated by transition metal catalysts under similar polymerization conditions as LLDPE (at low pressure and low temperature).[5-6, 8] Typically the polymer chain structure is linear with no or very few short chain branches which can be introduced by copolymerizing ethylene with a very minute amount of α-olefin.[7] HDPE polymer chains can be densely packed together and form crystal lattices which give it higher density (0.94 – 0.96 g/mL) and higher thermal resistance compared to LDPE and LLDPE.[6, 8] Other properties of HDPE include good chemical resistance, increased hardness, and increased stiffness and tensile strength. The materials produced using HDPE are hard and strong plastics but are typically brittle at low temperature and tend to crack under sufficient physical stress.[6, 8] HDPE is commonly used to make hard hats, plastic fuel tanks, and laundry detergent bottles.[4]

1.2 Traditional Ethylene Polymerization Technologies

1.2.1 Free Radical Polymerizations

Polyethylene was accidentally discovered in 1933 by Imperial Chemical Industries, Ltd. scientists R.O. Gibson and E.W.M. Fawcett, in England. They were testing the effects of high pressure and temperature on a mixture of ethylene and benzaldehyde and obtained a waxy solid that was identified as a polymer of ethylene.

It was determined that under the extreme reaction conditions, small amounts of oxygen or organic peroxides generate radicals that attack the π-bonds of ethylene monomers to initiate the polymerization. Active radicals continually add ethylene units at the end of the growing PE chain until the active site dies or transfers to other species in the reaction medium. This high-pressure high-temperature (e.g., 1000 atm and 300 °C) free-radical polymerization process is used to produce LDPE containing short and long chain branches. [2, 4]

However, the high production costs associated with extreme reaction conditions hindered the full potential of PE based materials. The development of coordinative polymerization processes with the use of transition metal catalysts, including Ziegler-Natta and metallocene catalysts has enabled efficient ethylene polymerization at milder reaction condition.

1.2.2 Ziegler-Natta Catalysts

One of the most significant innovations in ethylene polymerization technologies was the discovery of Ziegler-Natta catalysts in the 1950's. These transition metal-based catalyst systems were first used to produce new grades of PEs including HDPE and LLDPE. Ziegler-Natta catalyst processes proved much more cost effective than the free-radical processes due to the lower ethylene pressures and temperatures required.[11-12]

Ziegler-Natta catalysts are generally heterogeneous catalysts composed of a transition metal salt from groups IV–VIII (catalyst) and a metal alkyl from groups I–III (cocatalyst).[11-12] Not all catalyst-cocatalyst combinations are useful; certain combinations are only active for some monomers or under specific reaction conditions. For commercial processes, a mixture of titanium salts and aluminum alkyls is normally used. A typical Ziegler-Natta catalyst used in the industry is the $TiCl_3$ catalyst and $AlEt_3$ cocatalyst system. These catalysts often generate multi-type active polymerization sites, which differ in polymerization kinetic parameters. They can be soluble; however, for commercial production, the insoluble or supported Ziegler-Natta catalysts are often preferred due to

lower levels of metal contamination in the final polymer.[11-12] On an industrial scale, Ziegler-Natta catalyst technology has been applied in solution, slurry, and gas phase polymerization processes. [13]

There are several generations of Ziegler-Natta catalysts developed thus far. The first generation consisted of mixing metal alkyls with transition metal salts (e.g., $TiCl_3/AlEt_2Cl$). Their activity was low and the produced polymer contained unwanted catalyst residues. The second generation had improved productivity and stereo selectivity by using a Lewis base with the catalyst mixture (e.g., $TiCl_3/AlEt_2Cl$/Lewis base). The Lewis base coordinates with the catalyst metal centre and modifies the electronic environment. At this time, the majority of the metal catalysts were still inactive because they were located within the crystallites.[14-15]

Efforts to dilute or expose more active sites led to the discovery of the use of $MgCl_2$ as a support for Ti-based Ziegler-Natta catalysts. This third generation of catalysts was significantly more active than previous generations, and the removal of catalyst residues in the polymer product was no longer required. However, the polymers produced were regular and/or irregular powders, for which extrusion processing was often necessary in order to formulate polymer pellets for commercial applications.[14-15]

Control over polymer particle morphology was achieved with the fourth generation Ziegler-Natta catalysts. These catalysts most often possessed a spherical three-dimensional structure, which enables the production of globular-shaped polymer particles/granules having various sizes, internal morphologies (e.g., hollow, porous, compact, etc.), and polymer compositions, which were controlled by tuning polymerization conditions. Consequently, pelletization and blending processes were generally avoided, thus reducing production costs and expanding the variety of polymeric materials having new or improved properties.[14-15]

PEs produced by Ziegler-Natta catalysts are used for a wide variety of thermoplastic consumer goods. In general, these types of PEs have broad distributions in molecular weight and comonomer composition, two important parameters that influence material properties. This is due to the multi-site nature of the heterogeneous catalysts.

There are soluble Ziegler-Natta catalysts which can produce PEs with narrow molecular weight distribution and comonomer distributions but their activity is too low for commercial production.[11, 16]

1.2.3 Metallocene Catalysts

Metallocene catalysts were developed in the 1950's, when intense research efforts were focused on the next generation of Ziegler-Natta catalysts. Originally, this catalyst-cocatalyst system was comprised of a homogeneous titanium catalyst (e.g. $Cp_2TiEtCl$) ligated to bis(cyclopentadienyl) derivatives and an alkylaluminum cocatalyst (e.g. $EtAlCl_2$). Ethylene polymerization could be done at low pressures and low temperatures but this early generation of metallocene catalysts were unstable and their reactivity was low. They were revolutionized in the late 1970's when Kaminsky et al. observed a dramatic increase in catalyst activity when a small amount of water was added to the polymerization mixture.[17] Essentially, the water reacts with the alkylaluminum to form a significantly more effective cocatalyst, alkylaluminoxane (e.g., methylaluminoxane (MAO)), which in turn improved the productivity of this polymerization system.

Figure 1.2 (a) shows the traditional sandwich-style metallocene catalyst structure where M, a transition metal atom of group IV (Zr, Ti, and Hf), is coordinated in between two cyclopentadienyl ligands. Removable groups X, such as halogen atoms (e.g., Cl, Br) or alkyl groups, stabilize the transition metal centre. The ligands can be linked together by a bridge, A, which can be a bivalent alkyl radical or Si. Many different ligands and bridging ligands have been developed by varying their substituents, R and R', which alters the steric and electronic environment of the transition metal active site. A multitude of well-behaved metallocene catalysts, exhibiting good control on polymer characteristics, have been developed by varying the transition metal centre and its surrounding ligands.[13, 18]

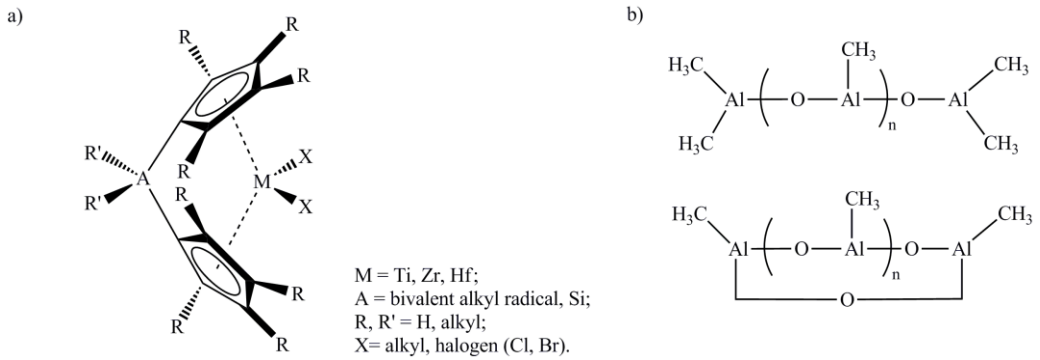

Figure 1.2 a) Generic structure of metallocene catalysts and b) the proposed linear and cyclic structures of methylaluminoxane cocatalyst, MAO.[19]

The high efficiency and high productivity of metallocene catalysts in the polymerization of PEs would not be possible without an effective cocatalyst. The most commonly used cocatalyst in metallocene polymerization is methylaluminoxane (MAO). Figure 1.2 (b) shows the proposed linear and cyclic structures of MAO. This cocatalyst is comprised of a mixture of oligomers that have varying numbers of the repeat unit -Al(CH_3)-O- (n = 5 to 20).[19-20] MAO is believed to have two major roles in the catalytic system: activating the metallocene catalysts and scavenging impurities in the polymerization system. During the activation process, MAO acts as an alkylation agent. It replaces the coordinating halogens of the transition metal with alkyl groups and subsequently removes one of the coordinating alkyl groups to generate a cationic active site with a vacant orbit ready for monomer insertion and polymerization.[18, 20] Unfortunately, it requires very high amounts of MAO in order to maintain the high activity of metallocene catalysts. Common aluminum to catalysts molar ratios can range from 1,000 to 20,000. In addition, the high cost of producing MAO makes the use of metallocene catalyst technology somewhat expensive.[20]

Compared to heterogeneous multi-site Ziegler-Natta catalysts, homogeneous single-site metallocene catalysts offer much higher productivity and better control of polymer chain microstructures and properties by tuning the ligand structures and polymerization conditions. PEs produced by metallocene catalysts have narrower

molecular weight distribution (typically with a theoretical polydispersity index, PDI, of 2) and narrower comonomer distribution compared to those by Ziegler-Natta catalysts. Consequently, new grades of LLDPE can be effectively produced on an industrial scale.[21]

1.2.4 Single-Site Late Transition Metal Catalysts

The high susceptibility to polar functionalities of Ziegler-Natta and metallocene catalysts based on early transition metals (Ti, Zr, V, and Cr) has prevented their use in the production of functionalized PEs. Therefore, the free-radical process is used to commercially produce this important type of PEs by copolymerizing ethylene with polar comonomers. Since the 1990's, there has been increasing research interest in developing and improving the capability of catalyst systems to incorporate polar functional monomers into PEs. Because of their reduced oxophilicity, late-transition metals (Co, Rh, Ni, Pd, etc.) were presumed to be more tolerant to functional monomers, therefore providing a potential solution to the production of functionalized PEs.[22-23]

The late transition metal catalysts initially developed were successfully used for ethylene dimerization and oligomerization, which are the foundation for the Shell Higher Olefin Process. However, their activity for ethylene polymerization was low.[24-27] In 1995, Brookhart et al. discovered a new class of highly active α-diimine-ligated single-site Ni(II) and Pd(II) catalysts for ethylene polymerization.[28] Figure 1.3 (a) shows the chemical structure of a typical cationic Pd(II) α-diimine catalyst with a SbF_6 counter anion (**1**). In their report, Brookhart and co-workers determined that the steric bulkiness of α-diimine ligands enabled both Ni and Pd catalysts to produce high-molecular-weight PEs. This is due to their unique square planar structure, characterized by four large *ortho-iso*propyl-groups on the aryl rings of the α-diimine ligand, which are nearly perpendicular to the metal-diimine plane. This configuration effectively blocks axial coordination sites (Figure 1.3 (b)) of the active metal centre from olefinic association and therefore significantly inhibits chain transfer reactions.[28-29] This mechanism has been theoretically proven through density functional theory and molecular mechanic modeling by Deng et al. [24, 29-31]

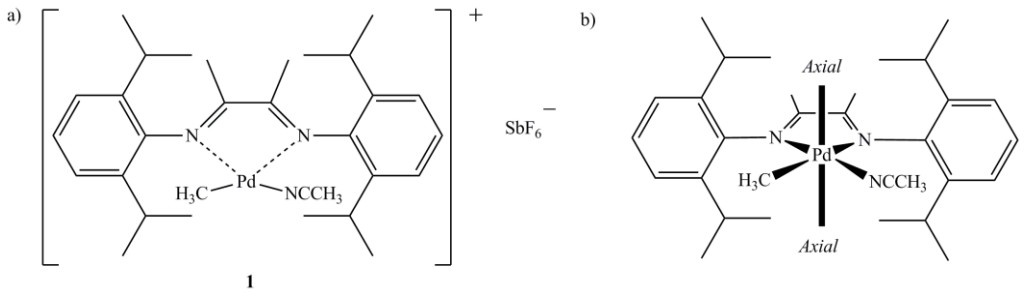

Figure 1.3 (a) Chemical structure of α-diimine cationic acetonitrile Pd(II) catalyst with SbF_6 counter-anion (**1**) and (b) axial coordination sites blocked by *ortho-iso*propyl groups on aryl rings of the diimine ligand. [29]

Compared to Ziegler-Natta and metallocene catalysts, this new type of single-site late transition metal catalysts have three outstanding polymerization features, including chain walking mechanism, olefin copolymerization with polar functional comonomers, and living polymerization. Figure 1.4 shows the steps involved in the chain walking ethylene polymerization mechanism of cationic Pd-diimine catalysts. Nuclear magnetic resonance (NMR) studies have shown that the alkyl-ethylene catalyst complex (**2** in Figure 1.4) is the catalyst resting state.[28, 31-33] Following monomer insertion, the cationic Pd centre coordinates with the β-hydrogen of the newly added ethylene unit. This Pd-complex (**3**) can isomerize/walk along the polymer backbone as a result of consecutive reactions involving β-hydride elimination (yielding an alkene-hydride complex **4**), bond rotation of the coordinated alkene, and re-addition of the hydride to yield a branched alkyl in complex **5**.[33-34] Chain walking and chain propagation are competing reactions, thus the cationic Pd centre in **5** can further undergo chain walking following the aforementioned steps or it can undergo chain propagation by coordinating and inserting an ethylene monomer which generates a methyl branch in the growing polymer chain. Mechanistic models and theoretical studies have verified and confirmed this mechanism.[30-35]

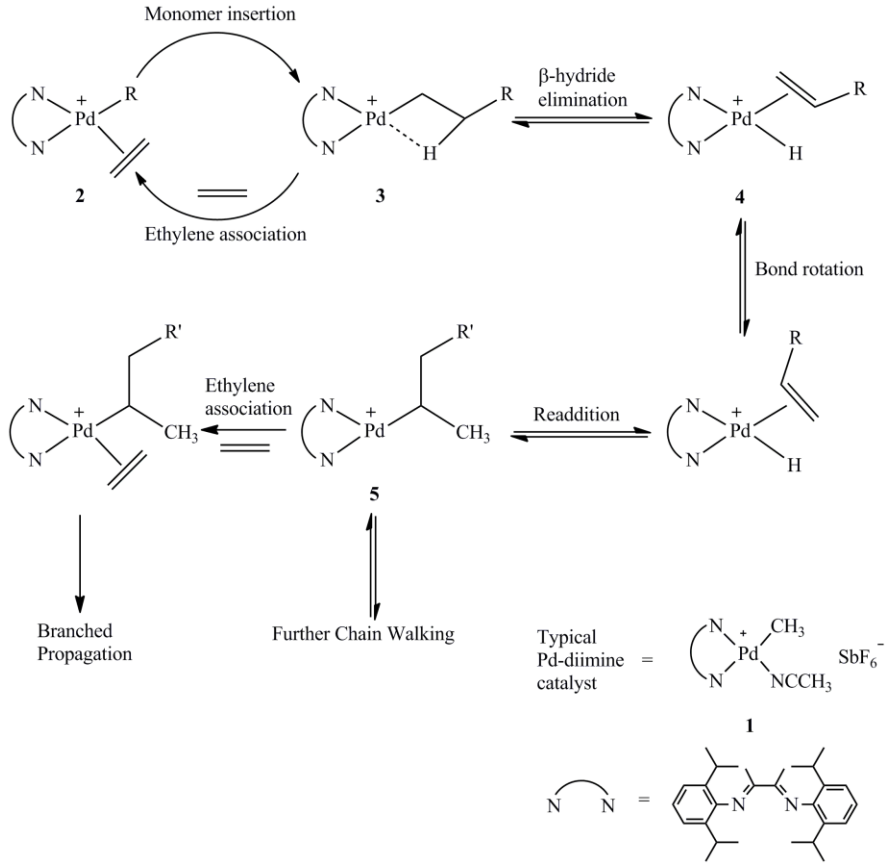

Figure 1.4 Schematic representation of the mechanism for ethylene chain walking polymerization and polymer branching by Pd-diimine catalyst.[33-34]

With a higher chain walking ability compared to its Ni-analog, Pd-catalysts produce a novel class of branched PEs known as hyperbranched polyethylenes (HBPEs). Typically, HBPEs have branching densities reaching up to 110 branches/1000 carbons, which are significantly higher than those found in ordinary types of LDPE and LLDPE. NMR analysis of Pd-catalyzed PEs shows the presence of *iso*-butyl groups as the smallest branch-on-branch structure in the polymer chains. This confirms the presence of branch-on-branch structures and also demonstrates that Pd-catalysts can walk/isomerize through tertiary carbons.[31, 34] On the other hand, Ni-catalysts produce linear PEs predominantly containing methyl branches.[24, 33] Using ethylene as the sole monomer source, chain walking Ni- and Pd-diimine catalysts enabled the production of structurally-variant branched PEs of

interesting and favourable properties, ranging from rigid plastomers to soft elastomers to viscous oils.[23-24]

Another important feature of Pd-diimine catalysts is their remarkably low oxophilicity. Their tolerance to oxygen-containing compounds and polar functionalities was confirmed by reports describing successful ethylene polymerizations conducted in the presence of air or in an aqueous/polar solvent (e.g., ethers, esters, organic acids, alcohols, etc.).[24] This feature also enabled the copolymerization of ethylene with various polar comonomers to produce functionalized PEs. Acrylates are the typical polar comonomers that have been extensively copolymerized with ethylene using Pd-diimine catalysts. NMR studies have elucidated the unique acrylate incorporation mechanism in Pd-diimine catalyzed ethylene copolymerization (Figure 1.5).[30] The Pd-catalyst incorporates acrylate double bonds primarily via a 2,1-insertion process, followed by two isomerization steps that yield a rearranged six-membered chelate (**6**), which can be dissociated by ethylene coordination to the Pd-centre (**7**). Further ethylene insertion and continued chain walking/propagation leads to PEs bearing unique microstructures in which the functional-ester groups of the acrylates are predominantly located at the ends of branches (**8**). [36-38] Given this unique feature, Pd-diimine catalysts have significantly expanded the application base of PEs.

A third key feature of Pd-diimine catalysts is their ability to facilitate ethylene living polymerization under specific reaction conditions. During living polymerization, all polymer chains are initiated instantaneously and grow simultaneously without significant chain breaking reactions (e.g., termination or chain transfer). Successful living ethylene polymerizations using Pd-diimine catalysts are generally conducted at low temperatures, typically ranging from 5 to 15 °C. The livingness is characterized by a linear increase in polymer molecular weight as a function of time and by a narrow molecular weight distribution (PDI $\approx$ 1).[39-40] The combination of these unique polymerization features has enabled the design and precision synthesis of a wide range of PEs and PE copolymers with complex architectures including block, telechelic, branched, hyperbranched, and star-shaped.[24, 41-50]

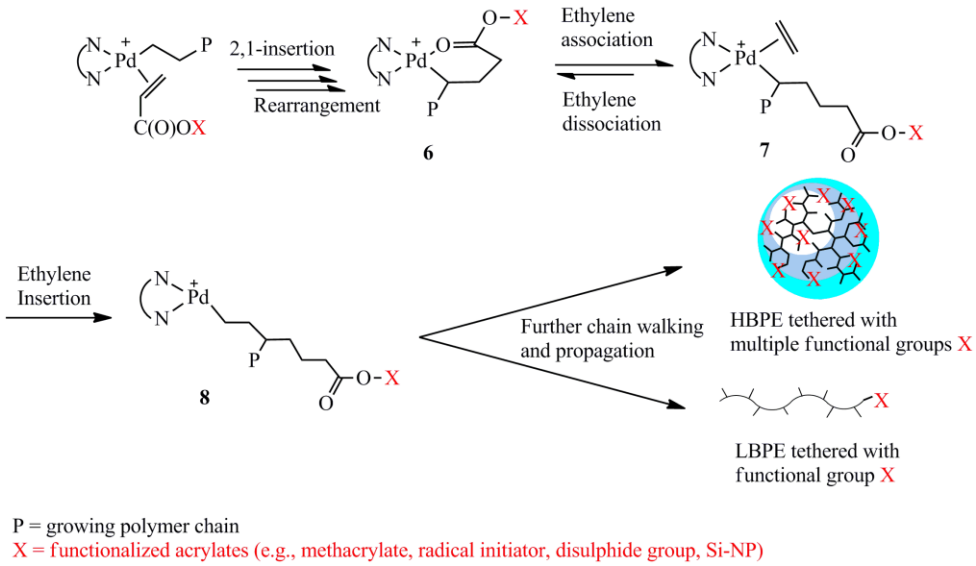

Figure 1.5 Mechanism of Pd-diimine-catalyzed ethylene copolymerization with functional acrylates for synthesis of functionalized branched PEs.

1.3 Branched Polyethylenes Produced by Pd-Diimine Catalysts

1.3.1 Synthesis and Topology Control of Branched Polyethylenes

The chain topology of polymers is one of the major factors determining the physical properties and applications of polymeric materials. In 1999, Guan et al. reported a very effective chain walking strategy to control PE chain topology by regulating polymerization conditions (i.e., ethylene pressure, polymerization temperature, and catalyst ligands) to adjust the competition between chain walking (R_w) and chain propagation (R_p) rates of Pd-diimine catalysts.[34]

During chain growth, at conditions where R_w is much higher than R_p, the catalyst will randomly walk longer distances (chain walking distance) on the polymer chain before trapping and inserting an ethylene unit. Under such conditions the catalyst will generate extensive branch-on-branch structures thus rendering hyperbranched chain topologies. In contrast, when R_p is much greater than R_w, the catalyst chain walking distance will be

shorter, thus resulting in a more linear chain topology with primarily short chain branches.[33-34, 51-52] Figure 1.6 shows a scheme of the Pd-catalysts chain walking ability to synthesize topologically different branched PEs.

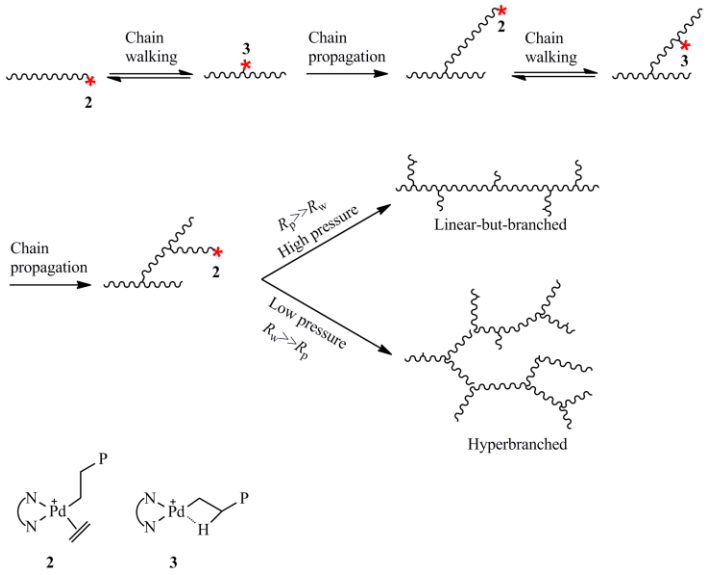

Figure 1.6 Polyethylene chain topology control by chain walking polymerization using Pd-diimine catalysts.[34]

Mechanistic and kinetic studies reported by Brookhart and coworkers have shown that, for Pd-diimine-catalyzed ethylene polymerization, R_p has a zero-order dependence on ethylene concentration whereas R_w has an inverse first-order dependence, from which Equation 1.1 was obtained.[31-34, 51-52] Researchers have successfully demonstrated that ethylene concentration ([ethylene]) and the relative rate constants for chain propagation (k_p) and chain walking (k_w) of Pd-diimine catalysts can be adjusted to effectively control PE chain topology. Ethylene concentration is easily manipulated by controlling ethylene pressure whereas varying polymerization temperature and catalyst structure/electronics influence the k_p/k_w ratio.[24, 33-34, 51-53]

$$\frac{R_p}{R_w} = \frac{k_p[\text{ethylene}]^0}{k_w[\text{ethylene}]^{-1}} = \left(\frac{k_p}{k_w}\right)[\text{ethylene}] \qquad 1.1$$

Controlling ethylene pressure is a straightforward and very effective strategy to tune PE chain topology due to the different relative dependencies of R_p and R_w on ethylene concentration, which allows for adjustable R_p/R_w ratio. NMR studies, conducted by Brookhart and coworkers, revealed that monomer insertion is the limiting step in chain propagation, which is governed by the ethylene-associated-Pd-complex (**2** in Figure 1.6), while chain walking is governed by the ethylene-dissociated Pd complex (**3**).[28, 31-32, 34] At high pressures (e.g., 30 atm), ethylene concentration is high; consequently, the relative concentration of **3** is lower compared to **2**. Kinetically, this translates to higher R_p/R_w ratios, which result in reduced chain walking distances and consequently polyethylenes of linear architectures but with primarily short branching structures. At low ethylene pressures/concentrations (e.g., 1 atm or lower), the chain walking distance increases significantly due to the increased R_w (higher concentration of **3**), rendering hyperbranched polyethylenes (HBPEs).[24, 34]

Polymerization temperature also has an effect on PE chain topology. Increasing polymerization temperature renders increasingly compact chain topology.[54-55] Although both k_p and k_w are enhanced with the increased polymerization temperature, k_w has a higher sensitivity towards the temperature change, thus resulting in lower k_p/k_w ratios. This leads to longer catalyst chain walking distances, which produce PE chains having increasingly compact topologies. However, using this temperature approach to control PE chain topology is restricted due to substantial catalyst deactivation at high polymerization temperatures.[33, 54-55]

The catalyst approach to control PE chain topology is based on altering the electronics of the α-diimine ligand.[53] At fixed polymerization conditions, Pd-diimine catalysts with electron-deficient ligands afford PEs with more compact chain topologies,, while the catalysts with electron-rich ligands produce PEs with more linear topologies. It is proposed that electron-rich ligands can better stabilize the catalyst transition state for

ethylene insertion/propagation.[53] Kinetically, this translates to higher k_p/k_w ratios, which ultimately yield more linear topologies. Differently, electron-deficient ligands can more effectively stabilize chain walking Pd species, which translates to lower k_p/k_w ratios and produce HBPEs.[53] Although both the catalyst and polymerization temperature strategies can provide some degree of freedom in controlling PE chain topology, ethylene pressure remains the preferred approach due to its simplicity and higher efficiency in rendering a broad range of topologies.

1.3.2 Structure and Properties of Branched Polyethylenes

The structural characterization of highly branched PEs produced by Pd-diimine catalysts is rather challenging due to their complex chain topologies comprised of randomly distributed branches and numerous branch-on-branch structures. Thus, a combination of multiple analytical techniques, including NMR spectroscopy, dynamic light scattering (DLS), and triple-detection gel permeation chromatography (GPC) incorporating on-line multi-angle light scattering (LS), viscosity, and differential refractive index (DRI) detectors, is required to accurately determine the chain topology of this type of branched PEs.

Quantitative ^{1}H and ^{13}C NMR spectroscopy are used in order to determine branching densities, short chain branching distributions, and branching microstructures for Pd-diimine PEs produced at various ethylene pressures (ranging from 0.1 to 34 atm). Due to the random chain walking, the produced PEs have high but similar total branching densities (ranging from 80 to 110 branches per 1000 carbons) and similar patterns of short chain branching distributions.[33, 36, 49, 56-59] Using two-dimensional NMR techniques, the methyl and ethyl groups of *sec*-butyl branches, the simplest branch-on-branch structure, were differentiated from the total amount of short chain branches and their amounts were found to increase in PEs produced at reduced ethylene pressures.[24, 33-34, 51, 59] Since hyperbranched polymers typically possess more branch-on-branch structures, this NMR result suggests that PEs produced at sufficiently low ethylene pressures may have a hyperbranched chain topology.

The chain topology of Pd-diimine PEs is also reflected by their dilute solution properties, particularly their chain compactness factor which is measured by the ratio of gyration radius (R_g, obtained from static LS in GPC) to hydrodynamic radius (R_h, obtained from DLS).[34] Typically, R_g/R_h ratios vary from 1.5 to 1.7 for linear polymers in good solvents whereas it is about 0.78 for rigid spherical polymers. The R_g/R_h ratio of Pd-diimine PEs produced at high ethylene pressure (34 atm) is 1.7, which indicates their linear chain topology; whereas it is 1.3 for PEs produced at low ethylene pressure (1 atm), which indicates their non-linear chain topology in dilute solution. At very low ethylene pressure (0.1 atm), the R_g/R_h ratio of the produced PEs is further reduced to 0.8, which is in good accordance with the predicted spherical hyperbranched chain structure.

Furthermore, the polymer intrinsic viscosity curve, i.e., the logarithmic plot of $[\eta]$ as a function of polymer M, also provides valuable information elucidating polymer chain topology. The curve is expressed by the Mark-Houwink Equation given by

$$[\eta] = K M^{\alpha} \qquad 1.2$$

where K is a constant and α corresponds to the slope of the curves. Both parameters (K and α) are dependent on the polymer conformation/chain topology. Typical α values for polymers of various chain conformations are: ~ 0 for solid spheres, 0.5 to 0.8 for flexible linear polymers, and 1.8 to 2.0 for rigid rod-like polymers.[45, 60-61] Through several GPC studies, Ye et al. have established two intrinsic viscosity-fitting curves for LBPEs ($[\eta] = 0.0621\ M^{0.61}$) and HBPEs ($[\eta] = 0.0407\ M^{0.59}$), which were synthesized with **1** under living polymerization conditions (27 atm/5 °C and 1 atm/15 °C, respectively).[47, 54-55, 59] In accordance with other reports [34, 51-52, 59], at the same M, the Pd-diimine PEs produced at 1 atm have lower $[\eta]$ and α values compared to those synthesized at 27 atm, which confirm their denser chain structures in comparison to their linear analog.[47, 54-55, 59] Based on these unique dilute solution properties and their dependence on ethylene pressure, it is possible to adequately differentiate linear and hyperbranched PE chain topologies.

1.3.3 Applications of Hyperbranched Polyethylenes

The hyperbranched topology gives Pd-diimine HBPEs many interesting and valuable properties for multiple applications. Due to their compact chain conformation, high molecular-weight HBPEs are very stable at high shear conditions, thus making them effective lubricant viscosity index (VI) improvers and polymer processing additives (PPAs).[33, 56, 62-63] In addition to lubricating purposes, HBPEs can non-specifically functionalize and solubilize multi-walled carbon nanotubes (MWCNTs) via non-covalent π-π interactions. This provides a way to facilitate the processing and applications of MWCNTs, while maintaining their valuable electrical and structural properties.[64]

Recently, functionalized HBPEs containing covalently tethered disulfide groups were successfully synthesized by copolymerization of ethylene with a disulfide-containing acrylate comonomer using Pd-diimine catalyst **1**.[65] The produced HBPEs were found to effectively trap the Pd(II) species *in situ* during the polymerization due to the coordinative capability of the disulfide functionality. Due to the hydrophobicity of HBPEs, these encapsulated Pd(II) catalysts have very good solubility in organic solvents, making them efficient as the recyclable catalyst in the Heck coupling reaction of iodobenzene and *n*-butyl acrylate. The strong affinity of Pd(II) species to the disulfide groups results in low Pd leaching in the reaction as well as easy recovery of the catalyst via precipitation or with biphasic solvent systems.[65]

1.4 Star-Structured Polyethylene Nanoparticles

In addition to hyperbranched polymers, soft star-structured polymer nanoparticles (NPs) are another class of uniquely branched macromolecules of highly compact chain architecture constructed with multiple polymer arms joined to a common central core.[66-67] Possessing a core-shell-structure, soft star polymer NPs have shown good application potential in numerous rapidly evolving technological fields including nanomedicine (e.g.,

DNA, siRNA, and drug delivery vector)[68-70], coatings[71], catalysis (e.g., recyclable catalyst and nanoreactor[72-75]), lubricants (e.g., VI improver)[76], emulsifiers[77-78], etc.

There are three main star polymer synthetic strategies as illustrated in Figure 1.7:

(a) Arm-first method which involves the synthesis of living polymer arms/macroinitiators (MIs) that are end-joined by initiating the polymerization of cross-linkable monomers (typically, divinyl monomers) to produce core cross-linked star polymers

(b) Core-first method which requires the synthesis of a core containing multiple initiators or catalysts capable of initiating simultaneous multi-directional living polymer arm growth

(c) Coupling-onto method which requires the synthesis of living polymer arms bearing a reactive group B and their subsequent joining to a core, functionalized with a certain number of reactive group A, via AB coupling reactions.[79-80]

Among all the living polymerization techniques, living radical polymerization techniques have been extensively used to synthesize star polymers from various monomer stocks (e.g., styrenics, methacrylates, and acrylates)[79-80], yet they cannot be used for the synthesis of star polyolefins. Star-structured polyethylene nanoparticles (SPE-NPs) had not been successfully synthesized until recently by our research group via Pd-catalyzed living ethylene coordination polymerization through both core-first and arm-first methods.[43, 45, 47, 81]

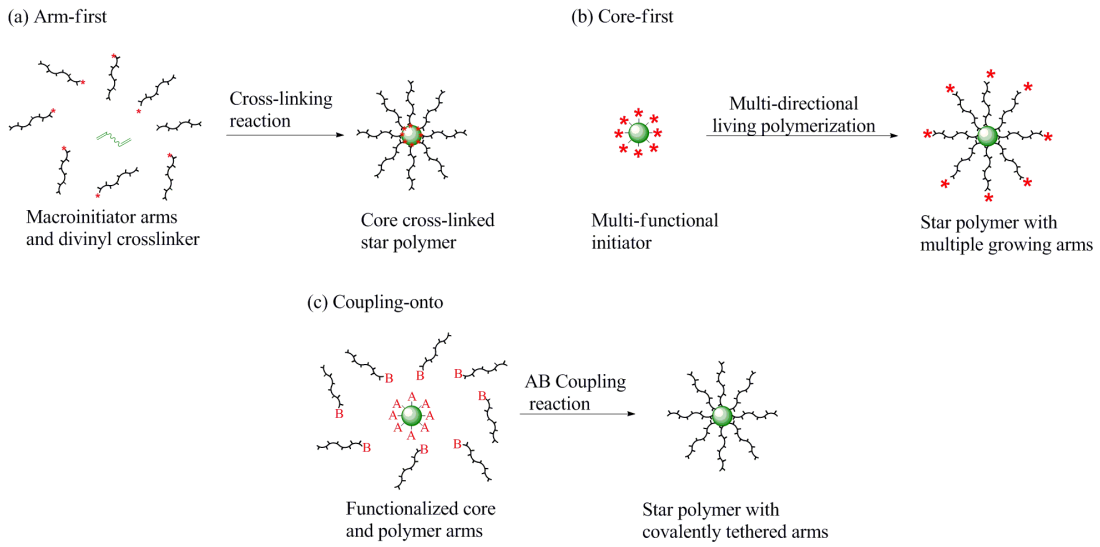

Figure 1.7 Schematic representations of the three general star polymer synthetic strategies: (a) arm-first; (b) core-first; and (c) coupling-onto.

Our research group was the first to report the successful synthesis of well-defined three-arm and multi-arm SPE-NPs via the core-first strategy.[45, 47] The major challenge in developing an efficient core-first synthetic approach to SPEs is the difficulty in designing multi-nuclear metal catalysts capable of initiating multi-directional living PE growth from a common central core.

Our group first developed a novel tri-nuclear Pd-catalyst (**10** in Figure 1.8) synthesized by immobilizing three acetonitrile Pd-diimine complexes (**1**) onto the acryloyl groups of a triacrylate complex (trimethylol propane, **9**) to produce three identical six-membered Pd-diimine centers bound to a tri-ester core. This catalyst was then used to mediate tri-directional living ethylene polymerization at high pressure and low temperature (27 atm and 5 °C). Due to the livingness of the polymerization, the M_n of the produced SPEs increased incrementally with the increase of polymerization time while at maintained narrow molecular weight distribution (e.g., M_n = 33 kg/mol at 1 h, PDI =1.05 and M_n = 136 kg/mol at 5 h, PDI = 1.12). Featured with a very small core, the M_n of these star polymers is essentially three times the size of its three identical LBPE arms produced by Pd-diimine catalyzed living ethylene polymerization (e.g., at 1 h: M_n = 11 kg/mol, PDI = 1.00; at 5 h:

M_n = 44 kg/mol, PDI = 1.03).[47]

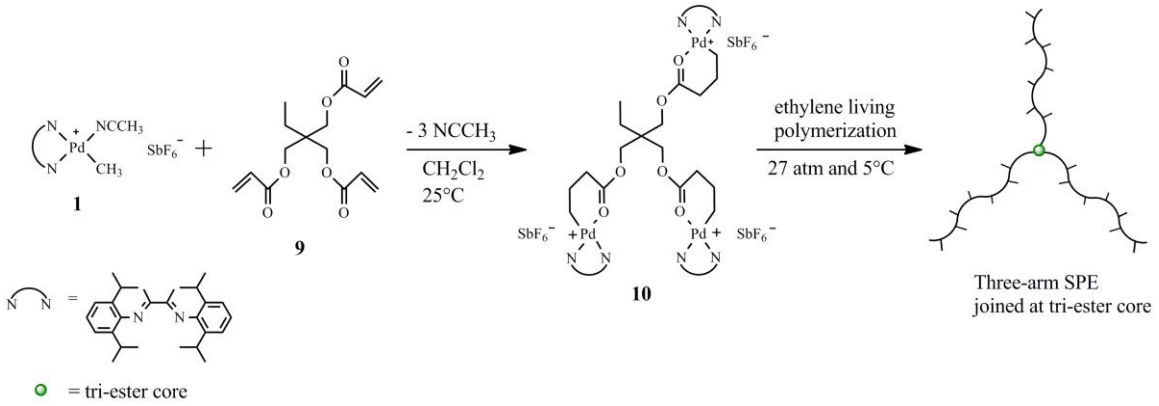

Figure 1.8 Schematic representation of the synthesis of the tri-nuclear Pd-diimine catalyst and the core-first synthesis of three-arm star polyethylenes via ethylene living polymerization.[47]

With the immobilization chemistry used to synthesize the trinuclear catalyst, our group further synthesized multi-nuclear Pd-diimine catalysts with multiple Pd-diimine centers (on average 17–23 per core) mounted onto acryloyl-functionalized HBPE cores, which were used to produce much larger SPE-NPs of high arm number (see Figure 1.9).[45] In the first step, a cationic acetonitrile Pd-diimine catalyst (**1**) was used to mediate non-living copolymerization of ethylene and divinyl 1,4-butanediol diacrylate (BDA, **14**) at low ethylene pressure (1 atm) and high BDA concentration, which produced HBPEs having pendant acryloyl groups.[45] In step two, Pd-diimine complex **1** was covalently anchored onto accessible acryloyl sites on the HBPE-cores to generate multi-nuclear HBPE-supported-Pd-diimine catalysts (**15**). Finally, multi-directional ethylene living polymerization was conducted using **15** at high ethylene pressure (27 atm) and 5 °C and sampled hourly for 6 h to monitor the size progression of the produced SPE-NPs via GPC-LS measurements.

Using this strategy, two separate multi-nuclear catalysts, HBPE-Pd-1 and HBPE-Pd-2, were synthesized having different M (M_n = 38 and 74 kg/mol; PDI = 1.3 and 1.8,

respectively), acryloyl content (average number of acryloyl groups per chain = 23 and 32, respectively), and Pd-catalyst content (average number of anchored Pd-catalysts per chain = 17 and 23, respectively). These two multi-nuclear catalysts produced spherical-shaped SPE-NPs with nearly identical sizes at the same polymerization times (e.g., at 1 h: $R_g \approx 16$ nm, $R_h \approx 15$ nm; at 6 h: $R_g \approx 30$ nm, $R_h \approx 30$ nm) with chain compactness factors of about unity ($R_g/R_h \approx 1$) which is in good agreement with R_g/R_h factors reported for spherical-shaped dendrimers and star polymers ($R_g/R_h \leq 1$).[82-84]

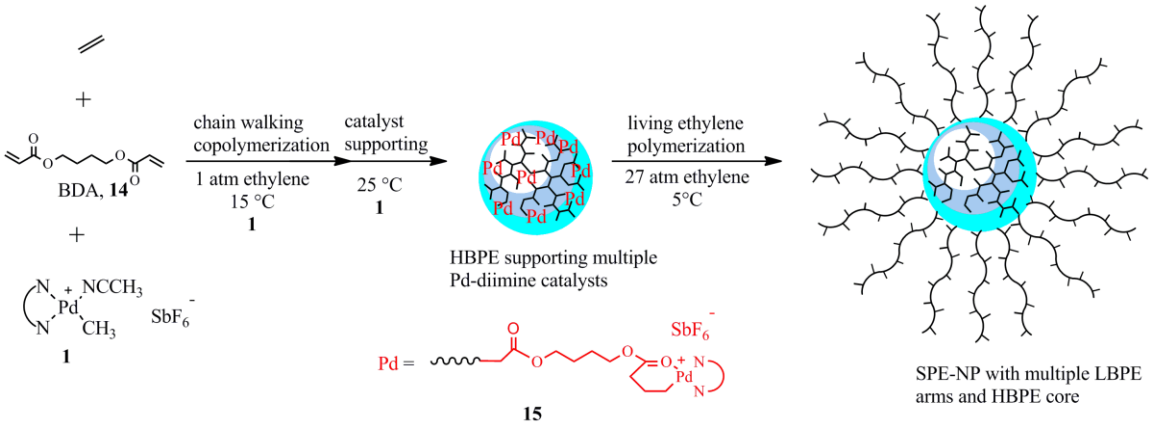

Figure 1.9 Schematic representation of the procedure used in the core-first synthesis of SPE-NPs composed of multiple LBPE arms joined at central HBPE core.[45]

Due to the livingness and identical conditions of the polymerization, the average M of both SPE-NPs increased incrementally from 1 h to 6 h while maintaining relatively narrow M distributions (SPE-1: M_n = 249 to 1496 kg/mol, PDI = 2.7 to 1.7; and SPE-2: M_n = 371 to 1436 kg/mol, PDI = 2.3 to 1.8). The average LBPE arm length in both sets of star polymers was also nearly identical at the same polymerization time (e.g., SPE-1 at 6 h: M_n = 49 kg/mol, PDI = 1.0; and SPE-2 at 6 h: M_n = 48 kg/mol, PDI = 1.0). The number average arm number (f_n) was found to be slightly higher in SPE-2 (f_n = 28) than in SPE-1 (f_n = 21) due to the higher average number of anchored Pd-catalysts in HBPE-Pd-2. This multi-step, core-first method enabled some control over star polymer parameters, like f_n, M, arm length, R_g, and R_h, by tuning ethylene polymerization time and by controlling the amount of acryloyl anchoring sites, hence the number of Pd-diimine centers, within the HBPE core.[45]

Sun and Guan have also reported a core-first, multi-step process to produce large star-structured dendritic PE-NPs using a multi-nuclear HBPE-Pd-diimine catalyst.[81] The synthesis of their multi-nuclear catalyst is more tedious than the method described above and consists of four main steps. In the first step, they used a chain walking Pd-diimine catalyst to copolymerize ethylene and a comonomer, containing a protected hydroxyl group, which needed to be deprotected (step 2) in order to be functionalized with butenoate groups (step 3), onto which were grafted Pd-diimine catalysts (step 4). The produced multi-nuclear catalyst was then used to mediate chain walking ethylene polymerization at very low pressure (0.1 atm) which produced very large and compact (R_g/R_h = 0.80) unimolecular dendritic PE-NPs (e.g., $M_{n,\,LS}$ = 3600 kg/mol, R_g = 48.1 nm, R_h = 59.6 nm, and PDI = 1.11) featured with a large HBPE core (e.g., $M_{n,\,LS}$ = 313 kg/mol) and high number of HBPE arms (e.g., f_n = 71).[81]

Our group also developed an "arm-first" method for synthesis of multiarm SPE-NPs via a tandem two-step polymerization process by combining Pd-catalyzed living ethylene polymerization and atom transfer radical polymerization (ATRP) of divinylbenzene (DVB), a well-known cross-linkable monomer (see Figure 1.10).[43] The first step involved the use of a cationic 2-(2-bromoisobutyryloxy)ethyl acrylate-Pd-diimine catalyst (BIEA-Pd-diimine catalyst, **16**) to synthesize living LBPE arms (at 27 atm ethylene and 5 °C) bearing a reactive ATRP initiating site at the starting end (referred to as LBPE macroinitiators or LBPE-MIs, **17**). In the second step, LBPE-MIs are used to initiate ATRP of DVB, thus joining several LBPE arms to a poly(divinylbenzene) or PDVB core, containing cross-linkable pendant double bonds. Further ATRP of those reactive double bonds facilitated the formation of SPE-NPs via a combination of star-star coupling, LBPE-MI addition, and intramolecular cross-linking reactions.[43]

With this arm-first method, three sets of SPE-NPs were synthesized using three separate narrowly distributed LBPE-MIs (PDI ≈ 1.01) of different lengths (M_n = 7.3, 10.3, and 13.7 kg/mol, respectively). Key polymerization parameters, including MI concentration, DVB to MI molar ratio, and MI length, were investigated for their effect on star parameters, including star yield, f_n, M_n, and R_h. By controlling these polymerization parameters a variety of SPE-NPs were formed with good yields (as high as 87 %), f_n

ranging from 5 to 43 per star, M_n as low as 50 kg/mol (PDI = 1.22) and as high as 740 kg/mol (PDI = 1.22), and R_h ranging from 6 to 14 nm.

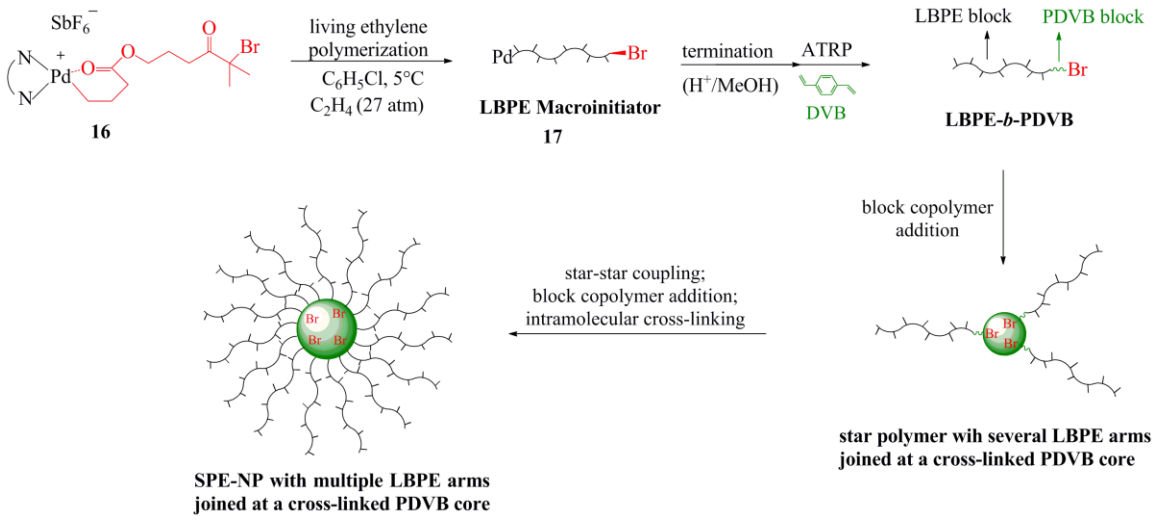

Figure 1.10 Schematic representation of the arm-first synthesis of SPE-NPs via a tandem two-step procedure combining Pd-catalyzed ethylene living polymerization and ATRP of divinylbenzene.[43]

Compared to the core-first methods, the arm-first method offers more flexible control over star polymer parameters. In particular, it has the advantages in the precise control of arm length, topology, and functionality, as well as the capacity to encapsulate reactive species within the cross-linked core of the star polymer. These features will be exploited in the arm-first synthesis of SPE-NPs and their catalytic applications detailed in this thesis.

1.5 Research Rationale and Objectives

Although Pd-diimine catalysts have been successfully used in the synthesis of SPE-NPs, the existing core-first and arm-first approaches require sophisticated synthesis of multi-nuclear or functional Pd-diimine catalysts and/or a combination of two different

polymerization reactions. The aim of this thesis was to further develop a more convenient arm-first synthesis of large unimolecular SPE-NPs via a simplified polymerization process conducted within a single reactor with the use of the conventional Pd-diimine catalyst **1**. The synthetic strategy will involve ethylene living polymerization with **1** for arm formation, followed with the addition of a divinyl cross-linker polymerizable by the Pd catalyst for star formation via cross-linking.

Generally, the selection of an appropriate cross-linking agent is vital to the successful arm-first synthesis of star polymers. It is particularly challenging in the case of Pd-catalyzed polymerization since typical divinyl cross-linking agents polymerizable by the Pd catalyst, such as diacrylates and diolefins, have a much weaker reactivity in comparison with ethylene. Therefore, it is difficult to synthesize the necessary diblock copolymers (which are comprised of a first long PE block and a short second block containing pendant vinyl groups) for star formation.

In this thesis research, bicyclo[2.2.1]hepta-2,5-diene, a strained symmetrical bicyclic diene also known as norbornadiene (NBD), was used as the cross-linker in the Pd-diimine catalyzed arm-first synthesis of SPE-NPs. It was chosen based on the fact that its monovinyl analogue, norbornene (NB), has high reactivity in the copolymerization with ethylene catalyzed with **1** as reported by our group, leading to ethylene-NB alternating, gradient, and gradient-block copolymers of tuneable microstructures.[41] The successful incorporation of NBD following the formation of living PE block was expected to generate efficiently, star-shell structured polymers constructed with PE arms and a cross-linked core via a one-pot process. Meanwhile, in this synthetic strategy, the Pd catalyst is simultaneously encapsulated into the cross-linked core, rendering unimolecular star polymer nanoparticles having core-encapsulated Pd catalysts. Such Pd-encapsulating nanoparticles are promising for applications as reusable supported catalysts for various Pd-catalyzed reactions.

Based on above hypotheses, there are three objectives in this thesis research.

The first objective of this thesis is to verify the effectiveness of the proposed arm-first strategy for the synthesis of SPE-NPs and to understand the polymerization chemistry

of NBD in the Pd-diimine catalyzed system.

The second objective is to investigate the effects of various polymerization parameters on star formation and structure of the resulting SPE-NPs, so as to tailor design the SPE-NPs of controllable star parameters, including arm length and number, and core size.

The third objective is to investigate and demonstrate the application of SPE-NPs as versatile reusable Pd-encapsulated catalysts for different reactions including the hydrogenation of alkenes and alkynes as well as the Heck coupling reaction.

1.6 Scope of Thesis

The experimental methodology employed in this thesis is described in Chapter 2, with details on the chemicals, materials, experimental setups and procedures, characterizations and measurements, and parameters of all analytical techniques used in this research.

Chapter 3 describes and discusses the results obtained from systematic investigations detailing the arm-first Pd-diimine-catalyzed synthesis of SPE-NPs. Section 3.1 discusses the star polymer formation at every stage of the synthetic process; Section 3.2 examines the polymerization chemistry of the NBD cross-linker with **1** as well as the effects of NBD reaction parameters on the formation of SPE-NPs; Sections 3.3-3.5 discuss a thorough investigation of the effects of PE arm topology and size, star polymer precipitation step, and drying step on the formation of SPE-NPs; and Section 3.6 describes and discusses TEM, AFM, and DLS morphological and size characterizations of the SPE-NPs synthesized at different reaction conditions.

In Chapter 4, the catalytic applications of SPE-NPs encapsulating Pd(II) species are demonstrated in hydrogenation and isomerization reactions of 1-octene and 1-hexyne (Section 4.1) and in Heck carbon-carbon coupling reactions of iodobenzene and butyl acrylate (Section 4.2). The recyclability of SPE-NPs in the Heck reaction was also

investigated and discussed in this chapter. NMR spectroscopy was used to determine reaction kinetics and to identify products in these reactions at different conditions.

Lastly, Chapter 5 summarizes the results obtained in this thesis with a discussion of the conclusions. Related to the research presented in this thesis, future works and potential applications are discussed in this concluding chapter.

CHAPTER 2: Experimental Methodology

2.1 Materials

The cationic acetonitrile Pd-diimine catalyst, [(ArN=C(Me)–(Me)C=NAr)Pd(CH_3)(NCMe)]$^+SbF_6^-$ (Ar = 2,6-(*i*Pr)$_2$C6H$_3$) **(1),** was synthesized following literature procedure [28] and its structure was confirmed with ^{1}H NMR in $CDCl_3$ (99.96 % D, Aldrich). The chemicals used in the synthesis of **1** include sodium tetrachloropalladate (Pressure Chemicals), 1,5-cyclooctadiene (99%, Aldrich), tretramethyltin (95%, Aldrich), 2,6-diisopropylaniline (tech, 90%, Aldrich), 2,3-butanedione (97%, Aldrich), acetonitrile (anhydrous, 99.8%, Sigma-Aldrich), silver hexaflurorantimonate (V) ($AgSbF_6$, 98%, Aldrich), and diethyl ether for purification purposes (anhydrous, American Chemical Society (ACS) reagent grade containing BHT as inhibitor, ≥99.0%, Sigma-Aldrich).

Polymer-grade ethylene and ultra-high purity nitrogen (99.998%, both purchased from Praxair) were purged from moisture and oxygen by flowing through 3Å/5Å molecular sieves and Oxiclear columns. Ultra-high purity hydrogen gas (99.9997%, Praxair) was used as purchased for hydrogenation reactions. Bicyclo[2.2.1]hepta-2,5-diene/norbornadiene (NBD 98%, contains 0.05-0.25% BHT inhibitor, Aldrich) was dried with molecular sieves and aluminum oxide. Chlorobenzene (ClBz), toluene, hexanes, and dichloromethane (HPLC grade, Fisher Scientific) were dried using a solvent purification system (Innovative Technology).

Other chemicals, including bicyclo[2.2.1]hept-2-ene/norbornene (NB, 99%, Aldrich), methanol (ACS reagent grade, Fisher Scientific), THF (ACS reagent and HPLC grade, Fisher Scientific), hydrochloric acid solution 1N (certified, Fisher Chemicals), 1-octene (98%, Aldrich), 1-hexyne (97%, Aldrich), bromobenzene (BrBz, 99.5%, Aldrich), iodobenzene (98%, Aldrich), butyl acrylate (99%, Aldrich), triethylamine (≥99%, Sigma-Aldrich), and liquid nitrogen (Praxair) were all used as purchased. All air/moisture

sensitive compounds were manipulated using standard Schlenk technique or in a nitrogen-filled glove box (Innovative Technology).

2.2 Experimental Procedures

2.2.1 Single-Reactor Arm-First Pd-Diimine-Catalyzed Synthesis of Star Polyethylene Nanoparticles

Low pressure living ethylene polymerizations, used to synthesize SPE-NPs made of multiple HBPE arms joined by a central cross-linked PNBD core, were conducted in an oven-dried 500 mL jacketed glass reactor equipped with medium sized egg-shaped stir bar, sealed with a rubber stopper and Parafilm® (registered trademark of Bemis Company, Inc.), and temperature controlled by a refrigerating water circulator set to 15 °C. The reactor was purged three or four times with 1 atm ethylene (vacuumed 10 min/cycle), then 40 mL of anhydrous chlorobenzene (ClBz) was injected into the ethylene-pressurised reactor. The reaction solution was mixed for 15 min to homogenize and thermally equilibrate the ethylene-ClBz mixture to 15 °C.

Step 1 of the SPE-NP synthesis consists of synthesizing living HBPE arms/blocks catalyzed by **1**. It was initiated by injecting 0.1 mmol of catalyst **1**, which was dissolved in 10 mL of anhydrous ClBz, into the jacketed reactor at constant absolute ethylene pressure of 1 atm and 15 °C. Living ethylene polymerization catalyzed by **1** was carried out for 1, 2, 3, or 5 h to produce HBPE arms/blocks of tunable lengths. A 5 mL sample of the reaction solution from step 1 was collected and the polymer product was precipitated in a large volume of HCl-acidified methanol solution (2% (v/v) HCl solution in methanol; H^+/MeOH). The polymer sample was washed several times, by dissolution in THF and precipitation in methanol (MeOH, now referred to as THF/MeOH wash cycle), to neutralize the polymer's alkalinity and remove the majority of Pd(0) black deposits. The washed polymer sample was then dried *in vacuo* overnight at 70 °C. Characteristics of the

HBPE arm were obtained with triple-detection-GPC (with on-line LS, DRI, and viscometer detectors) using THF as elution solvent at 33 °C (see Section 2.3.3 for GPC procedure).

Step 2 consists of polymerizing a short PNBD block, containing pendant cross-linkable vinyl groups, by chain extension of the growing living HBPE block catalyzed by **1**. Immediately after sampling the reaction solution in step 1, NBD polymerization was initiated by adding a prescribed amount of NBD (5.43 to 32.5 mmol) into the reaction mixture for a fixed polymerization time of 2 h in the presence of ethylene (1 atm absolute pressure) at 15 °C. In selected polymerizations, a 5 mL sample of the reaction solution was sampled at 2 h, then diluted in THF and directly injected into the GPC system to obtain polymer characteristics of the HBPE-*b*-PNBD block copolymer product. The kinetics of the HBPE chain extension by the polymerization of NBD with **1** is investigated in a separate set of experiments (see Section 2.2.2 for the procedure).

In step 3, the block copolymers produced in step 2 are precipitated, via centrifugation at 5000 rpm for ~ 10 min, in H^+/MeOH in order to initiate the formation of SPE-NPs via cross-linking reactions of the pendant vinyl groups in the NBD segment of HBPE-*b*-PNBD block copolymers. Finally, in step 4, the polymer product was dried *in vacuo* at 120 °C for 6 h in order to accelerate the cross-linking process and form large unimolecular SPE-NPs composed of multiple HBPE arms emanating from a cross-linked PNBD core.

Differently, the synthesis of SPE-NPs made of multiple LBPE arms joined by a central cross-linked PNBD core was conducted in a 500 mL Autoclave Engineers Zipperclave reactor equipped with a MagnaDrive mixer, a water/ethylene glycol circulation jacket connected to a heating/cooling circulator, and a sampling port. The reactor was purged three to four times with 1 atm ethylene (vacuumed 10 min/cycle) and 40 mL of anhydrous ClBz was injected into the ethylene-pressurized reactor (ca. 1 atm). The reaction solution was mixed for 15 min in order to homogenize and thermally equilibrate the ethylene-ClBz solution to 5 °C.

In step 1, living LBPE arms/blocks were grown by injecting 0.1 mmol of **1**, dissolved in 10 mL of anhydrous ClBz, into the Zipperclave reactor under positive ethylene

pressure and the polymerization was immediately started by pressurizing the reactor to an ethylene pressure of 27 atm (absolute). Living ethylene polymerizations were conducted for 2, 3, or 5 h, followed by reduction in reactor pressure to 1 atm ethylene by venting-out the excess pressure. A 5 mL sample was collected through the sampling port and the polymer was precipitated (via centrifugation at 5000 rpm for ~ 10 min) in H^+ MeOH, washed by three or four cycles of THF/MeOH dissolution/ precipitation, and dried *in vacuo* overnight at 70 °C. Characteristics of the LBPE arms produced in step 1 were obtained with triple-detection-GPC (with on-line LS, DRI, and viscosity detectors) using THF as elution solvent at 33 °C.

Immediately after reducing ethylene pressure to 1 atm and sampling the polymerization solution, step 2 was initiated by injecting a prescribed amount of NBD (5.43 to 32.5 mmol) into the reactor. NBD polymerization was carried for 2 h, catalyzed by **1** at an absolute ethylene pressure of 1 atm and 5 °C. Steps 3 and 4, consisting of H^+ MeOH precipitation and drying of the polymer product, were executed exactly as described in the low ethylene pressure procedure described above. Both types of SPE-NPs (having HBPE arms or LBPE arms) were characterized by triple detection GPC in THF at 33 °C.

2.2.2 Determination of Norbornadiene Conversion in Pd-Diimine-Catalyzed Synthesis of Star Polyethylene Nanoparticles

This SPE-NP synthesis was conducted utilizing the same reaction conditions as described above (in section 2.2.3), and carried out in a jacketed glass reactor equipped with egg-shaped magnetic stir bar and sealed with a rubber stopper and Parafilm®. First, living ethylene polymerization catalyzed by **1** was carried out at 1 atm ethylene and 15 °C to form HBPE arms. A reference solution containing 21.73 mmol of NBD and 19.96 mmol of bromobenzene (BrBz), used as internal standard for GC analysis, was precisely diluted to 10 mL with anhydrous ClBz. The GC reference sample at time 0 h was prepared by diluting 100 μL of the reference solution in exactly 10 mL of methanol.

Stage 2 was initiated by adding the reference solution, containing NBD and BrBz, into the polymerization mixture at an absolute ethylene pressure of 1 atm and 15 °C. Samples (1 mL each) were collected at 0.25, 0.5, and 1 h of NBD polymerization and the polymer products were precipitated in exactly 10 mL of methanol, respectively. The precipitated polymer was removed from the polymerization samples by syringe filtration (0.2 μm porous filters), and the filtrate (containing unreacted NBD monomer, BrBz, ClBz, and MeOH) analyzed by GC to determine NBD conversion (see Section 2.3.2 for GC procedure including sample preparation).

A control NBD homopolymerization was conducted in a flame-dried Schlenk flask equipped with small egg-shape magnetic stir bar and sealed with a rubber stopper and Parafilm®. The polymerization was done at an absolute nitrogen pressure of 1 atm at 25 °C using 0.1 mmol of **1** with total volume of 20 mL in ClBz. Initially **1** was dissolved in 10 mL of ClBz and added into the pre-purged reactor filled with 1 atm nitrogen. A reference solution containing NBD (33.30 mmol) and BrBz (32.85 mmol) was diluted to 10 mL in ClBz, and added into the reactor to start the polymerization. Samples were collect at 0.25, 0.5, and 1 h to determine NBD conversion by GC analysis (see Section 2.3.2 for GC procedure including sample preparation).

2.2.3 Pd-Diimine-Catalyzed Norbornadiene Homopolymerization via *in situ* ^{1}H NMR

A NMR tube was charged with 0.011 mmol of catalyst **1** dissolved in 0.5 mL of deuterated chloroform ($CDCl_3$) and a ^{1}H spectrum was collected using 500 MHz NMR at 25 °C. The tube was ejected and prescribed amounts of NBD (0.594-3.56 mmol) along with equimolar amounts of dichloromethane (used as internal standard) were added to start the polymerization. A ^{1}H spectrum was immediately collected in order to give the initial amount of NBD in the polymerization system at time 0 h. The polymerization was monitored by collecting ^{1}H spectrums at regular intervals for 3 h (e.g., every 15 min during the first hour then every 30 min) using the same 500 MHz NMR spectrometer at 25 °C.

2.2.4 Pd-Diimine-Catalyzed Norbornadiene Homopolymerization & Copolymerization with Ethylene

A flame-dried round bottom Schlenk flask was purged three times, following a 10 min vacuum period per cycle, with either 1 atm nitrogen (N_2) or 1 atm ethylene (C_2H_4) for NBD homopolymerization or copolymerization with ethylene, respectively. Under 1 atm N_2 or 1 atm C_2H_4, the reaction solutions containing 32.5 mmol of NBD and 10 mL of anhydrous dichloromethane were added to the respective Schlenk flasks and mixed for 10 min to assure the reaction mediums were homogeneous. After thermal equilibration to 25 °C, NBD homopolymerization and ethylene copolymerization reactions were initiated by adding a solution of 0.1 mmol of catalyst **1** dissolved in 10 mL of anhydrous dichloromethane into each Schlenk flask.

The polymer products were recovered after 1 h of polymerization via vacuum evaporation of the reaction solvent and unreacted NBD monomer. The solubility of the polymer products, obtained in both homo- and copolymerizations, were tested in common organic solvents (e.g., THF, chloroform, dichloromethane, chlorobenzene, hexanes, etc.) prior to and after being washed three times with acidified methanol (2% v/v concentrated HCl in methanol) and dried under air flow at 25°C and/or *in vacuo* at 120°C.

2.2.5 Hydrogenation Reactions of 1-Octene & 1-Hexyne Catalyzed by Pd(II)-Catalysts Encapsulated in Star Polyethylene Nanoparticles

Hydrogenation reactions were carried out in a 20 mL stainless steel high pressure reaction vessel equipped with a pressure gauge, an on-off 2-way Swagelok ball valve used as the injection/sampling port and a switching 3-way Swagelok ball valve with inlets connected to a hydrogen (H_2) gas line and a vacuum line. The reaction temperature was regulated by submerging the reaction vessel into an oil bath equipped with magnetic stir bar that was heated and stirred by a hot plate/magnetic stirrer unit. The reaction temperature was monitored with a thermometer submerged in the oil bath (depicted in Figure 2.1). Before starting a hydrogenation reaction, the vessel was purged three times with 1 atm of

hydrogen (vacuumed 10 min/cycle) to remove air and moisture. Meanwhile, the oil bath was heated to maintain the desired reaction temperature under constant stirring.

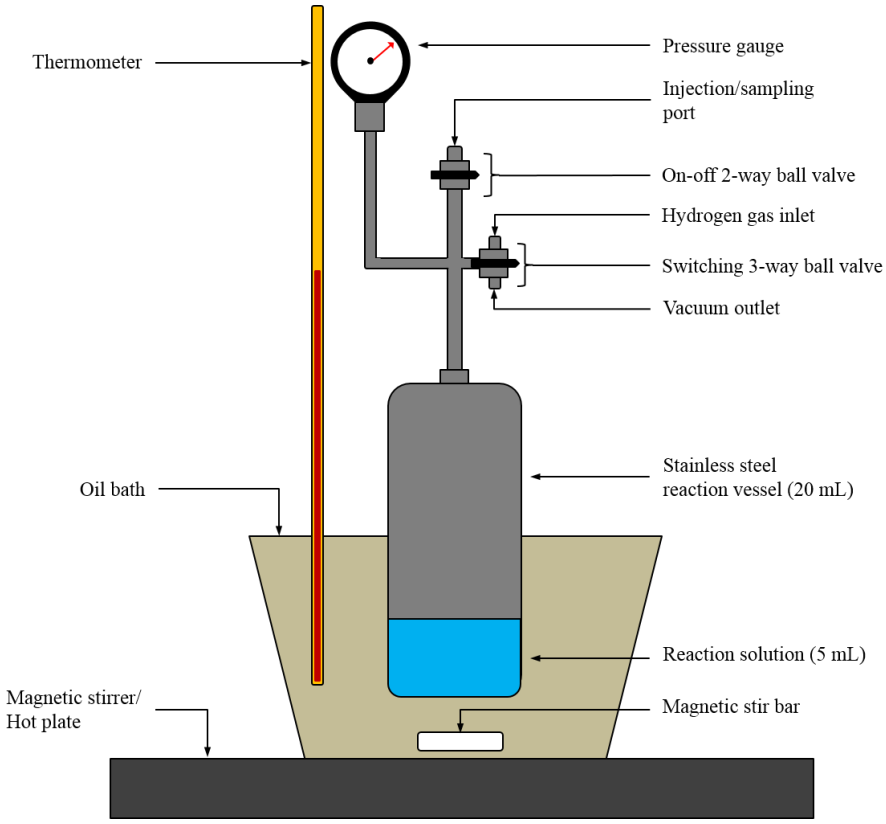

Figure 2.1 Schematic representation of the hydrogenation reaction setup displaying the principle assembly of the 20 mL stainless steel reaction vessel equipped with a pressure gauge, an injection/sampling port, a hydrogen gas inlet and vacuum outlet.

Hydrogenations of two α-unsaturated hydrocarbons (1-octene or 1-hexyne, respectively) were catalyzed by Pd(II) catalysts encapsulated in two different star polymer NPs, one bearing HBPE arms and the other LBPE arms (SPE-NP-52 and SPE-NP-20, respectively). A typical hydrogenation reaction mixture was prepared by dissolving 0.05 g of SPE-NP-52 or 0.08 g of SPE-NP-20 (ca. Pd(II) amount ≈ 5 μmol/ polymer sample) in a solution containing equimolar amounts (1330 μmol) of 1-octene/1-hexyne and anisole (the

internal standard used to normalize ^{1}H NMR integrations) and diluted to a total reaction volume of 5 mL with hexanes (solvent). An initial sample (100 µL) was collected, then the mixture was added to the H_2-filled reactor which was immediately pressurized with H_2 to the targeted absolute pressure of 1 atm or 10 atm, and submerged into the temperature controlled oil bath at 25, 35, 45, or 65 °C to start the hydrogenation reaction.

In order to calculate the amount of Pd(II) catalyst (mol) contained within the mass of SPE-NP used in each hydrogenation reaction, it was assumed, given the livingness of the polymerization, that every Pd catalyst mediating the growth of a living arm (PE-*b*-PNBD block copolymer), which was used in the construction of a star polymer, was considered trapped inside its cross-linked PNBD core. Therefore, an approximate Pd(II) catalyst amount was calculated by dividing the mass of the SPE-NP (g) used in the hydrogenation reaction by the M_n (g/mol) of the PE arm multiplied by the star yield (Equation 2.1).

$$\text{Pd amount (mol)} = \left[\frac{\text{mass of SPE-NP (g)}}{M_n \text{ of PE arm (g/mol)}}\right] * \text{ star yield} \qquad 2.1$$

Reaction kinetics was determined by ^{1}H NMR analysis of samples collected periodically (ca., every 2 h for the first 12 h, then every 12 h to 96 h, and every 24 h to 144 h). Sampling of hydrogenation reactions was done by quickly cooling the reactor in an iced water bath, and then H_2 pressure was reduced to a continuous flow of 1 atm in order to collect 0.2 mL of reaction solution through the sampling port. Subsequently, H_2 pressure was readjusted and the reaction vessel was re-submerged in the hot oil bath to continue the hydrogenation. ^{1}H NMR samples were prepared by diluting 100 µL of the hydrogenation reaction samples with 500 µL of $CDCl_3$ and analyzed using a Varian Gemini 2000 NMR spectrometer (200 MHz) at 25 °C .

2.2.6 Heck Coupling Reaction of Iodobenzene & Butyl Acrylate Catalyzed by Pd(II)-Catalysts Encapsulated in Star Polyethylene Nanoparticles

Heck coupling reactions of iodobenzene and butyl acrylate were conducted using a sufficient amount (0.1 g) of two different star polymers, one constructed with HBPE arms the other with LBPE arms (SPE-NP-52 and SPE-NP-20) in order to effectively recycle the polymer-encapsulated Pd(II) catalyst after each reaction/cycle. Approximate Pd amounts contained in the 0.1 g samples of SPE-NP-52 and SPE-NP-20 were calculated at 10 μmol and 6 μmol, respectively, using Equation 2.1. The reaction solution was prepared in a clean test tube equipped with a magnetic stir bar by combining 0.1 g of SPE-NP (Pd(II) catalyst), 2.45 mmol of iodobenzene (limiting reactant), 3.68 mmol of butyl acrylate (1.5 molar equivalents of iodobenzene), 3.68 mmol of triethylamine (Et_3N, organic base), and 3 mL of anhydrous toluene (solvent).

The test tube was sealed with a rubber stopper, air was purged from the reaction mixture following three freeze-thaw cycles in liquid nitrogen and finally filled to 1 atm with nitrogen gas. Under vigorous mixing, the reaction solution was heated to 100°C in a hot oil bath to initiate the Heck coupling reaction of iodobenzene and butyl acrylate. Samples (0.1 mL) of the reaction solution were collected periodically for 24 h to determine the product yield and reaction kinetics by ^1H NMR. These NMR samples were prepared by diluting 100 μL of reaction sample with 500 μL of $CDCl_3$ and ^1H spectrums were collected using a Bruker AV500 NMR spectrometer (500 MHz) at 25°C.

During the Heck reaction, Pd (0) black deposits were observed in the salt precipitate consisting of a complexion of the base adduct (HEt_3NI) and the leached Pd catalysts. After 24 h, the Heck reaction solution was recovered and the salt/Pd black precipitate was washed three times with petroleum ether to remove any residual SPE-NPs, reactants, and coupling products. The salt precipitate was dried overnight *in vacuo* at 70 °C. The recovered reaction solution was concentrated and the SPE-NPs were precipitated in MeOH, washed several times by THF dissolution and MeOH precipitation cycles, and dried overnight *in vacuo* at 70°C.

2.3 Characterization Techniques and Measurements

2.3.1 Gel Permeation Chromatography with On-Line Triple Detection

Polymer characterizations with gel permeation chromatography (GPC) were carried out using a Polymer Laboratories PL-GPC220 system with high temperature on-line triple-detection incorporating a differential refractive index (DRI) detector (from Polymer Laboratories), a three-angle (45, 90, and 135°) miniDAWN light scattering (LS) detector (from Wyatt Technology) at a laser wavelength of 687 nm, and a four-bridge capillary viscometer (from Polymer Laboratories). All polymer samples (1-5 mg/mL) were injected (200 μL) and separated by passing through a guard column (PL# 1110-1120) and three 30 cm columns (PLgel 10 μm MIXED-B 300 × 7.5 mm) at a flow rate of 1.0 mL/min in HPLC-grade THF at 33°C.

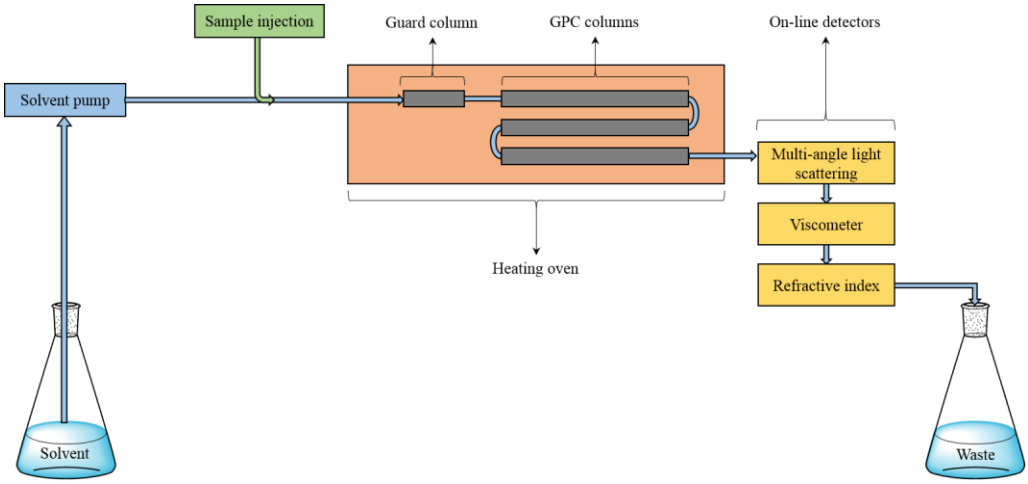

Figure 2.2 Schematic representation of the arrangement of the principal components of the triple detection GPC instrument incorporating on-line three-angle light scattering detectors, differential refractive index detector, and viscometer.

Data from the three detectors was collected and analyzed with Wyatt Technology's Astra software. Two polystyrene narrow standards (from Pressure Chemicals) with weight-average molecular weight (M_w) of 30 and 200 kg/mol were used to normalize the three angle LS signals, the interdetector delay volume, and band broadening, respectively. The DRI increment (d*n*/d*c*) values used for HBPE, LBPE and SPE-NPs was 0.078 mL/g, and 0.185 mL/g for polystyrene.

M_n, M_w, and PDI of the polymers synthesized here-in were determined with the LS detector; the weight-average intrinsic viscosity ($[\eta]_w$) was measured with the viscometer; and the mass fraction of the eluting polymer was measured with DRI detector. The star yield was determined from the area percentage of star polymer to overall polymer product by fitting the curves obtained from the DRI detector and calculated using Equation 2.1, where A_{SPE} and $A_{PE\ arm}$ are the areas under the DRI curves for the SPE peak and its PE arm, respectively. The number-average arm number (f_n) per star was calculated from the ratio of the M_n of the star polymer to its PE arm (Equation 2.2) with the assumption that the low M_n of the short PNBD blocks, that constitute the small cross-linked core, has negligible influence on the overall M_n of the SPE-NP. $[\eta]_w$ ratio was determined from the ratio of the $[\eta]_w$ of the SPE-NPS to the $[\eta]_w$ of its PE arm. Mark Houwink exponent α was obtained from the logarithmic relationship of the star polymer $[\eta]$ as a function of M (Equation 1.2).

$$\text{star yield} = \left(\frac{A_{SPE}}{A_{SPE} + A_{PE\ arm}}\right) * 100 \qquad 2.2$$

$$f_n = \frac{M_n \text{ of SPE}}{M_n \text{ of PE arm}} \qquad 2.3$$

For catalytic applications, the SPE-NPs produced in Runs 52 (bearing HBPE arms) were purified by GPC fractionation method described in our earlier work.[45] A Waters 2695 Separation System incorporating a Waters 2414 DRI detector and comprised of one

guard column (PL# 1110-1120) and three separation columns (30 cm, PLgel 10 µm MIXED-B 3000 × 9.5 mm) was operated using HPLC-grade THF at a flow rate of 1.0 mL/min for the fractionation of SPE-NPs contained in the as-produced polymer. GPC polymer samples were prepared at high concentration c.a. 50-100 mg/mL. Purification of the star polymer nanoparticles was done by 100 µL injections and the eluting high-molecular-weight and low-molecular-weight signals detected from DRI were collected separately and corresponded to purified SPE-NPs and free unattached HBPE-b-PNBD copolymer arms, respectively.

2.3.2 Nuclear Magnetic Resonance Spectroscopy

A Bruker AV500 NMR spectrometer (500 MHz) was used at 25 °C to collect ^{1}H NMR spectrums of *in situ* NBD homopolymerizations and Heck reaction samples using $CDCl_3$ as solvent. It was also used (at 25 °C using $CDCl_3$ as solvent) to analyze ^{13}C NMR spectrums of NBD homopolymers, ethylene-NBD copolymers, and 1-hexyne hydrogenation reaction samples. All other ^{1}H NMR spectra including hydrogenation/isomerization reaction samples, were recorded on a Varian Gemini 2000 NMR spectrometer (200 MHz) at 25 °C using $CDCl_3$ as solvent.

NBD conversion data were obtained from H integration of the resonance signal of the growing NBD homopolymer chain (I_c; peak c, 5.8-6.3 ppm, 2 H) over the total amount of NBD including the combined H integration of signals of unreacted NBD monomer (I_C; peak C, 6.8 ppm, 4 H) and the growing PNBD chain (I_c). ^{1}H NMR integration signals were normalized with internal standard CH_2Cl_2 (singulet, 5.3 ppm, 2 H) added into the reaction mixture in equimolar amounts to the initial NBD. Percent conversion results of NBD homopolymerization (x_{NBD}) catalyzed by **1** were calculated using Equation 2.4.

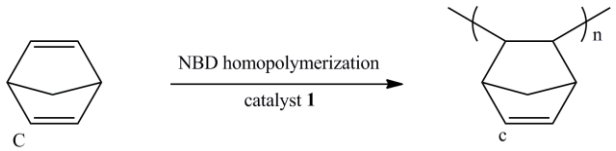

$$x_{\mathrm{NBD}} = \left(\frac{I_c/_2}{I_c/_2 + I_C/_4} \right) * 100 \qquad 2.4$$

For all ^{1}H NMR spectra analyzed in the hydrogenation/isomerization reactions of alkenes (i.e., octene, hexene) and terminal alkyne (1-hexyne), the resonance peak integrations were normalized with the singulet peak arising at 3.75 ppm of anisole's (internal standard) 3 H of its methyl group.

The kinetics of the hydrogenation/isomerization reaction of 1-octene catalyzed by Pd(II)-encapsulated SPE-NPs were assessed by monitoring the ^{1}H NMR integration of resonance peaks arising from the vinyl protons of unsaturated octene species. The initial octene percentage present in the 0 h sample was calculated from the combine H resonance peak integrations of 1-octene ($I_{a\ at\ 0h}$, peak a: 5.7 ppm, 1 H) and, possibly present, *n*-octene isomers ($I_{b\ at\ 0h}$, peak b: 5.47-5.34 ppm, 2 H) using Equation 2.5.

$$\%\ \text{initial octene} = \left(I_{a\ at\ 0h} + I_{b\ at\ 0h}/_2 \right) * 100 \qquad 2.5$$

See below for a schematic representation of the chemical structures of 1-octene and *n*-octene isomers with annotated protons used in these equations.

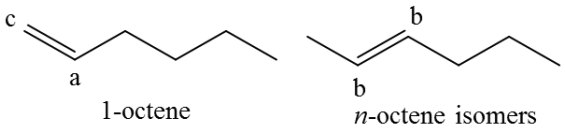

1-octene *n*-octene isomers

The percent yield of isomerization products, *n*-octene isomers, present in samples collected periodically during the reaction, were calculated from the H resonance peak intensity of 1-octene (I_c, peak c: 4.97-4.91 ppm, 2 H) over the initial octene content using Equation 2.6. The percent yield of hydrogenation product, octane, was calculated with Equation 2.8, by subtracting the total octene content present in the sample (which was calculated from the combine H integrations of peaks a, b, and c using Equation 2.7) from the initial octene percentage (calculated in Equation 2.5). Finally the percent residual octene content was determined from the H resonance peak integrations of vinyl protons a and b from 1-octene and *n*-octene isomers, respectively, using Equation 2.9.

$$\%\ \text{n-octene isomers} = \left[\frac{\left(I_c/_2\right)}{\left(I_{a\ at\ 0h} + I_{b\ at\ 0h}/_2\right)}\right] * 100 \qquad 2.6$$

$$\%\ \text{total octene} = \left(I_a + I_b/_2 + I_c/_2\right) * 100 \qquad 2.7$$

$$\%\ \text{octane} = \%\ \text{initial} - \text{total octene} \qquad 2.8$$

$$\%\ \text{residual 1-octene} = \left[\frac{\left(I_a + I_b/_2\right)}{\left(I_{a\ at\ 0h} + I_{b\ at\ 0h}/_2\right)}\right] * 100 \qquad 2.9$$

Similarly, for the Pd(II) encapsulated SPE-NP-catalyzed hydrogenation of 1-hexyne, the reaction kinetics were also assessed by monitoring the ^{1}H NMR integration of resonance peaks arising from the secondary protons ($I_{d\ at\ 0h}$, peak d: 2.18 ppm, 2 H) of initial 1-hexyne content and double bond protons of, possibly present, 1-hexene ($I_{a\ at\ 0h} + I_{c\ at\ 0h}$,

peak a: 5.8ppm, 1 H; peak c: 4.96-4.22 ppm, 2 H) and *n*-hexene isomers ($I_{b\ at\ 0h}$, peak b: 5.44-5.37 ppm , 2 H), respectively. Using these resonance peak integrations, the percent initial and total unsaturation content in the samples collected during the hydrogenation/isomerization reaction was calculated using Equation 2.10-2.11, respectively.

$$\%\ \text{initial unsaturation} = \left(\frac{I_{d\ at\ 0h}}{2} + \frac{I_{a\ at\ 0h} + I_{c\ at\ 0h}}{3} + \frac{I_{b\ at\ 0h}}{2}\right) * 100 \qquad 2.10$$

$$\%\ \text{total unsaturation} = \left(\frac{I_d}{2} + \frac{I_a + I_c}{3} + \frac{I_b}{2}\right) * 100 \qquad 2.11$$

See below for a schematic representation of the chemical structures of 1-hexyne, 1-hexene, and *n*-hexene isomers with annotated protons used in these equations.

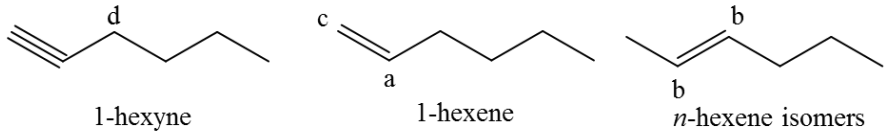

1-hexyne 1-hexene *n*-hexene isomers

The percent yield of isomerization products, 1-hexene and *n*-hexene isomers, were determined from the resonance peak integrations of their vinyl protons ($I_a + I_c$, and I_b, respectively) over the percent initial unsaturation content calculated using Equation 2.12-2.13, respectively. The percent yield of hexane, representing completely hydrogenated 1-hexyne and hexenes, was calculated by subtracting the percent initial and total unsaturation present in the samples collected during the reaction using Equation 2.14. Finally, the percent residual amount of 1-hexyne was determined from the resonance peak integration of secondary protons adjacent to the triple bond (I_d) over the initial content of unsaturated substrates (1-hexyne, 1-hexene, and *n*-hexene isomers) calculated using Equation 2.15.

$$\% \text{ 1-hexene} = \left[\frac{\left(\frac{I_a + I_c}{3} \right)}{\left(\frac{I_{d\ at\ 0h}}{2} + \frac{I_{a\ at\ 0h} + I_{c\ at\ 0h}}{3} + \frac{I_{b\ at\ 0h}}{2} \right)} \right] * 100 \qquad 2.12$$

$$\% \text{ n-hexene amount} = \left[\frac{I_b/_2}{\left(\frac{I_{d\ at\ 0h}}{2} + \frac{I_{a\ at\ 0h} + I_{c\ at\ 0h}}{3} + \frac{I_{b\ at\ 0h}}{2} \right)} \right] * 100 \qquad 2.13$$

$$\% \text{ hexane} = \text{initial} - \text{total unsaturation} \qquad 2.14$$

$$\% \text{ residual 1-hexyne} = \left[\frac{I_d/_2}{\left(\frac{I_{d\ at\ 0h}}{2} + \frac{I_{a\ at\ 0h} + I_{c\ at\ 0h}}{3} + \frac{I_{b\ at\ 0h}}{2} \right)} \right] * 100 \qquad 2.15$$

Determination of the product yield in Pd(II) encapsulated SPE-NP-catalyzed Heck coupling reactions of *n*-butyl acrylate (BA) and iodobenzene (IBz) was based on ^{1}H NMR integration of the resonance signals arising from analogous vinyl protons of the excess reactant (1.5 X molar excess), BA (peak A, 6.21-6.18 ppm, 1 H), and the coupling product (peak a, 6.26-6.22 ppm, 1 H). ^{1}H NMR peak integrations were normalized by specifying 2 H as the integration for the combined resonance peaks B (doublet, 4.03-4.00 ppm, 2 H) and b (doublet, 3.95-3.98 ppm, 2 H). See below a schematic representation of the Heck reaction for the annotation of theses protons on their chemical structures.

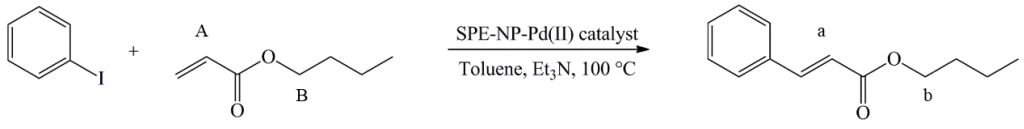

BA conversion was determined by the increase in the integration of the resonance signal arising from the vinyl proton of yielded product (I_a) divided by the combined integration for the resonance peaks of vinyl proton of unreacted BA (I_A) and the final product (I_a). The product yield was then calculated simply by multiplying the BA conversion by its molar excess factor of 1.5 using Equation 2.16.

$$\text{Iodobenzene conversion} = \left(\frac{I_a}{I_a + I_A}\right) * 1.5 \qquad 2.16$$

2.3.3 Gas Chromatography with Flame Ionization Detector

All gas chromatography (GC) samples were prepared by diluting 200 μL of the reference sample or reaction samples with 1000 μL of chloroform (used as the elution solvent). GC measurements were carried out on a Varian CP-3800 Gas Chromatograph system equipped with a Varian CP-8400 Autosampler, a Varian 1170 injector, and a Flame Ionization Detector (FID). The GC column used was an Rtx-5 (30 m x 0.32 mm ID, film composition = 5 % diphenyl-95 % dimethyl polysiloxane, film thickness = 0.25 μm) manufactured by Restek. Ultra-high purity He and N_2 used as carrier gas in the GC measurements were purified by passing through gas-clean moisture, oxygen, and charcoal columns. The following GC program conditions were used for all measurements:

- Total gas flow: 30 mL/min
- FID detector temperature set to 280 °C
- 5 μL samples were injected into a vaporisation port set to 260 °C
- Oven temperature program:
    1) Column temperature was held at 35 °C for 3.6 min;
    2) Column temperature was ramped from 35 to 100 °C at 20 °C/min;
    3) Followed by ramping from 100 to 280 °C at 50 °C/min; and
    4) Final column temperature held at 280 °C for 10 min.

NBD conversion (x_{NBD}) results were calculated using Equation 2.17 by subtracting the GC elution peak area of unreacted NBD monomer at t_{NBD} ($A_{NBD\ at\ tNBD}$) from the initial amount of NBD ($A_{NBD\ at\ 0\ h}$). Areas for the GC elution peaks at different t_{NBD} were normalized by the GC elution peak area of BrBz (internal standard), which was added in equimolar amounts to initial NBD.

$$x_{NBD} = \left(\frac{A_{NBD\ at\ 0\ h}}{A_{BrBz\ at\ 0\ h}} - \frac{A_{NBD\ at\ tNBD}}{A_{BrBz\ at\ tNBD}}\right) * 100 \qquad 2.17$$

2.3.4 Dynamic Light Scattering

A Malvern Zetasizer Nano S90 Dynamic Light Scattering (DLS) detector was used to measure the particle size of freshly ultrasonicated SPE-NPs solutions (with concentrations ranging from 1 to 10 mg/mL in THF) in aperture glass cuvettes. A typical standard operating procedure was setup by specifying the dispersant as THF at 25 °C, material criteria set to polystyrene latex (RI of 1.59, absorption of 0.010), the attenuator set to automatic, and laser positioned at the centre of the cuvette (4.65 mm). The intensity of scattered light detected at a 90-degree angle was used to measure the particle size and size distributions, which were calculated with Stoke-Einstein Equations based on the diffusion of particles moving by Brownian motion. A schematic representation of the dynamic light scattering apparatus showing the principal arrangement of the various instrument components is illustrated in Figure 2.3.

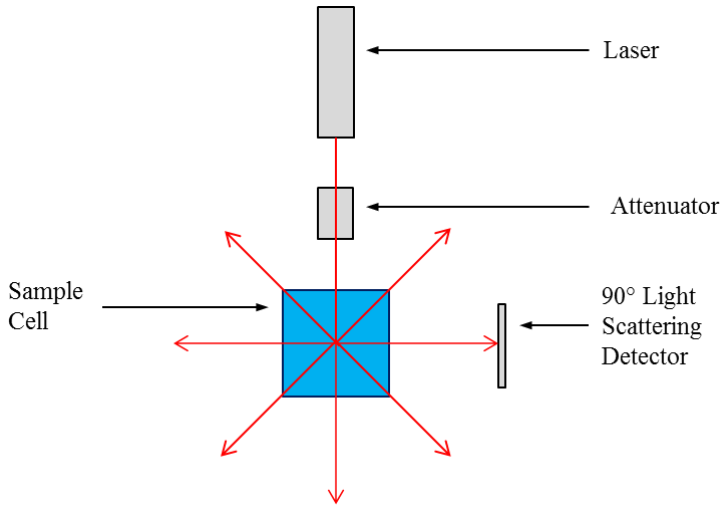

Figure 2.3 Schematic representation of a typical DLS setup displaying the principle arrangement of the laser, sample cell, and 90° light scattering detector.

2.3.5 Transmission Electron Microscopy

Transmission electron microscopy (TEM) and scanning tunnelling microscopy (STM) imaging of SPE-NPs produced in Runs 17 (constructed with HBPE arms) and Runs 20 (constructed with LBPE arms) were carried out with a JEOL 2010F Transmission Electron Microscope operated at 200 keV. Polymer samples were dissolved in THF to a concentration of 0.1-0.5 mg/mL and ultrasonicated overnight. TEM samples were prepared by adding one or more drops of freshly sonicated SPE-NP solution onto a 400-mesh Cu-grid coated with silicon monoxide and immediately dried under a hot lamp. Given the hydrophobicity of PE, we selected TEM grids with a hydrophilic coating surface in order to better preserve the macromolecular shape of the SPEs. A technician at the Canadian Centre collected TEM and STM images for Electron Microscopy at McMaster University in Hamilton, Ontario, Canada. Figure 3.19 shows TEM images of as produced SPE-NPs synthesized in Runs 17 (a, b, c) and in Runs 20 (d, e) at different magnifications. Image (f) shows an STM characterization of a single SPE-NP produced in Runs 20).

2.3.6 Atomic Force Microscopy Imaging and Particle Analysis

AFM characterization was done in tapping mode using a Bruker Multimode AFM IIID equipped with a Veeco TESPA Model cantilever tip (0.01-0.025 Ohm-cm Antimony dipped silicon, force constant: 20-80 N/m). Polymer samples were dissolved in THF at room temperature under sonication overnight at concentrations of ca. 0.1-0.5 mg/mL. The following morning, polymers were deposited onto a freshly cleaved mica sheet by submerging it in the polymer solution overnight. Upon removal, the excess solvent was quickly removed by dabbing the fine edge of the mica sheet on a tissue paper and dried under a hot lamp before imaging.

Typically, the cantilever raster scans the mica surface in tapping mode at a scan rate of 1.49 Hz with 512 samples per line in order to obtain high-resolution images. Based on sample properties (e.g., softness, separation between nanoparticles, etc.) other parameters including the amplitude set point, drive frequency, and drive amplitude were adjusted accordingly with typical ranges of 0.4-1.5 V, 362-372 kHz, and 8-20 mV, respectively. The 2010 Veeco 1.2 NanoScope Analysis software was used for image optimization and statistical nanoparticle analysis. Figures 3.20-22 display the 2D & 3D tapping mode AFM images and statistical particle analysis of SPE-NPs produced in Runs 17, 5, and 20.

CHAPTER 3: Arm-First Pd-Diimine–Catalyzed Synthesis of Star Polyethylene Nanoparticles

The arm-first synthesis of SPE-NPs described in this thesis entails four straightforward steps:

(1) Synthesis of living PE arms by ethylene living polymerization catalyzed with cationic acetonitrile Pd-diimine catalyst (**1**, in Figure 3.1) for a desired polymerization time
(2) Addition of NBD as the cross-linking agent directly into the ethylene polymerization system for Pd-catalyzed arm extension for a specified reaction time to synthesize PE-*b*-PNBD block copolymers bearing pendant reactive double bonds in the short PNBD segment
(3) Precipitation of the polymer product in acidified methanol (2 vol.% of HCl)
(4) Drying of the polymer precipitate at high temperature (i.e., 70, 100, or 120 °C) under vacuum to produce SPE-NPs.

Figure 3.1 illustrates the four-step synthetic procedure. In the synthesis, the topology and size of the PE arms are controlled in this first step by tuning the polymerization condition (i.e., ethylene pressure and polymerization time) following chain-walking mechanism of Pd-diimine catalysts. SPEs constructed with multiple hyperbranched (HBPE) or linear-but-branched (LBPE) arms joined at central cross-linked PNBD core are produced at low (1 atm) and high (27 atm) ethylene pressure, respectively, in the first step.

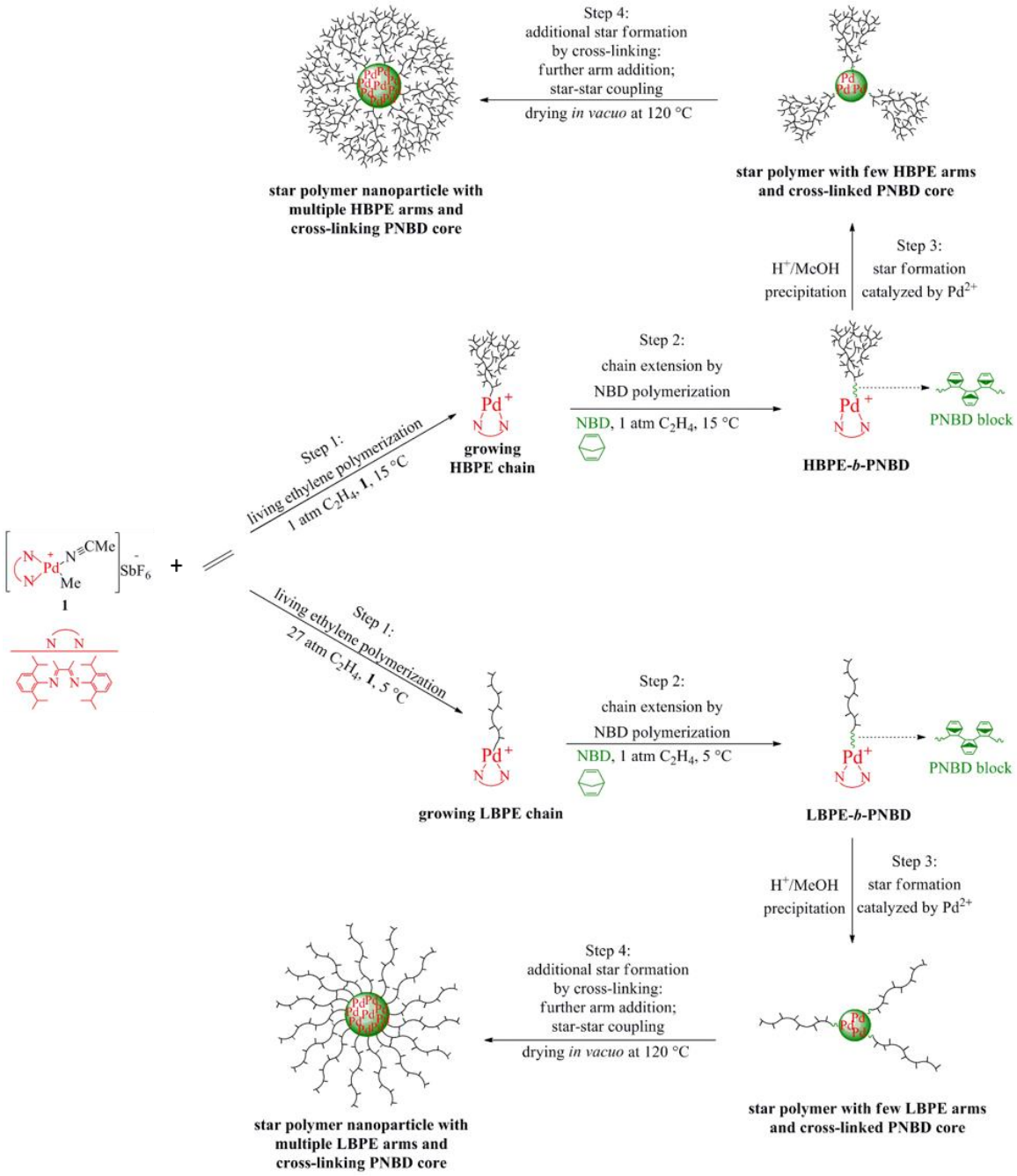

Figure 3.1 Arm-first synthesis of SPE-NPs with HBPE or LBPE arms joined to central cross-linked PNBD cores via a four-step procedure.

The success of this convenient, simplistic Pd-catalyzed arm-first synthesis of SPE benefits from the valuable polymerization chemistry of NBD as a unique cross-linker in

the presence of the Pd-diimine catalyst, which was discovered during this research. In the second step, chain extension occurs by adding a short PNBD homopolymer block containing pendant norbornenyl double bonds from the PE block through Pd-diimine catalyzed mono-vinyl insertion polymerization of NBD. In the third and four steps, star formation occurs through rapid Pd-catalyzed inter- and intra-molecular cross-linking reactions of the pendant vinyl groups in the PNBD sequence of PE-*b*-PNBD block copolymers to render large unimolecular SPE-NPs. In the following sections of this chapter, the mechanism of star polymer formation in the synthesis (Section 3.1), and the effects of NBD-step reaction conditions (Section 3.2), PE arm topology and length (Section 3.3), precipitation conditions (Section 3.4), and melt-state drying conditions (Section 3.5) on star formation are discussed. The size and morphology of the as-produced SPE-NPs are investigated via DLS and direct TEM and AFM imaging (Section 3.6). Systematic investigations were conducted to examine the effects of important reaction parameters, including ethylene pressure, ethylene polymerization time (t_E), NBD to catalyst **1** molar ratio ($[NBD]_0/[\mathbf{1}]_0$), NBD-step reaction time (t_{NBD}), acidified vs. non-acidified methanol precipitation (H^+/MeOH vs. MeOH PPT), drying temperature, and drying time (t_d), on star polymer parameters, including star yield, average arm number (f_n), average molecular weight (M_n, M_w), and size (D_h).

3.1 Effects of Synthetic Steps 1-4 on Star Formation

To study the mechanism of star formation in this synthetic procedure, we performed one run (Run 17) where the polymer molecular weight development in the four-step process was monitored. Figure 3.2 shows the GPC elution curves (obtained from DRI detector) for the as-produced polymer samples at every step of the star polymer synthesis.

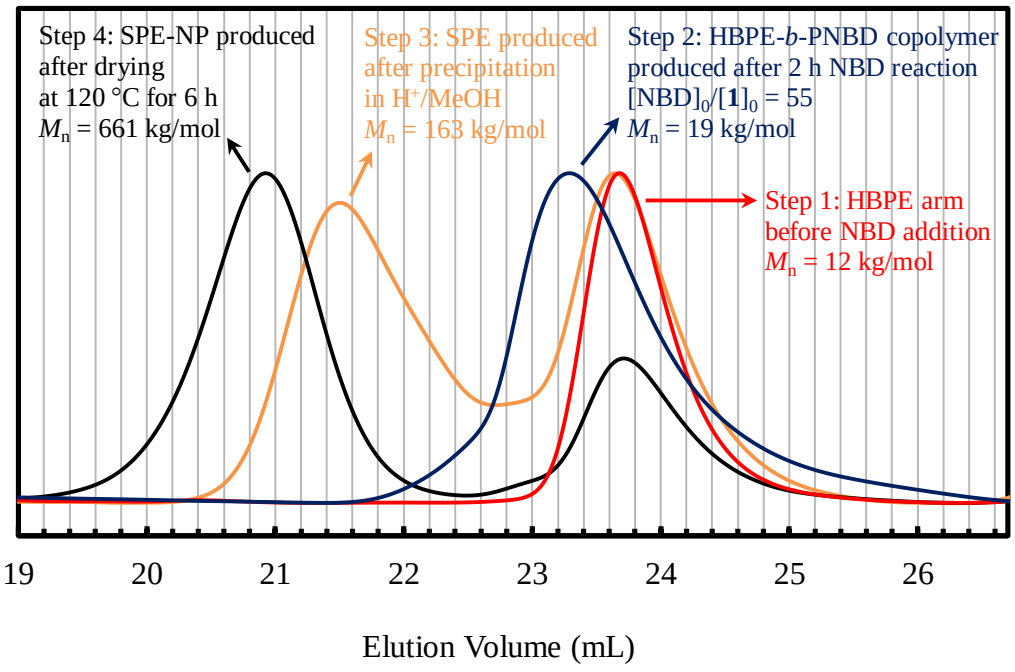

Figure 3.2 GPC elution curves obtained from DRI detector in THF at 33 °C of polymers produced in every step of the SPE-NP synthesis in Run 17, including HBPE arms in Step 1, HBPE-*b*-PNBD block copolymers in Step 2, SPEs in Step 3, and SPE-NPs in Step 4. Reaction conditions for Run 17: living C_2H_4 polymerization step was carried out using 0.1 mmol of **1** in 50 mL of ClBz at C_2H_4 pressure of 1 atm/15 °C for t_E = 1 h and t_{NBD} = 2 h.

In the first step, living ethylene polymerization was catalyzed with **1** at 1 atm/15 °C for t_E = 1 h. The polymer produced at the end for the first step (HBPE arm) was narrow-distributed with M_n = 12 kg/mol and PDI = 1.01. In the second step, NBD was added at $[NBD]_0/[\mathbf{1}]_0$ = 55 and the reaction was carried out for t_{NBD} = 2 h. A small increase in M_n = 19 kg/mol with slightly higher PDI = 1.20 was observed with the polymer collected at the end of 2nd step compared to the HBPE arm. Given the minor increase in M_n, star formation should be non-existent at this point.

Subsequently, the polymer product was precipitated via centrifugation at 5000 rpm for about 10 min in H^+/MeOH followed by drying *in vacuo* at 120 °C for 6 h. Both the precipitated polymer and the dried polymer had bimodal GPC elution traces, typical for

star polymers produced via the arm-first method [43, 85-86] (Figure 3.2). Both traces have a clearly separated high molecular weight peak deemed as the produced SPE-NP (M_n = 163 kg/mol and 661 kg/mol, respectively, and low PDIs of 1.28 and 1.16, respectively) and a low molecular weight peak which overlaps closely with the elution trace for the HBPE arm used in this star polymer construction.

Comparing the GPC elution traces, we can clearly see the SPE peak of the dried polymer sample shifted to lower elution volumes (higher M) and the relative intensity of its HBPE arm peak was significantly decreased compared to the precipitated sample. The star yield, determined from the area percentage of star polymer to overall polymer product using Equation 2.2, increased significantly from 51% for the precipitated polymer to 71 % for the dried polymer. Furthermore, the number-average arm number (f_n) per star, calculated from the ratio of the M_n of the star polymer to its PE arm (Equation 2.3), also increased drastically from 14 for the precipitated polymer to 57 for the dried polymer. These GPC evidences confirm the occurrence of star formation in Steps 3 and 4.

In comparison to the SPEs produced via the tandem two-step arm-first approach (combining Pd-catalyzed living ethylene polymerization to produce LBPE macroinitiators/arms subsequently joined by core cross-linking ATRP of DVB), this arm-first approach is much more convenient, simple, and fast. To produce narrowly distributed SPEs (i.e., PDI ≈ 1.05-1.80) of high M (i.e., ≥ 500 kg/mol), the former method requires long (i.e., 22 h) and tedious ATRP reaction of its DVB cross-linker, whereas the latter only requires a short NBD-step reaction (i.e., 2 h) followed by conventional polymer purification processes.

The fast intermolecular and intramolecular cross-linking reactions responsible for the formation of large SPE-NPs is believed to be catalyzed by ligandless or NBD-ligated Pd^{2+} catalysts [87-88] generated *in situ* during the H^+/MeOH PPT step by which the acidified-diimine ligand of catalyst **1** is removed. Fast core cross-linking reactions may also be catalyzed via radicals generated during the high temperature-drying step.

3.2 Effects of Norbornadiene Concentration and Reaction Time on Star Formation

While the first step of "living" ethylene polymerization has been well demonstrated, the second polymerization step involving NBD has not been previously studied and reported in the literature. A thorough understanding of NBD polymerization with Pd-diimine catalysts is thus important to elucidate the star formation mechanism in this arm-first synthesis of SPE. It was often noted in the polymerization run undertaken at 1 atm of ethylene pressure that, within few minutes following the addition of NBD ($[NBD]_0/[\mathbf{1}]_0$ = 53-326) in the second step, ethylene consumption rate, monitored through a bubbler, dropped quickly to a complete stop. With this observation, it is reasoned that ethylene was not consumed during the second step, which appeared to involve only the homopolymerization of norbornene.

NBD has been previously reported to undergo alternating copolymerization with CO by Pd-diimine catalysts [89-90], and other Pd(II) catalysts [89-93] to produce low-*M* alternating copolymers. Meanwhile, it was also copolymerized with ethylene using several homogeneous metallocene/MAO catalyst systems.[94] However, Pd-diimine catalysts have not yet been reported for NBD homopolymerization or copolymerization with ethylene.

3.2.1 Pd-Diimine-Catalyzed Norbornadiene Homopolymerization and Copolymerization with Ethylene

To verify the above hypothesis, two single-step NBD polymerizations (Run 33 and 34) were carried out with $[NBD_0]/[\mathbf{1}]_0$ = 327 at 20 °C in the absence (1 atm N_2) and presence of ethylene (1 atm C_2H_4), respectively. Following a reaction time t_{NBD} = 1 h, the solvent and unreacted monomer were evaporated via vacuum at room temperature. The resulting polymer products in both runs were visually and physically identical, consisting of brittle yellow-coloured crystal-like powders. Polymer samples of each run were dissolved in $CDCl_3$ for ^1H NMR analysis.

From Figure 3.3, the ^{1}H spectrum of the polymer produced in the presence of ethylene has no clear resonance peak attributable to incorporated ethylene units and is nearly identical to the spectrum of the NBD homopolymer (PNBD) produced in the absence of ethylene. In both spectra, the resonance peaks c (5.8-6.4 ppm, 2 H), b (3.0-2.2 ppm, 2 H), and d (0.9-1.9 ppm, 3 H) arise from pendant endocyclic vinyl and bridge head protons, respectively, of the norbornene repeat units and have similar integration areas. Peak **a** (0.9-1.9 ppm, 3 H) is assigned to the backbone protons and the bridge protons of the NBD homopolymer chain. These results indicate that NBD has a much greater binding affinity to the Pd^{2+} active site of **1** than ethylene. It also confirms that **1** polymerizes NBD via only one of its endocyclic double bonds without involving double bond, leaving the other pendant within the polymer chain. The pendant norbornene-type double bonds are not copolymerizable either in the presence of NBD.

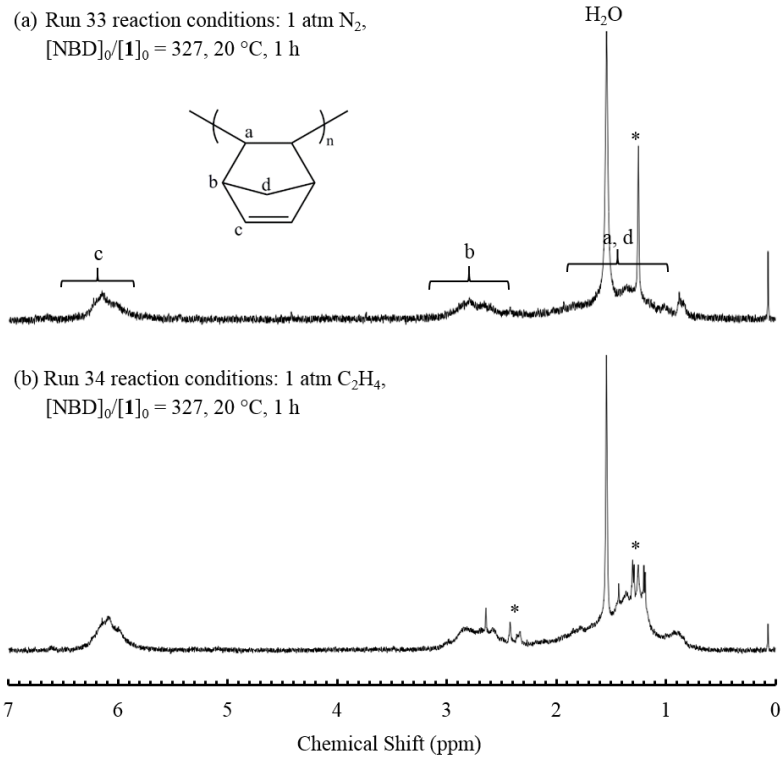

Figure 3.3 ^{1}H NMR (500 MHz) spectrums of NBD homopolymers synthesized by **1** under N_2 (1 atm) in Run 33 (a) and C_2H_4 (1 atm) in Run 34 (b). Peak at 1.5 ppm arises from residue H_2O present in the $CDCl_3$ solvent and the peaks marked with an asterisk (*) arise from residual catalyst **1**.

The PNBD products from the control runs are soluble in solvents like chloroform and THF. From GPC characterization, the polymers have low molecular weight since their elution peak overlaps significantly with solvent peaks. This makes the molecular weight determination through GPC difficult. Upon washing with acidified methanol and vacuum drying (at 120 °C, <1 mmHg, for 6 h), both PNBD polymers produced in the two runs became completely insoluble in chloroform or THF. Consistent with the star formation observed above in the precipitation and drying steps for SPE synthesis, this indicates the occurrence of rapid intermolecular cross-linking of the pendant norbornene type double bond in the polymer. Traditionally, cyclic norbornene-type monomers can be polymerized/oligomerized through catalytic vinyl addition, ring-opening metathesis, radical, or cationic mechanism. While catalytic vinyl addition and ring-opening metathesis can render high-molecular-weight polymers, radical and cationic mechanisms only give rise to oligomers.[95] The latter three mechanisms can be ruled out for the cross-linking here, given the absence of the metathesis, radical or cationic initiating species in the precipitation and drying steps. Here, the cross-liking should be facilitated via the catalytic vinyl addition mechanism by the residual catalytic Pd(II) species trapped within the polymers. Cationic Pd(II)-based catalysts have been extensively used in the vinyl polymerization of norbornene at high activities.[95] Given the heterogeneous nature of the polymerization system, the precise structure of the responsible catalytic species here cannot be exclusively determined. It is speculated that the reactive species responsible for the NBD polymerization are ligandless or NBD-ligated cationic Pd(II) species which are generated when the diimine ligands are protonated and washed out during the acidic condition of the polymer precipitation step. NBD has been previously demonstrated to act as a ligand for various Pd(II) compounds.[96] Following the loss of the diimine ligand, NBD may coordinate with the cationic Pd(II) species to render NBD-ligated catalytic species during the precipitation step.

3.2.2 Pd-Diimine–Catalyzed Norbornadiene Homopolymerization via *in situ* ^{1}H NMR

Polymerization kinetics were investigated in Runs 42, 44, 45, and 31 via *in situ* ^{1}H NMR study of NBD homopolymerization catalyzed with **1** at 20 °C over t_{NBD} = 3 h. Four $[NBD]_0/[\mathbf{1}]_0$ molar ratios of 55, 109, 218, and 326, respectively, similar to those used in SPE synthesis, were used in these runs. Figure 3.4 shows the ^{1}H spectrum at t_{NBD} = 3 h in Run 31 conducted at $[NBD]_0/[\mathbf{1}]_0$ = 326. Resonance peaks C (singlet, 6.8 ppm, 4H), B (singlet, 3.6 ppm, 2 H), and D (singlet, 2.0 ppm, 2 H) belong to the unreacted NBD monomer whereas peaks **c** (5.8-6.3 ppm, 2 H) and **b** (2.6-3.1 ppm, 2 H), and **a** and **d** (1.0-1.7 ppm) arise from the protons of the repeat units in the NBD homopolymer.

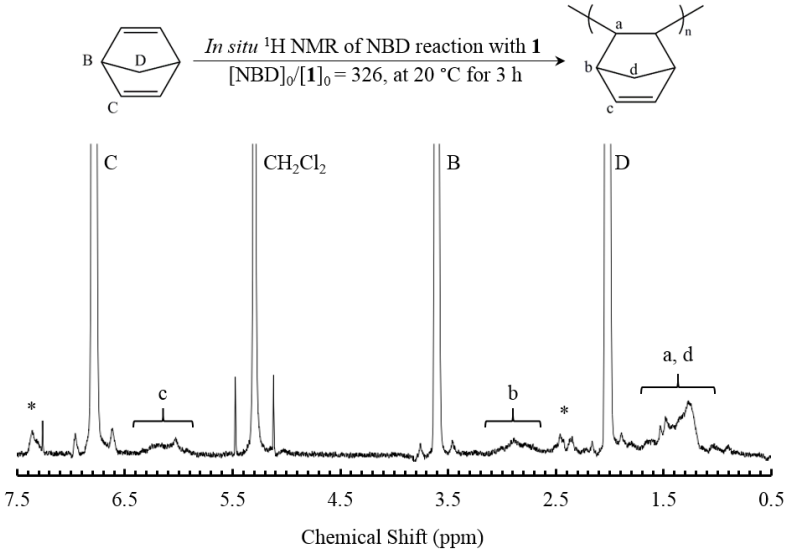

Figure 3.4 *In situ* ^{1}H NMR spectrum (500 MHz) of NBD homopolymerization catalyzed with **1** for 3 h (Run 31). Peaks marked with an asterisk (*) (at around 2.5 and 7.4 ppm) arise from catalyst **1**. CH_2Cl_2 (singlet, 5.3 ppm, 2 H) was added into the reaction in equimolar amount to the initial NBD as an internal standard.

NBD conversion data were calculated from the integration areas of peak C for unreacted NBD and peak c for incorporated NBD according to Equation 2.4. The

conversion data are summarized in Table 3.1. For all four runs, we observed slow and low NBD conversions only ranging from $x_{NBD} \approx 1$ %, immediately after NBD addition, up to $x_{NBD} \approx 7$ % after $t_{NBD} = 3$ h. The kinetic plots of x_{NBD} as function of t_{NBD} for Runs 42, 44, 45, and 31 are compared in Figure 3.5. Following the addition of NBD, x_{NBD} show a slow increase with only small final conversions in the range of 5.3–7.3% reached at $t_{NBD} = 3$ h in all runs despite at their very different $[NBD]_0/[\mathbf{1}]_0$ ratios.

Table 3.1. Conversion Data in Norbornadiene Homopolymerization via *in situ* ^{1}H NMR Study[a]

		Percent NBD conversion (x_{NBD}) at different t_{NBD} (h)[b]								
Run	$[NBD]_0/[\mathbf{1}]_0$	0	0.25	0.5	0.75	1	1.5	2	2.5	3
42	55	1.3	2.7	3.7	6.3	–	6.4	6.9	6.9	7.3
44	109	0.9	3.1	3.1	3.1	4.8	4.8	4.8	5.7	5.3
45	218	1.3	1.7	2.6	3.9	3.9	4.3	5.2	6.0	6.0
31	326	1.6	4.0	–	3.9	–	5.4	–	6.1	5.4

[a] Reaction conditions: $[NBD]_0/[\mathbf{1}]_0$ listed above were catalyzed by 0.011 mmol of **1** in 1 mL of $CDCl_3$ at 20 °C and monitored during NBD reaction times (t_{NBD}) listed in the table. [b] Percent conversion of NBD (x_{NBD}) was calculated from ^{1}H NMR spectra using Equation 2.4.

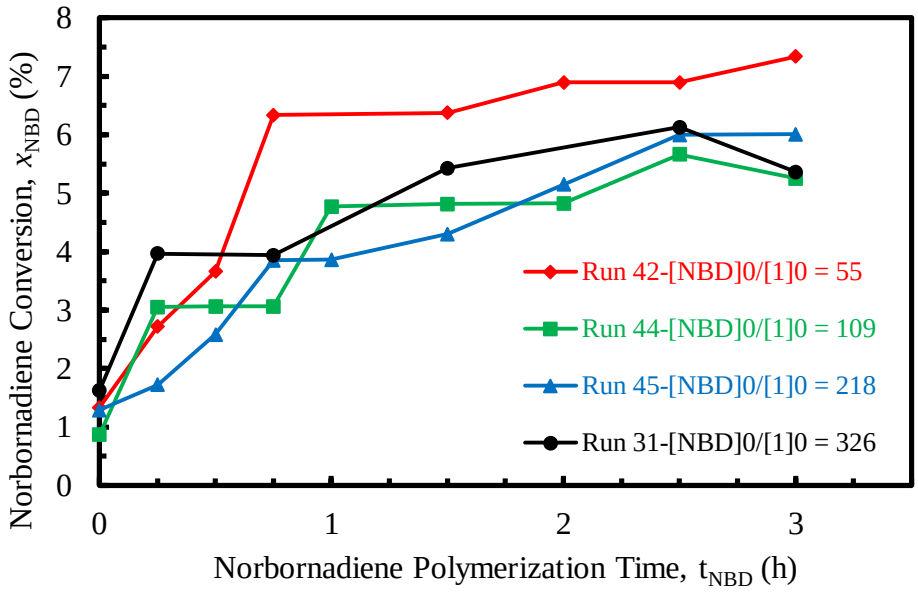

Figure 3.5 Kinetic plots of *in situ* ^{1}H NMR study of NBD homopolymerizations catalyzed by **1** at different $[NBD]_0/[\mathbf{1}]_0$.

3.2.3 Norbornadiene Conversion in Pd-Diimine-Catalyzed Synthesis of Star Polyethylene Nanoparticles

An additional kinetic study was conducted in parallel to directly determine NBD conversion in the second step of SPE-NP synthesis. Run 53 was carried out with 0.1 mmol of **1** at 1 atm ethylene pressure and 15 °C for t_E = 1 h followed by the addition of $[NBD]_0/[\mathbf{1}]_0$ = 218, along with an equimolar amount of bromobenzene (BrBz) as internal GC standard. Samples were collected periodically at t_{NBD} = 0.25, 0.5, and 1 h and analyzed with GC to determine x_{NBD}. The control Run 60 was also carried out as a single-step NBD homopolymerization catalyzed with 0.1 mmol of **1** with $[NBD]_0/[\mathbf{1}]_0$ = 336 (also in the presence of equimolar amount of BrBz) under 1 atm N_2 pressure at 15 °C for 1 h. NBD conversion data were calculated according to Equation 2.17 from the area under the GC elution peak for unreacted NBD monomer and the GC elution peak area for the NBD fed at the beginning of the reaction. The conversion data for both runs are summarized in Table

3.2. Figure 3.6 shows x_{NBD} as a function of t_{NBD} in both runs. A maximum $x_{NBD} \approx 4$ % was reached in Run 53 as opposed to 11 % in the control NBD homopolymerization of Run 60. These low conversion data are in good agreement with those determined through *in situ* NMR study. Meanwhile, the higher conversion obtained in Run 60 should result from the absence of the bulky HBPE block, which limited the diffusion of NBD in Run 53.

Table 3.2. Norbornadiene Conversion Data in Norbornadiene-Reaction Step of the Star Polyethylene Synthesis [a] and Norbornadiene Homopolymerization [b] Catalyzed with **1**

Run	Catalyst **1** (mmol)	NBD amount (mmol)	$[NBD]_0/[\mathbf{1}]_0$	t_{NBD} (h)	x_{NBD} [c] (%)
53	0.100	21.7	218	0.00	0.0
				0.25	2.4
				0.50	3.7
				1.00	2.6
60	0.099	33.3	336	0.00	0.0
				0.25	7.1
				0.50	8.3
				1.00	10.7

[a] SPE-NP synthesis (Run 53): ethylene reaction step was carried out at 1 atm C_2H_4/15 °C for 3 h in 50 mL ClBz and NBD reaction step conditions are listed in table. [b] NBD Homopolymerization conditions (Run 60): 1 atm N_2/15 °C in 20 mL of ClBz. [c] Percent conversion of NBD (x_{NBD}) was calculated from GC results using Equation 2.17.

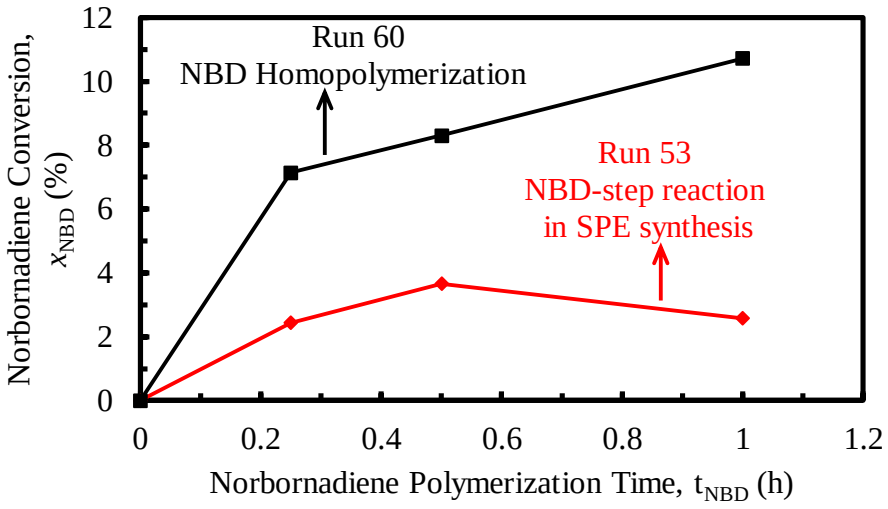

Figure 3.6 NBD conversion curves of the NBD polymerization step in SPE-NP synthesis (Run 53) and NBD homopolymerization (Run 60).

3.2.4 Effect of $[NBD]_0/[1]_0$ Ratio and t_{NBD} on Star Polyethylene Formation

On the basis of the above mechanistic study on NBD homopolymerization runs, we can conclude that the second block in the block copolymer produced via chain extension in the second step of the SPE synthesis should contain a PNBD sequence. Given the low NBD conversion in the second step, the PNBD sequence should be short but effective for star formation via cross-linking. The SPE star polymers synthesized in this method are thus constructed with a shell of PE arms joined together to a cross-linked PNBD core. The length of the short NBD block should be critical to the structural parameters of the resulting SPEs (such as average arm number, average molecular weights, etc.). Despite the low NBD conversions at different $[NBD]_0/[\mathbf{1}]_0$ ratios, it is hypothesized that the length of the PNBD block might be related to the $[NBD]_0/[\mathbf{1}]_0$ ratio and t_{NBD}. A study on the effects of $[NBD]_0/[\mathbf{1}]_0$ ratio and t_{NBD} on the structural parameters of the resulting SPEs was thus performed. Runs 16, and 4–6 (see Tables 3.3 and 3.4) were carried out with the first step undertaken at identical conditions (1 atm/15 °C, for t_E = 3 h) to produce HBPE arms of similar length (M_n = 28, 26, 29, and 27 kg/mol, respectively, and PDI ≈ 1.07). In step two, NBD at different $[NBD]_0/[\mathbf{1}]_0$ molar ratios of 53, 106, 220, and 326, respectively, was

added into the polymerization mixtures of these runs. Polymer samples were then collected periodically during the 2nd-step reaction (t_{NBD} = 0.25–4 h), precipitated in H^+/MeOH, and dried *in vacuo* at 120 °C for 6 h, and were characterized by triple-detection GPC.

Figure 3.7 shows GPC elution traces (recorded with DRI detector) of the polymer samples collected at t_{NBD} = 0.25, 1, 2, and 4 h for all runs. All polymer products show the characteristic bimodal elution traces with a high-*M* peak (i.e., low elution volume, 19.0–21.5 mL) corresponding to the SPEs and a low-*M* peak belonging to unreacted HBPE arms (elution volume = 21.5–24.5 mL). The absolute *M* data including M_n, M_w, and PDI were obtained from the three-angle (45°, 90°, and 135°) LS detector using a dn/dc value of 0.072 mL/g for olefins in THF. At each given $[NBD]_0/[1]_0$, SPEs with high *M* and narrow distribution (M_n = 594–735 kg/mol; PDI ≈ 1.08) were produced even at a short t_{NBD} of 0.25 h. Extension of t_{NBD} to 1 h only led to slight but noticeable improvements in M_n of the SPEs to the range of 810–952 kg/mol (PDI ≈ 1.11). Further extension of t_{NBD} up to 4 h, however, only rendered marginable changes in the M_n values. These results indicate that t_{NBD} in the second step does not exert significant effects on the structural parameters of the resulting SPEs. In sharp contrast, SPEs produced via the tandem-two step method required much longer DVB reaction times as high as 22 h, in order to reach similar star polymer *M*.[43] Comparing the SPEs produced at $[NBD]_0/[\mathbf{1}]_0$ ratios but at a fixed t_{NBD}, their M_n values are also very similar without clear effects resulting from the change in the $[NBD]_0/[\mathbf{1}]_0$ ratio.

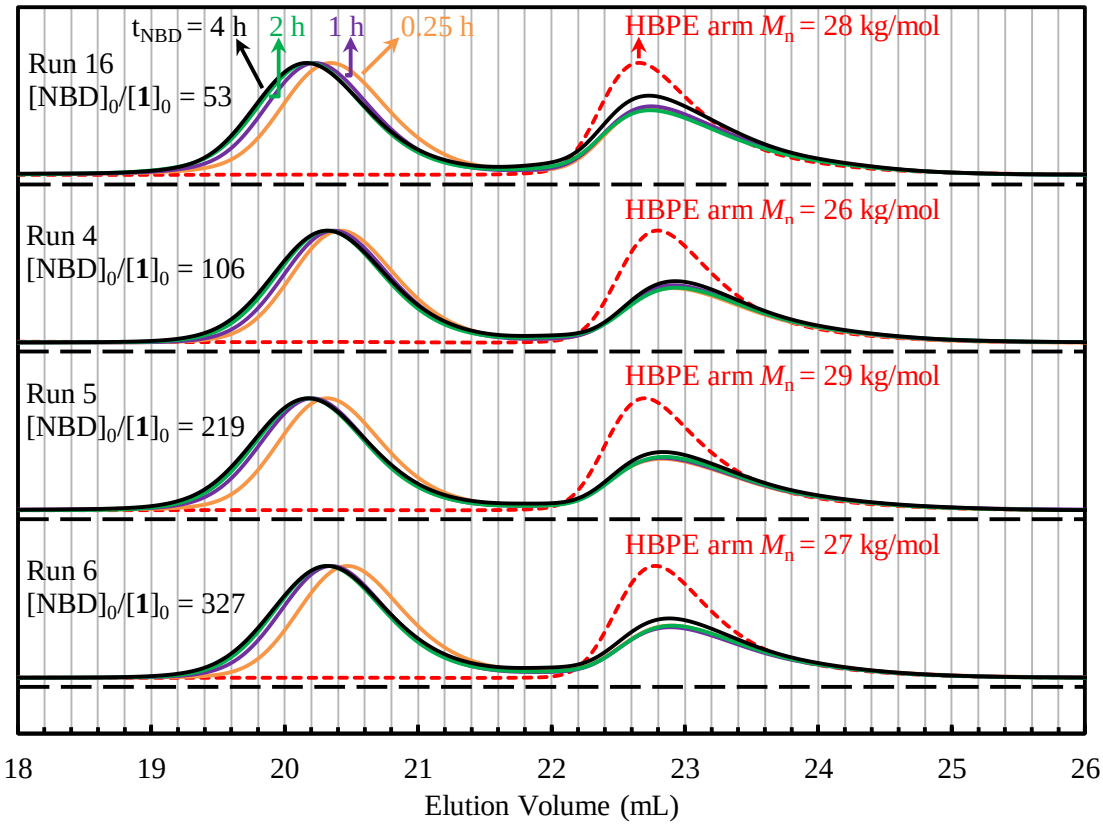

Figure 3.7 GPC elution traces (obtained from DRI detector in THF at 33 °C) of the polymer products obtained in Runs 16, and 4–6 carried out at different $[NBD]_0/[\mathbf{1}]_0$ and t_{NBD} in the second step of SPE synthesis. See Tables 3.3 and 3.4 for detailed polymerization conditions and GPC results of the polymers.

Figure 3.8 shows the dependencies of number-average arm number (f_n) and star yield as a function of t_{NBD} for the four runs. Star yields were calculated using Equation 2.2 from the area fraction of the SPE peak in the GPC elution curve recorded with the DRI detector in GPC characterization. Although the cross-linked PNBD core size and M_n are unknown, we know that NBD conversion during the 2nd step of the SPE synthesis is in the low range of 4–7%. We can thus reasonably assume that the core size is very small compared to the large HBPE shell.[43] Hence, the f_n per star was calculated using Equation 2.3 as the ratio of the M_n of the star polymer to the M_n of its constituting HBPE arm.

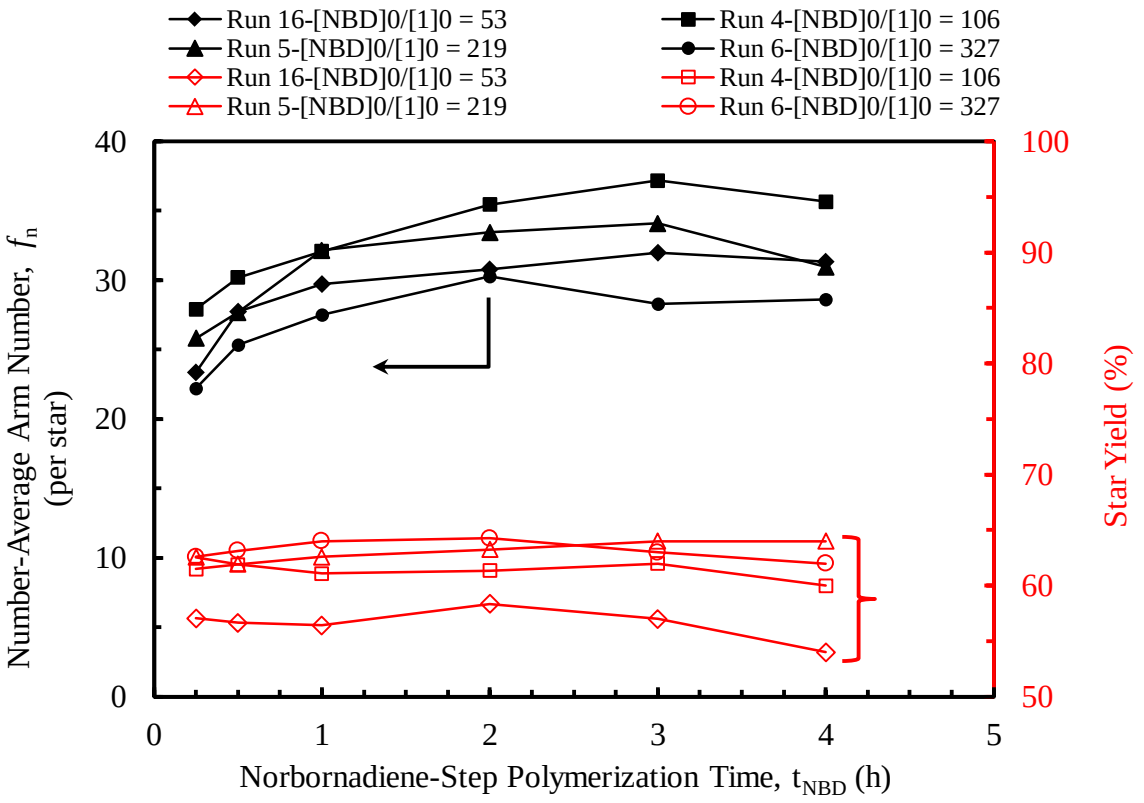

Figure 3.8 Effects of NBD-step polymerization parameters, $[NBD]_0/[\mathbf{1}]_0$ and t_{NBD}, on the number-average HBPE arm number (f_n) of the produced SPE-NPs and the resulting star yield. Reaction conditions and results are listed in Tables 3.3 and 3.4.

Following a similar trend in the M_n values of SPEs, f_n increase from 22 to 37 in response to the increase of t_{NBD} from 0.25 h to 4 h, but with no clear trend resulting from the change in the $[NBD]_0/[\mathbf{1}]_0$ ratio. In all four runs, the star polymer yields were in the range of 54–64 % as t_{NBD} increased. Increasing the $[NBD]_0/[\mathbf{1}]_0$ ratio leads to a small but clear enhancement in star yield. In comparison to the higher yields (75–87%) obtained with SPE produced with LBPE arms/MIs joined together by cross-linker PDVB core in the tandem two-step arm-first approach, the relatively lower yields obtained herein are due to steric hindrance from the bulkier HBPE arms used to construct these star polymers.[43] However, the f_n values are similar in both types of SPEs, with f_n = 22–37 reached herein compared to f_n = 20–30 achieved in the other arm-first method. The high M_n and f_n obtained

herein proves that this one-pot method to SPE-NPs is very effective and much simpler compared to the other tandem two-step method.

Dilute solution properties of the core cross-linked SPEs produced in these runs, including weight-average intrinsic viscosity ($[\eta]_w$) and Mark-Houwink exponent (α), were determined with the viscosity detector in combination with the LS detector in triple-detection GPC characterization. These data are also summarized in Tables 3.3 and 3.4. According to the dependence of SPE's intrinsic viscosity ($[\eta]$) on the *M*, their star architecture can be confirmed. Despite their high *M*, the SPE's show low $[\eta]_w$ values, which are about 1.5–1.6 times the $[\eta]_w$ of the corresponding HBPE arms used in its synthesis (see $[\eta]_w$ ratio in Tables 3.3 and 3.4), which is characteristic of star polymers. [43, 45, 47]

Table 3.3. Effects of $[NBD]_0/[\mathbf{1}]_0$ Ratio and t_{NBD} on Star Polymer Formation [a] in Runs 16 and 4

	GPC results of HBPE arms							GPC results of SPE-NPs							
Run	t_E (h)	M_n (kg/mol)	M_w (kg/mol)	$[\eta]_w$ (mL/g)	PDI	$[NBD]_0/[\mathbf{1}]_0$	t_{NBD} (h)	Star yield [b] (%)	M_n (kg/mol)	M_w (kg/mol)	PDI	$[\eta]_w$ (mL/g)	$[\eta]_w$ ratio[c]	f_n [d]	α [e]
16	3	28	30	16.7	1.07	53	0.25	57	661	705	1.07	27.0	1.6	23	-0.18
							0.50	57	784	827	1.05	26.7	1.6	28	-0.17
							1.00	56	840	892	1.06	26.1	1.6	30	-0.22
							2.00	58	870	935	1.08	25.0	1.5	31	-0.16
							3.00	57	904	973	1.08	24.8	1.5	32	-0.18
							4.00	54	886	988	1.12	25.6	1.5	31	-0.18
4	3	26	31	16.8	1.09	106	0.25	62	682	723	1.06	24.6	1.6	28	-0.18
							0.50	62	737	787	1.07	25.9	1.5	30	-0.17
							1.00	61	784	837	1.07	26.2	1.6	32	-0.22
							2.00	61	866	935	1.08	25.4	1.5	35	-0.20
							3.00	62	908	995	1.10	25.5	1.5	37	-0.20
							4.00	60	871	974	1.12	25.5	1.5	36	-0.20

[a] SPE-NP reaction conditions: catalyzed by 0.1 mmol of **1**, 1 atm C_2H_4/15°C in 50 mL of ClBz, precipitated in H^+/MeOH, and dried 6 h *in vacuo* at 120 °C. [b] Star yield was calculated from the area percentage of star polymer to overall polymer product by fitting DRI curves using Equation 2.2. [c] $[\eta]_w$ ratio was calculated from $[\eta]_w$ SPE-NP and HBPE arm. [d] Arm number (f_n) was calculated from the M_n of SPE-NP and HBPE arm using Equation 2.3. [e] α is the Mark-Houwink exponent of the SPE-NPs.

Table 3.4. Effects of $[NBD]_0/[\mathbf{1}]_0$ Ratio and t_{NBD} on Star Polymer Formation [a] in Runs 5 and 6

	GPC results of HBPE arms							GPC results of SPE-NPs							
Run	t_E (h)	M_n (kg/mol)	M_w (kg/mol)	$[\eta]_w$ (mL/g)	PDI	$[NBD]_0/[\mathbf{1}]_0$	t_{NBD} (h)	Star yield [b] (%)	M_n (kg/mol)	M_w (kg/mol)	PDI	$[\eta]_w$ (mL/g)	$[\eta]_w$ ratio[c]	f_n [d]	α [e]
5	3	29	31	17.2	1.07	220	0.25	63	735	787	1.07	27.0	1.6	26	-0.22
							0.50	62	788	850	1.08	26.7	1.6	28	-0.27
							1.00	63	915	1,002	1.10	26.1	1.6	32	-0.24
							2.00	63	952	1,081	1.14	25.0	1.5	33	-0.20
							3.00	64	971	1,150	1.18	25.9	1.5	34	-0.20
							4.00	64	882	1,100	1.24	26.0	1.5	31	-0.20
6	3	27	28	16.1	1.06	326	0.25	63	594	652	1.10	24.6	1.6	22	-0.14
							0.50	63	677	734	1.08	25.9	1.6	25	-0.16
							1.00	64	736	820	1.11	26.2	1.6	28	-0.18
							2.00	64	810	916	1.13	25.4	1.6	30	-0.16
							3.00	63	757	922	1.22	24.6	1.5	28	-0.14
							4.00	62	766	931	1.22	24.9	1.5	29	-0.15

[a] SPE-NP reaction conditions: catalyzed by 0.1 mmol of **1**, 1 atm C_2H_4/15°C in 50 mL of ClBz, precipitated in H^+/MeOH, and dried 6 h *in vacuo* at 120 °C. [b] Star yield was calculated from the area percentage of star polymer to overall polymer product by fitting DRI curves using Equation 2.2. [c] $[\eta]_w$ ratio was calculated from $[\eta]_w$ SPE-NP and HBPE arm. [d] Arm number (f_n) was calculated from the M_n of SPE-NP and HBPE arm using Equation 2.3. [e] α is the Mark-Houwink exponent of the SPE-NPs.

The Mark-Houwink plots of the resulting SPEs obtained at t_{NBD} = 0.25, 2, and 4 h in the four runs are shown in Figures 3.9 and 3.10 (a), (b), (c), and (d), respectively. The slopes (i.e., α value) of the intrinsic viscosity curves for all star polymers were found to have α values ranging from -0.27 to -0.14 demonstrating very low dependencies of their intrinsic viscosities to their molecular weights. From α value, important polymer chain confirmation can be deduced according to previous reports defining typical values of 0 for rigid spherical chains, 0.5-0.8 for flexible polymers, and 2 for rod-like chains.[60] Multi-arm star polymers and dendrimers have been reported to have rigid spherical chain confirmations with low negative and positive α values near 0.[43, 45, 97-99] Their low $[\eta]_w$ and negative α values are the solid evidence, confirming their rigid sphere-like chain confirmation. Similar results were obtained in other studies, for SPEs synthesized via the core-first and tandem two-step arm-first methods. [43, 45, 47]

Summarizing this section, we discovered from Runs 33 and 34 that NBD has a much great binding affinity to **1** compared to ethylene and that only one of its endocyclic double bonds is polymerized into NBD homopolymer. ^{1}H NMR spectra of the polymers synthesized in the presence and absence of ethylene were nearly identical, thus confirming that ethylene was not copolymerized in the presence of NBD. The ^{1}H spectra elucidated the PNBD chain microstructure comprised of norbornene repeat units bearing unreacted pendant double bonds. The cross-linking reaction of these pendant vinyl groups in the 3rd and 4th steps are essential to join multiple PE arms together at a cross-linked PNBD core during the one-pot arm-first star polymer synthetic strategy presented in this thesis.

Kinetic studies on NBD reaction with **1** show low conversions (4-7 %) after t_{NBD} = 1–3 h for reactions carried out at several high $[NBD_0/[\mathbf{1}]_0$ molar ratios (55–327). These molar ratios were tested in the SPE-NPs synthesis and were sufficiently large enough to quickly quench accessible Pd^{2+} active sites of **1**, thus inhibiting ethylene polymerization and allowing the formation short oligomerized PNBD segments from the growing living HBPE arm/block. For all runs, the resulting SPEs produced at different $[NBD_0/[\mathbf{1}]_0$ ratios had very similar high M (e.g., M_n = 594–952 kg/mol), high f_n (e.g., 23–37), and relatively good yields (e.g., 54–64%) after extending the NBD-step reaction time followed by H^+/MeOH precipitation and drying *in vacuo* at 120 °C for 6 h. All SPEs behaved like

compact solid spheres or dendrimers in dilute solution with a negative dependence of their $[\eta]_w$ on M.

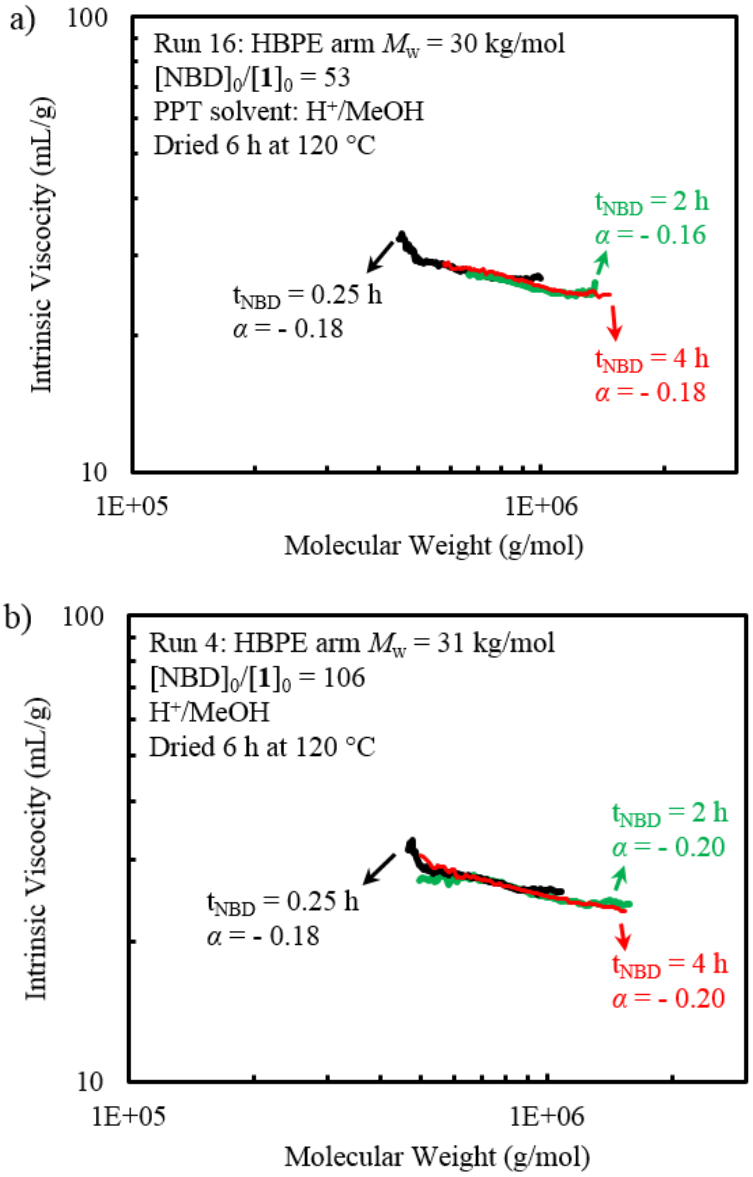

Figure 3.9 Mark-Houwink plots of the SPEs produced in Runs 16–4. See Tables 3.3 and 3.4 for details on the polymerization conditions and GPC data.

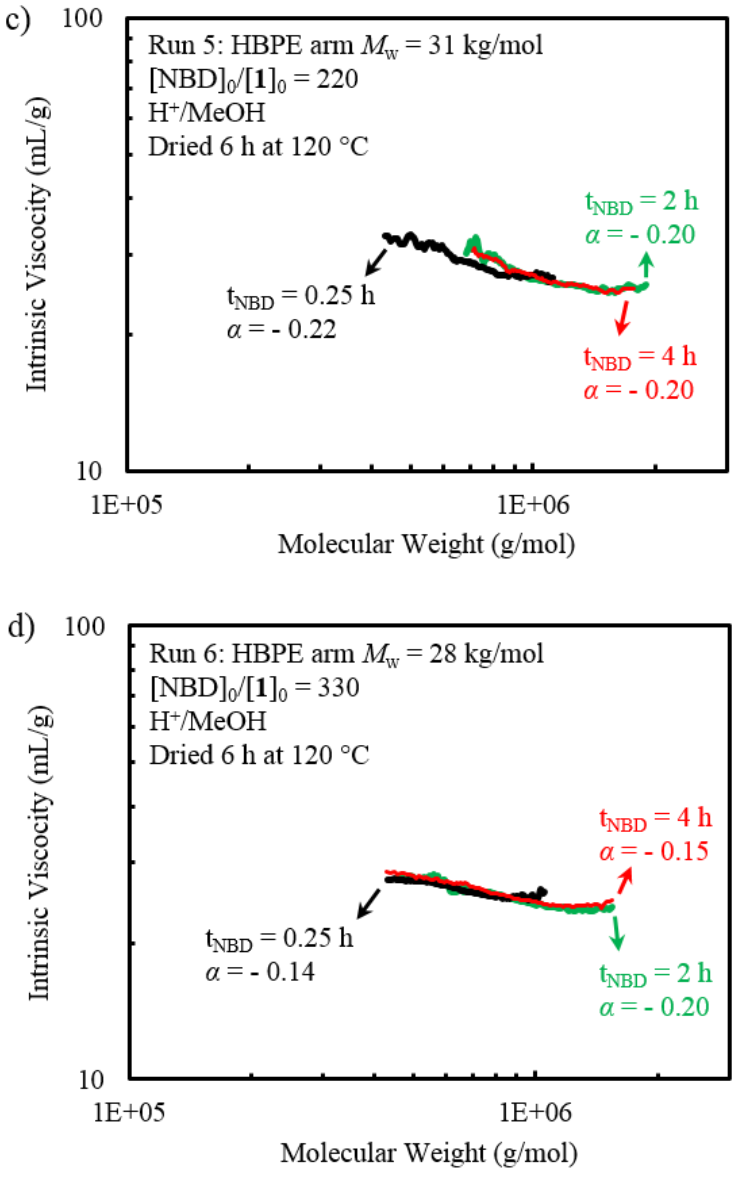

Figure 3.10 Mark-Houwink plots of the SPEs produced in Runs 5–6. See Tables 3.3 and 3.4 for details on the polymerization conditions and GPC data

3.3 Effects of Polyethylene Arm Topology & Length on Star Formation

Generally, the arm/macroinitiator length and topology are important factors affecting significantly the structural parameters of the resulting star polymers in

conventional arm-first synthesis. To facilitate star formation and enhance star parameters including star yield, arm number, and molecular weight, the preferred arm chain topology is typically linear, which consequently reduces steric hindrance for the cross-linking reactions.[43, 86, 100-101] To study the effects of arm length and topology, two sets of polymerizations were undertaken to synthesize SPEs constructed with PE arms of different length and topology (Table 3.5). In the first set (Set 1 in Table 3.5), three runs (7–9) were undertaken with the first-step ethylene "living" polymerization performed at 1 atm/15 ºC for t_E of 1, 2, and 5 h, respectively, to render HBPE arms of different length, which was then followed by subsequent 3 steps with $[NBD]_0/[\mathbf{1}]_0$ = ca. 110 and t_{NBD} = 2 h in the 2nd step. In the second set (Set 2 in Table 3.5), three other runs (20–22) were carried out with the first step ethylene "living" polymerization performed at 27 atm/5 °C for t_E = 2, 3, and 5 h, respectively, to render linear-but-branched PE arms (LBPE) of different length,[33-34] followed by subsequent 3 steps with $[NBD]_0/[\mathbf{1}]_0$ = ca. 330 and t_{NBD} = 2 h in the 2nd step. For both sets of runs, the third and fourth steps were performed under identical conditions, i.e., polymer precipitation in H^+/MeOH and subsequent drying at 120 °C under vacuum for 6 h.

In Set 1, the living HBPE arms synthesized at t_E = 1, 2, and 5 h have M_n of 12, 21, and 43 kg/mol, respectively, with PDI values below 1.1 (see Table 3.5 for GPC results and Figure 3.11 (a) for comparison of the GPC elution curves). Increasing the HBPE arm length, led to a reduction in star yield from 77% in Run 7 (t_E = 1 h) to 66% in Run 8 (t_E = 2 h) and to 46% (t_E = 5 h) in Run 9. Correspondingly, the M of SPEs changed only marginally, with a slight increase of M_n from 929 kg/mol in Run 7 to 968 kg/mol in Run 8 and to 1,050 kg/mol in Run 9 while at similar PDI values (*ca.* 1.08). On the other hand, f_n drops significantly from 85 in Run 7 to 46 in Run 8 to 25 in Run 9, with the increase of HBPE arm length. In Set 2, the LBPE arms synthesized at t_E = 2, 3, and 5 h have M_n of 14, 20, and 29 kg/mol, respectively, also at low PDIs (below 1.07). With increase of arm length, the star yield shows a gradual decrease from 85 in Run 20 to 80 in Run 21 and to 72 in Run 22; similarly, f_n drops sharply from 391 in Run 20 to 88 in Run 21 and to 72 in Run 22. The M values of SPEs in this latter set are very high, with M_n being 5,380, 1,770, and 2,070 kg/mol, respectively, in Runs 20–22. Clearly, increasing the arm length leads to

significant reductions in both star yield and f_n due to the enhanced steric recumbence for arm-addition and/or star-star coupling.

Table 3.5. Effects of PE arm Topology and Size on Star Polymer Formation [a]

		GPC results of HBPE arms							GPC results of SPE-NPs							
Set	Run	C_2H_4 (atm)	t_E (h)	M_n (kg/mol)	M_w (kg/mol)	$[\eta]_w$ (mL/g)	PDI	$[NBD]_0/[\mathbf{1}]_0$	Star yield [b] (%)	M_n (kg/mol)	M_w (kg/mol)	PDI	$[\eta]_w$ (mL/g)	$[\eta]_w$ ratio [c]	f_n [d]	α [e]
1	7	1	1	11	11	11.2	1.00	113	77	929	1,270	1.36	14.3	1.3	85	0.10
	8	1	2	21	22	14.6	1.02	108	66	968	1,030	1.06	19.9	1.4	46	-0.13
	9	1	5	43	47	20.7	1.09	114	46	1050	1,140	1.08	33.6	1.6	25	-0.22
2	20	27	2	14	14	20.2	1.03	329	85	5,380	9,720	1.81	24.7	1.2	391	0.16
	21	27	3	20	21	23.8	1.02	330	80	1,770	2,110	1.19	29.3	1.2	88	-0.12
	22	27	5	29	31	30.9	1.07	329	72	2,070	2,290	1.11	43.5	1.4	72	-0.21

[a] SPE-NP reaction conditions: catalyzed by 0.1 mmol of **1**, 1 atm C_2H_4/15°C (Set 1) and 27 atm C_2H_4/5°C (Set 2) in 50 mL of ClBz, precipitated in H^+/MeOH, and dried 6 h *in vacuo* at 120 °C. [b] Star yield was calculated from the area percentage of star polymer to overall polymer product by fitting DRI curves using Equation 2.2. [c] $[\eta]_w$ ratio was calculated from $[\eta]_w$ SPE-NP and HBPE arm. [d] Arm number (f_n) was calculated from the M_n of SPE-NP and HBPE arm using Equation 2.3. [e] α is the Mark-Houwink exponent of the SPE-NPs.

a) Set 1: avg. $[NBD]_0/[\mathbf{1}]_0$ = 112

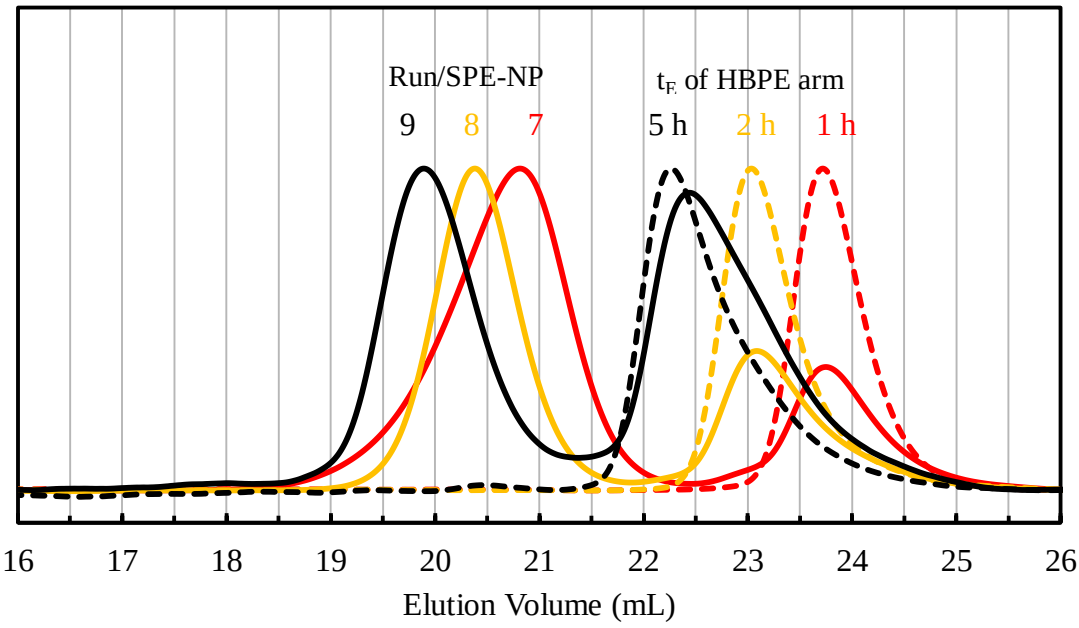

b) Set 2: avg. $[NBD]_0/[\mathbf{1}]_0$ = 329

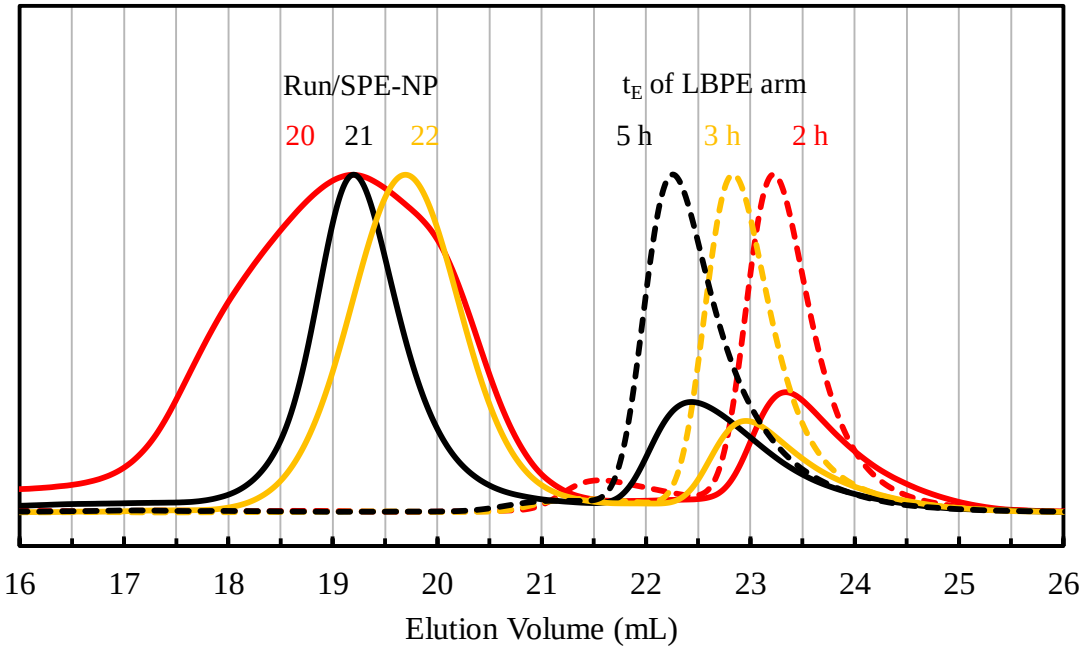

Figure 3.11 GPC elution traces (recorded with DRI detector) of the two sets of polymer products with different arm length and arm topology (see Table 3.5).

Comparing Run 8 in Set 1 and Run 21 in Set 2 with similar arm molecular weight (20 kg/mol) but different chain topology (hyperbranched vs. linear), the SPE constructed the more sterically hindering hyperbranched arm is featured with much lower values in all three structural parameters, star yield (66 vs. 80), M_n (1,030 vs. 1,770 kg/mol), and f_n (46 vs. 88). This further confirms that the chain topology of the arms also affect significantly the star formation, with more sterically hindering arm topology giving rise to reduced star yield, molecular weight, and arm number values. Meanwhile, SPEs synthesized in Set 2 have much broad molecular weight distributions with significantly higher PDI values (up to 1.81), which is indicative of the presence of significant star-star coupling reactions.

Constructed with polymer arms of different arm length and topology, the two sets of polymers synthesized herein enable us to study their important dilute solution properties along with their dependencies on the arm length and topology. Figure 3.11 shows the Mark-Houwink plots of the two sets of SPE. For the purpose of comparison, two fitting lines, $[\eta]_w = 0.0407\ M_w^{0.59}$ and $[\eta]_w = 0.0621\ M_w^{0.61}$(mL/g), reported in our group's earlier studies on narrow-distributed HBPE and LBPE produced with **1** at 1 atm C_2H_4/15 °C and 27 atm C_2H_4/5 °C, respectively, are included in the figure. [45, 47, 49]

From Figure 3.12, the intrinsic viscosity values for the PE arms in both sets of runs are all located on their respective fitting curve, thus confirming their corresponding hyperbranched and linear chain topology. Despite their dramatically higher molecular weight relative the constituting arms, all SPEs synthesized in the two sets have their $[\eta]_w$ being about 1.2–1.6 times those of the arms, reflecting their highly compact star conformation. Meanwhile, for all SPEs, the dependency of $[\eta]$ on M is all very weak, with the α values in the range from -0.22 to 0.16, which are in good agreement with typical α values obtained for rigid globular-shaped chain confirmation determined for other star polymers. [60]. Meanwhile, in each set, the α value of the SPEs decreases with the increase of arm length. In Set 1, the α values are 0.10, -0.13, and -0.22 at the arm M_n of 11, 21, 43 kg/mol, respectively. In Set 2, it decreases from 0.16 to -0.21 with the increase of arm M_n from 11 to 43 kg/mol. This indicates that, at enhanced arm length, these star polymers approach more to behave like the dendrimers.

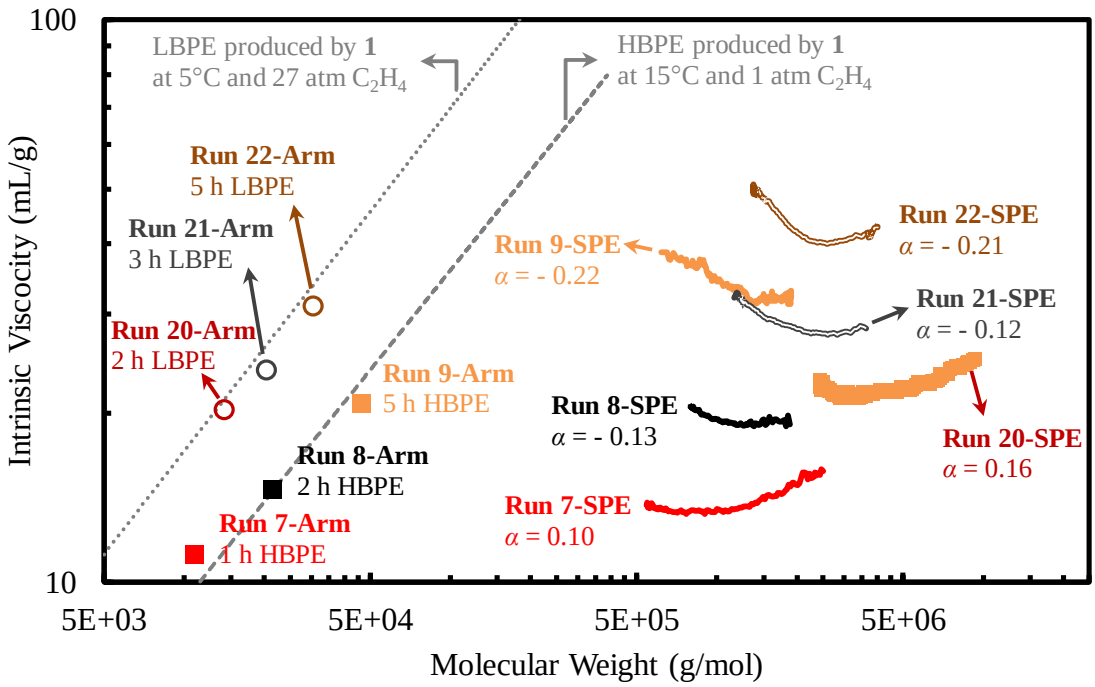

Figure 3.12 Mark-Houwink plots of SPE-NPs constructed with HBPE arms (Runs 7-9) or LBPE arms (Runs 20-22) of different lengths. Two fitting curves in dotted gray lines ($[\eta]_w = 0.0407\ M_w^{0.589}$ for HBPE & $[\eta]_w = 0.0621\ M_w^{0.61}$ for LBPE) were obtained in our earlier studies on HBPE & LBPE synthesized via living C_2H_4 polymerization using **1** at 1 atm C_2H_4/15 °C and 27 atm C_2H_4/5 °C, respectively.[45, 47, 49]

In summary, the increase of arm steric hindrance by either increasing arm length or changing the chain topology from linear to hyperbranched has significant effects on star formation, with star polymers of significantly reduced M, f_n, and star yield produced. Commonly observed in the "arm-first" synthesis of star polymers, this results from the enhanced steric hindrance in the star shell, which restricts the further incorporation of more arms and the occurrence of star-star coupling.[43, 86]

3.4 Effect of Precipitation-Step on Star Formation

Unlike the usual arm-first approaches where the formation of diblock polymer containing a short block of the cross-linker and star formation via cross-linking occur simultaneously in a single step,[43] the approach herein requires the precipitation of the polymer product in order to form high *M* stars of high arm number and good yields. As discussed above, SPEs produced in this approach were precipitated in 2% (v/v) HCl-acidified methanol (H^+/MeOH), where star formation occurred. In Run 17, a sample was taken immediately after precipitation for triple-detection GPC characterization. From the DRI detector, the sample's GPC curve was bimodal showing a well separated high *M* peak for the SPE and low *M* peak for free HBPE-*b*-PNBD block copolymer arms. These results coupled with NBD's polymerization mechanism and chemistry with **1** suggest ligandless or NBD-ligated Pd^{2+} catalysts being the catalyst facilitating fast intermolecular cross-linking reactions of the pendant norbornene groups present in the diblock polymer formed during the second step, which leads to the formation of SPEs.[87-88]

Traditionally, cyclic norbornene-type monomers can be polymerized/oligomerized through catalytic vinyl addition, ring-opening metathesis, radical, or cationic mechanism. While catalytic vinyl addition and ring-opening metathesis can render high-molecular-weight polymers, radical and cationic mechanisms only give rise to oligomers.[95] The latter three mechanisms can be ruled out for the cross-linking here given the absence of the metathesis, radical or cationic initiating species in the precipitation and drying steps. Here, the cross-liking should be facilitated via the catalytic vinyl addition mechanism by the residual catalytic Pd(II) species trapped within the polymers. Cationic Pd(II)-based catalysts have been extensively used in the vinyl polymerization of norbornene at high activities.[95] Given the heterogeneous nature of the polymerization system, the precise structure of the responsible catalytic species here cannot be exclusively determined. We hypothesize that it is most likely the ligandless or NBD ligated cationic Pd(II) species since the loss of the basic diimine ligand should occur given the acidic condition in the precipitation step. NBD has been previously demonstrated to act as a ligand for various Pd(II) compounds.[96] Following the loss of the diimine ligand, NBD may coordinate with

the cationic Pd(II) species to render NBD-ligated catalytic species during the precipitation step.

In this section, the effects of precipitation solvents, methanol or acidified methanol, on the star parameters of the resulting SPEs are discussed. Runs 1 and 2 were conducted at the exact same conditions with different initial $[NBD]_0/[\mathbf{1}]_0$ amounts (i.e., 109 and 230, respectively). Living ethylene polymerization catalyzed by 0.1 mmol of **1** was carried out at 1 atm C_2H_4 and 15 °C for t_E = 3 h followed by NBD addition and reaction for t_{NBD} = 2 h. Half of the polymerization mixture was then precipitated in H^+/MeOH and the other in MeOH. Polymer products were isolated after 10 min of centrifugation at 5000 rpm. The samples, specified with drying time (t_d) of 0 h, were characterized by triple-detection GPC. The precipitated polymers were then split into two equal amounts to be dried at room temperature (20 °C) under air flow and *in vacuo* at 120 °C for t_d = 0.25, 1, 2, 3, 4, and 6 h. The GPC results of the SPE-NPs produced in Runs 1 and 2 including, M_n, M_w, PDI, $[\eta]_w$, star yield, f_n and α values, are listed in Tables 3.6-3.7 and Tables 3.8-3.9, respectively.

On the contrary, the polymer samples collected immediately after MeOH precipitation have monomodal elution curves but with a high *M* shoulder beginning to evolve. This shoulder presumably corresponds to early stages of the star polymer formation with few HBPE arms attached to the slow growing PNBD core. These broadened peaks for Runs 1 and 2 are characterized with M_n = 63 and 45 kg/mol with PDI values of 1.42 and 1.58, respectively. According to their M_n values, the polymers formed after MeOH precipitation are the dimer or trimer of the HBPE-*b*-PNBD block copolymers. These results support our hypothesis that the use H^+/MeOH either generates NBD-ligated or non-ligated Pd^{2+} catalysts, which catalyze fast inter- and intra-molecular cross-linking reactions of the pendant norbornene groups to form the SPEs.

From Figure 3.13, when the MeOH precipitated polymers are dried at 20 and 120 °C, the high *M* elution peak (in both runs) progressively separate from the unreacted HBPE-*b*-PNBD block copolymer peak (which overlaps the HBPE arm peak) and shift to lower elution volume as the drying time increases from t_d = 0.25–6 h. According to the light scattering data, the M_n of SPEs produced after drying at 20 °C under air flow is in the range

of 315–486 kg/mol with PDI's = 1.26–1.58 whereas those formed at 120 °C have drastically higher M_n in the range of 560–1,140 kg/mol with PDI's within 1.02–1.41 (Tables 3.6-3.9). The changes in star polymer M are much more pronounced when dried at high temperature. Also, the molecular weight distribution becomes narrower as t_d increases.

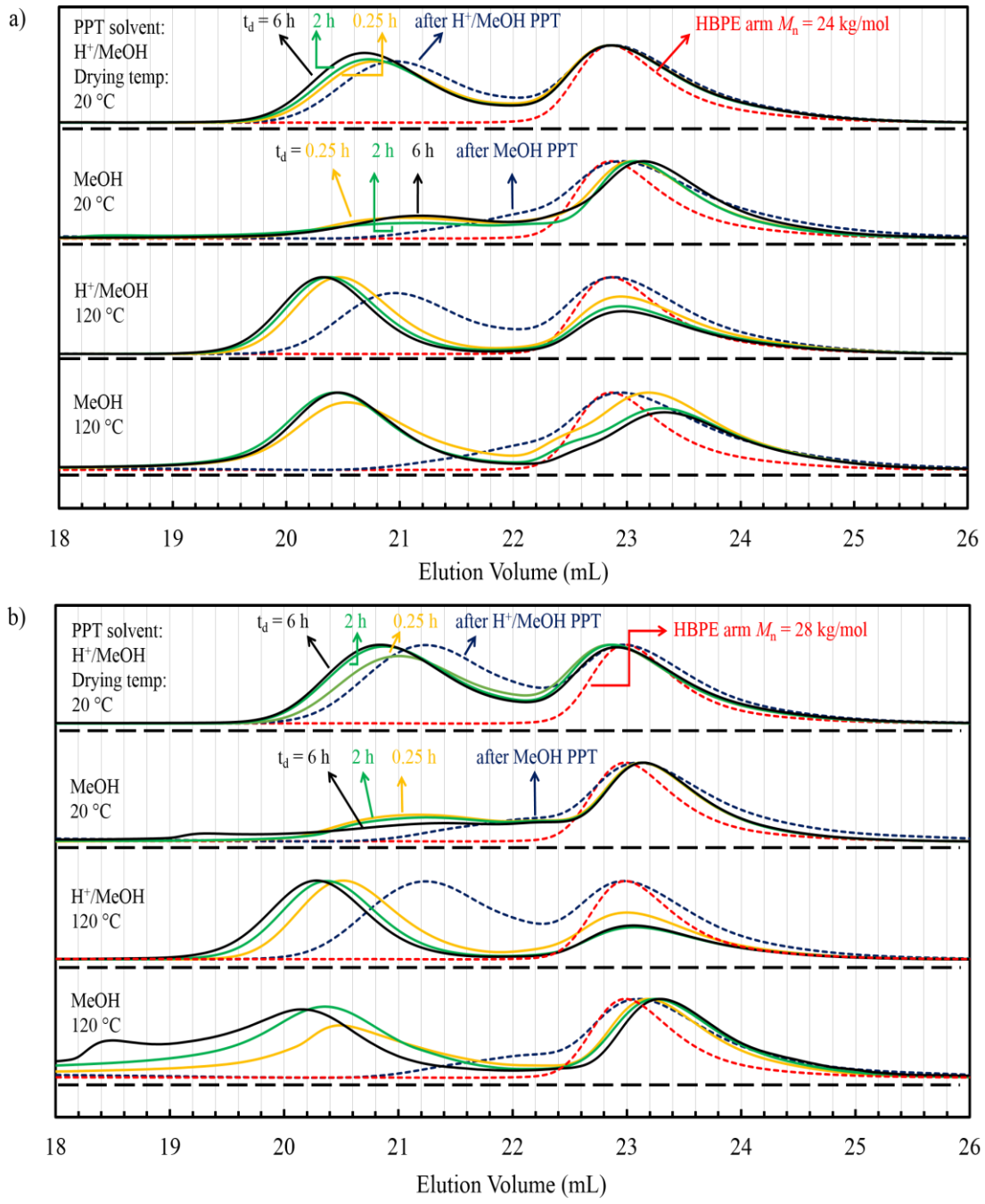

Figure 3.13 GPC elution traces of Run 1 (a) and 2 (b) (recorded with DRI detector) showing the effects of PPT solvent and drying temperature on the formation of SPEs constructed with identical HBPE arms. Other reaction conditions and GPC data of polymer arms and produced star polymers are listed in Tables 3.6/3.7 and 3.8/3.9 for Runs 1 and 2, respectively.

Figure 3.14 and 3.15 shows the effects of non-acidified versus acidified methanol (MeOH vs. H^+/MeOH) precipitation on f_n and star yield of the SPEs, respectively. By comparing plots a, c (Run 1) and b, d (Run 2), we can clearly see that the results are consistent, with similar f_n and star yield curves for H^+/MeOH and MeOH precipitated star polymers formed during the drying periods (t_d) at both drying temperatures. Star yields are significantly improved when H^+/MeOH is used to precipitate the polymers (see Figures 3.14 a and b for comparison of the plots). This difference is clear at the drying temperature of 20 °C, and there is a large gap between the yields for stars formed after H^+/MeOH (i.e., yield range = 42–51 %) and MeOH (i.e., yield range = 0–30 %). However, at the drying temperature of 120 °C, the difference in star yield is not so pronounced for SPEs precipitated in both solvent systems with yields increasing from 44–66 % with longer t_d = 0.25–6 h.

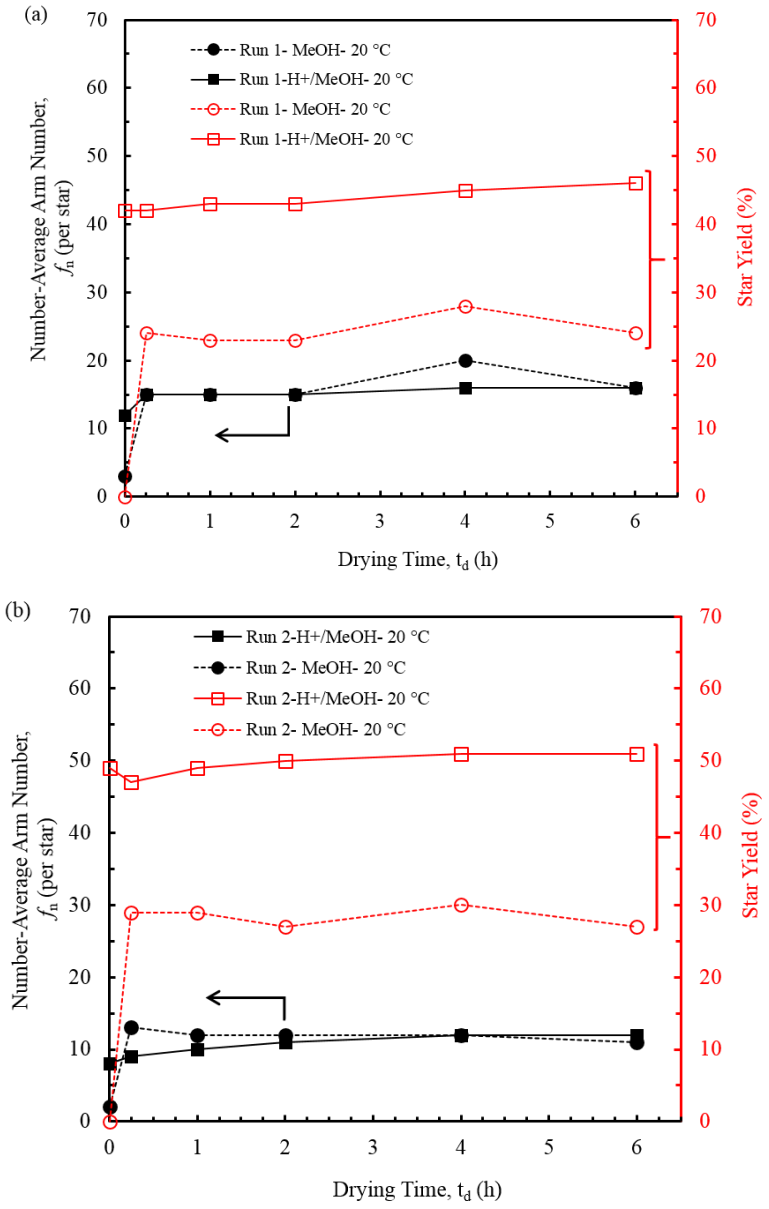

Figure 3.14 Effects of MeOH vs. H^+/MeOH precipitation on f_n and star yield of the SPEs produced in Runs 1 and 2 when dried at 20 °C (a, b) respectively.

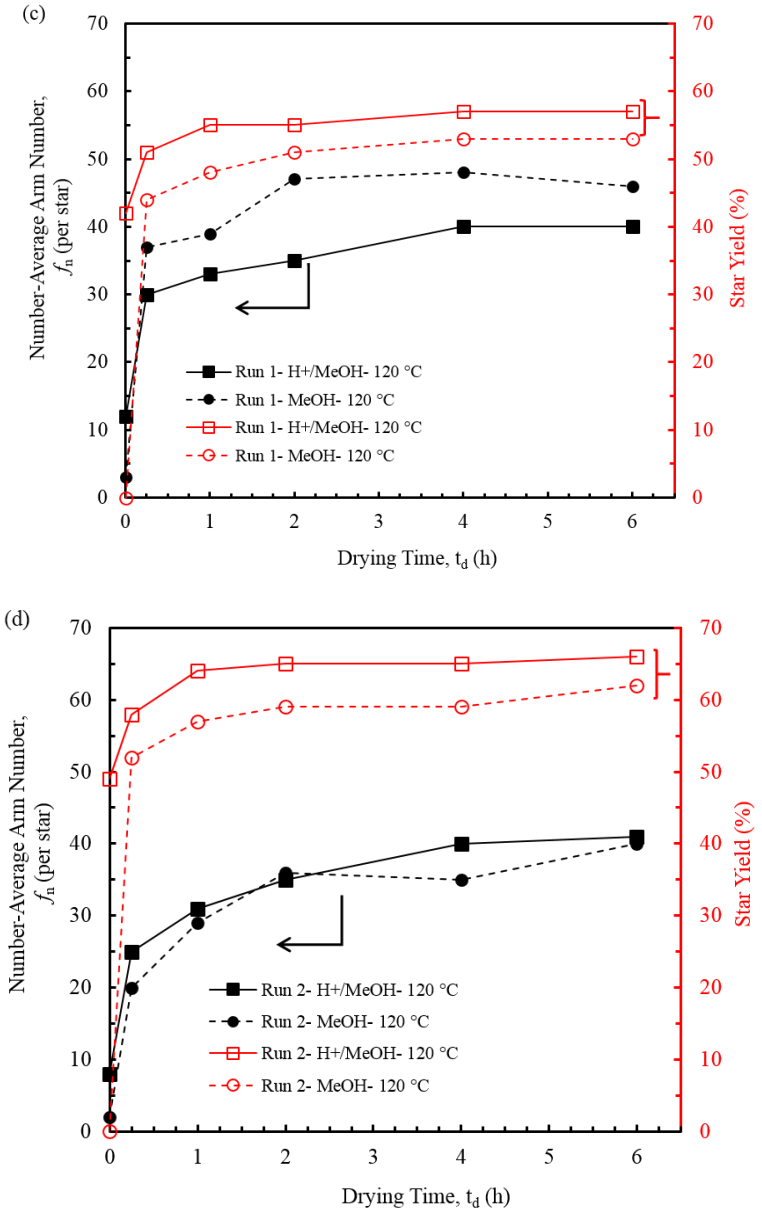

Figure 3.15 Effects of MeOH vs. H^+/MeOH precipitation on f_n and star yield of the SPEs produced in Runs 1 and 2 when dried at 120 °C (c, d), respectively.

On the other hand, the f_n values are within similar ranges for SPEs precipitated in both solvent systems and dried at both 20 °C (i.e., f_n range = 2–20) and 120 °C (i.e., f_n range = 2–48), respectively. Note that these arm numbers are rather constant after drying at 20 °C but are continuously increased when dried at 120 °C. At the same conditions, this

increasing trend in f_n is also observed for M_n of SPEs (see Tables 3.7-3.9). Though the precipitation method has an immediate effect on star formation before drying, it does not seem to influence the resulting star parameters once the drying step begins. There are, however, significant enhancements in star parameters (e.g., M_n, f_n, and star yield) when the drying temperature is increased.

Star architecture was also confirmed for these polymers based on their dilute solution behavior in THF at 33 °C. Figure 3.16 demonstrates the Mark-Houwink plots for H^+/MeOH and MeOH precipitated SPEs dried under air flow at 20 °C and dried *in vacuo* at 120 °C for 6 h (**a** for Run 1) and 4 h (**b** for Run 2). For all polymer samples characterized, $[\eta]_w$ of the produced SPEs was marginally affected by the increase in molecular weight. Consistent with our previous findings, the star polymers' $[\eta]_w$ are 1.1–1.8 times that of their constituting HBPE arm (see $[\eta]_w$ ratio data in Tables 3.6-3.9). Note that the MeOH precipitated star polymers have lower $[\eta]_w$ ratios in the range of 1.1–1.4 compared to 1.6–1.8 for their H^+/MeOH precipitated counterpart, thus indicating a more compact chain configuration for MeOH precipitated SPEs. The Mark-Houwink exponent, α, of all star polymer samples analyzed in Runs 1 and 2 are in the range of 0.02 to -0.32, which is indicative of rigid nanoglobular chain confirmations consistent with α values obtained in the above Runs and those found for other star polymers and SPEs.[43, 45, 47, 60]

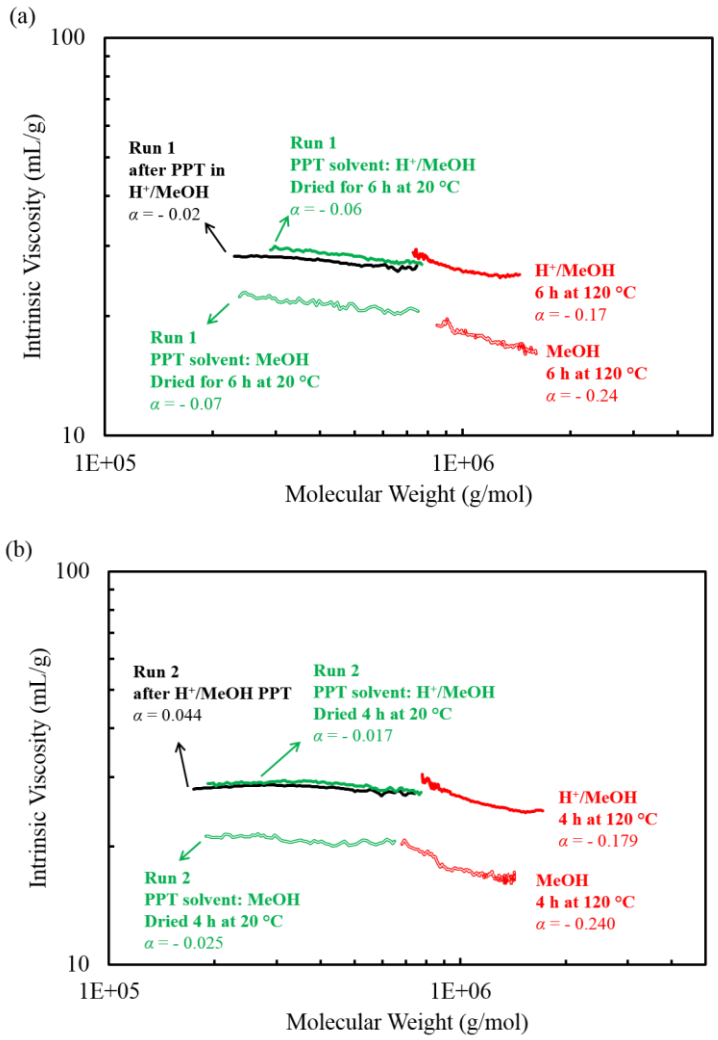

Figure 3.16 Mark-Houwink plots of SPEs produced in Run 1 (a) and 2 (b) by precipitation in H^+/MeOH and MeOH, respectively, and subsequent drying at 20 °C and 120 °C.

In summary, the core cross-linking reactions forming the SPEs in H^+/MeOH seem to be catalyzed by NBD-ligated or non-ligated Pd^{2+} catalysts generated from the removal of protonated diimine ligand of **1.** There is no significant formation of SPEs immediately after MeOH precipitation. Furthermore, when dried at 20 °C under airflow, the star yields are markedly lower for SPEs precipitated in MeOH (i.e., 0–30 %) versus H^+/MeOH (i.e., 42–51 %). For both precipitation methods, after drying at 20 °C for t_d = 0.25–6 h, there is no significant enhancement of the resulting star polymer M_n (i.e., 315–486 kg/mol) and f_n

(i.e., 9–20). When the drying temperature is increased to 120 °C, the resulting M_n (i.e., 560–1,140 kg/mol) and f_n (i.e., 20–48) of SPEs are drastically improved. Given these results, the effects of drying temperature and drying time on the resulting SPEs merits a more detailed investigation.

Table 3.6. Run 1: Effects of Precipitation Solvent and Drying Time at 20 °C on Star Formation [a]

			GPC results of star polymers							
drying temperature (°C)	precipitation solvent	drying time (h)	star yield [b] (%)	$M_{n,LS}$ (kg/mol)	$M_{w,LS}$ (kg/mol)	$[\eta]_w$ (mL/g)	$[\eta]_w$ [c] ratio	PDI	f_n [d]	α [e]
20	H^+/MeOH	0	42	278	347	27.6	1.7	1.25	12	-0.02
		0.25	42	352	430	28.5	1.8	1.22	15	-0.03
		1	43	358	441	28.0	1.7	1.23	15	-0.03
		2	43	369	454	28.4	1.8	1.23	15	-0.04
		4	45	378	465	27.5	1.7	1.23	16	-0.02
		6	46	386	477	28.1	1.8	1.24	16	-0.06
	MeOH	0	0	63	89	20.0	1.2	1.42	3	0.33
		0.25	24	351	551	21.7	1.4	1.57	15	-0.05
		1	23	362	478	21.0	1.3	1.32	15	-0.02
		2	23	352	459	21.6	1.3	1.30	15	0.07
		4	28	486	716	20.5	1.3	1.47	20	-0.08
		6	24	390	544	20.3	1.3	1.40	16	-0.07

[a] Run 1 conditions: catalyzed by 0.1 mmol of **1**, 1 atm C_2H_4/15°C in 50 mL of ClBz for t_E = 3 h, addition of $[NBD]_0/[\mathbf{1}]_0$ = 109, t_{NBD} = 2 h, precipitation and drying. Run 1 HBPE arm: M_n, 24 kg/mol; M_w, 27 kg/mol; PDI, 1.11; $[\eta]_w$, 16.1 mL/g. [b] Star yield was calculated from the area percentage of star polymer to overall polymer product by fitting DRI curves using Equation 2.2. [c] $[\eta]_w$ ratio was calculated from $[\eta]_w$ SPE-NP and HBPE arm. [d] Arm number (f_n) was calculated from the M_n of SPE-NP and HBPE arm using Equation 2.3. [e] α is the Mark-Houwink exponent of the SPE-NPs.

Table 3.7. Run 1: Effects of Precipitation Solvent and Drying Time at 120 °Con Star Formation [a]

			GPC results of star polymers							
drying temperature (°C)	precipitation solvent	drying time (h)	star yield [b] (%)	$M_{n,LS}$ (kg/mol)	$M_{w,LS}$ (kg/mol)	$[\eta]_w$ (mL/g)	$[\eta]_w$ [c] ratio	PDI	f_n [d]	α [e]
120	H^+/MeOH	0	42	278	347	27.6	1.7	1.25	12	-0.02
		0.25	51	717	786	27.2	1.7	1.10	30	-0.14
		1	55	794	846	27.2	1.7	1.07	33	-0.14
		2	55	839	895	26.7	1.7	1.07	35	-0.16
		4	57	951	1,010	27.7	1.7	1.06	40	-0.02
		6	57	963	1,014	26.7	1.7	1.05	40	-0.17
	MeOH	0	0	63	89	20.0	1.2	1.42	3	0.33
		0.25	44	886	944	18.5	1.2	1.07	37	-0.27
		1	48	936	994	19.2	1.2	1.06	39	-0.28
		2	51	1,138	1,176	18.1	1.1	1.03	47	-0.32
		4	53	1,144	1,168	18.3	1.1	1.02	48	-0.41
		6	53	1,102	1,159	17.1	1.1	1.05	46	-0.24

[a] Run 1 conditions: catalyzed by 0.1 mmol of **1**, 1 atm C_2H_4/15°C in 50 mL of ClBz for t_E = 3 h, addition of $[NBD]_0/[\mathbf{1}]_0$ = 109, t_{NBD} = 2 h, precipitation and drying. Run 1 HBPE arm: M_n, 24 kg/mol; M_w, 27 kg/mol; PDI, 1.11; $[\eta]_w$, 16.1 mL/g. [b] Star yield was calculated from the area percentage of star polymer to overall polymer product by fitting DRI curves using Equation 2.2. [c] $[\eta]_w$ ratio was calculated from $[\eta]_w$ SPE-NP and HBPE arm. [d] Arm number (f_n) was calculated from the M_n of SPE-NP and HBPE arm using Equation 2.3. [e] α is the Mark-Houwink exponent of the SPE-NPs.

Table 3.8. Run 2: Effects of Precipitation Solvent and Drying Time at 20 °C on Star Formation [a]

			GPC results of star polymers							
drying temperature (°C)	precipitation solvent	drying time (h)	star yield [b] (%)	$M_{n,LS}$ (kg/mol)	$M_{w,LS}$ (kg/mol)	$[\eta]_w$ (mL/g)	$[\eta]_w$ [c] ratio	PDI	f_n [d]	α [e]
20	H^+/MeOH	0	49	229	294	27.9	1.7	1.29	8	0.04
		0.25	47	259	329	29.0	1.8	1.27	9	0.02
		1	49	274	353	28.7	1.8	1.29	10	0.02
		2	50	294	378	28.7	1.8	1.29	11	-0.01
		4	51	326	414	28.6	1.7	1.27	12	-0.02
		6	51	329	415	28.6	1.7	1.26	12	-0.02
	MeOH	0	0	45	71	16.6	1.0	1.58	2	0.45
		0.25	29	349	545	21.2	1.3	1.56	13	0.02
		1	29	341	492	20.4	1.2	1.44	12	-0.02
		2	27	319	462	20.6	1.3	1.45	12	-0.02
		4	30	335	462	20.5	1.3	1.38	12	-0.03
		6	27	315	396	20.3	1.2	1.26	11	-0.05

[a] Run 2 conditions: catalyzed by 0.1 mmol of **1**, 1 atm C_2H_4/15°C in 50 mL of ClBz for t_E = 3 h, addition of $[NBD]_0/[\mathbf{1}]_0$ = 230, t_{NBD} = 2 h, precipitation and drying. Run 2 HBPE arm: M_n, 28 kg/mol; M_w, 30 kg/mol; PDI, 1.06; $[\eta]_w$, 16.4 mL/g. [b] Star yield was calculated from the area percentage of star polymer to overall polymer product by fitting DRI curves using Equation 2.2. [c] $[\eta]_w$ ratio was calculated from $[\eta]_w$ SPE-NP and HBPE arm. [d] Arm number (f_n) was calculated from the M_n of SPE-NP and HBPE arm using Equation 2.3. [e] α is the Mark-Houwink exponent of the SPE-NPs.

Table 3.9. Run 2: Effects of Precipitation Solvent and Drying Time at 120 °C on Star Formation [a]

			GPC results of star polymers							
drying temperature (°C)	precipitation solvent	drying time (h)	star yield [b] (%)	$M_{n,LS}$ (kg/mol)	$M_{w,LS}$ (kg/mol)	$[\eta]_w$ (mL/g)	$[\eta]_w$ [c] ratio	PDI	f_n [d]	α [e]
120	H^+/MeOH	0	49	229	294	27.9	1.7	1.29	8	0.04
		0.25	58	698	772	28.4	1.7	1.11	25	-0.22
		1	64	852	920	27.0	1.7	1.08	31	-0.19
		2	65	959	1,037	26.6	1.6	1.08	35	-0.15
		4	65	1,116	1,194	26.3	1.6	1.07	40	-0.18
		6	66	1,130	1,215	25.4	1.6	1.08	41	-0.21
	MeOH	0	0	45	71	16.6	1.0	1.58	2	0.45
		0.25	52	560	788	18.8	1.2	1.41	20	-0.10
		1	57	812	972	17.9	1.1	1.20	29	-0.22
		2	59	994	1,102	16.9	1.0	1.11	36	-0.24
		4	59	969	1,119	18.0	1.1	1.16	35	-0.24
		6	62	1,114	1,213	18.8	1.2	1.09	40	-0.24

[a] Run 2 conditions: catalyzed by 0.1 mmol of **1**, 1 atm C_2H_4/15°C in 50 mL of ClBz for t_E = 3 h, addition of $[NBD]_0/[\mathbf{1}]_0$ = 230, t_{NBD} = 2 h, precipitation and drying. Run 2 HBPE arm: M_n, 28 kg/mol; M_w, 30 kg/mol; PDI, 1.06; $[\eta]_w$, 16.4 mL/g. [b] Star yield was calculated from the area percentage of star polymer to overall polymer product by fitting DRI curves using Equation 2.2. [c] $[\eta]_w$ ratio was calculated from $[\eta]_w$ SPE-NP and HBPE arm. [d] Arm number (f_n) was calculated from the M_n of SPE-NP and HBPE arm using Equation 2.3. [e] α is the Mark-Houwink exponent of the SPE-NPs.

3.5 Effect of Drying Temperature and Time on Star Formation

Although the use of H^+/MeOH in polymer precipitation is clearly beneficial compared to MeOH to the formation of star polymers immediately after precipitation, the drying temperature seems to be the major condition governing SPE-NP formation. In this section we examine the effects of drying at different temperatures. The H^+/MeOH precipitated polymer products of Runs 1 and 2 conducted in Section 3.4 were used in this study.

The polymer products obtained following the precipitation in H^+/MeOH were split into four parts and dried under air flow at 20 °C and *in vacuo* at 70, 100, and 120 °C, respectively. Samples were collected at t_d = 0.25, 0.5, 1, 2, 4, and 6 h and were characterized via triple-detection GPC. GPC results are listed in Tables 3.10–3.11 and Tables 3.12–3.13 for Runs 1 and 2, respectively. The results obtained for Run 1 were replicable in Run 2, thus validating this investigation and further confirming that the $[NBD]_0/[\mathbf{1}]_0$ ratio has no distinct effect on the star formation.

The drying temperature affects significantly the M_n of resulting SPEs. The range of M_n following drying for 0.25–6 h changes from 259–370 kg/mol (PDI range = 1.24–1.29) at 20 °C, to 363–654 kg/mol (PDI = 1.26–1.15) at 70 °C, to 491–887 kg/mol (PDI = 1.25–1.07) at 100 °C, and finally to 687–1,130 kg/mol (PDI = 1.12–1.06) at 120 °C (Tables 3.10–3.13). Note that the PDI's of the star polymers decreases throughout the drying period. These results indicate more efficient core cross-linking reactions (i.e., HBPE-*b*-PNBD addition and star-star coupling) as the drying temperature and time are increased. This would increase the activities of the postulated catalysts (Pd^{2+} catalysts) that are suspected to mediate core cross-linking reactions.

Figure 3.17 demonstrates the GPC elution curves (obtained from DRI detector) for polymer samples dried at different temperatures which were collected at t_d = 0.25 h and 6 h in Runs 1 (a) and 2 (b). Elution curves for the HBPE arms (red dotted line) and freshly H^+/MeOH precipitated polymers (blue dotted line) are also included for comparison. Both plots (a) and (b) show the same trend in which the high *M* peak corresponding to SPEs shifts to lower elution volumes (i.e., higher *M*) with the increase in drying temperature

from 20-120 °C and also in response to longer drying times. Furthermore, the low *M* elution peaks which overlap with the HBPE arm peak corresponds to free unreacted HBPE-*b*-PNBD block copolymer arms. The mass fraction of these peaks is gradually reduced as drying temperature and time are increased. Consequently, the mass fraction (i.e., star yield) of the corresponding SPE-NP is also increased.

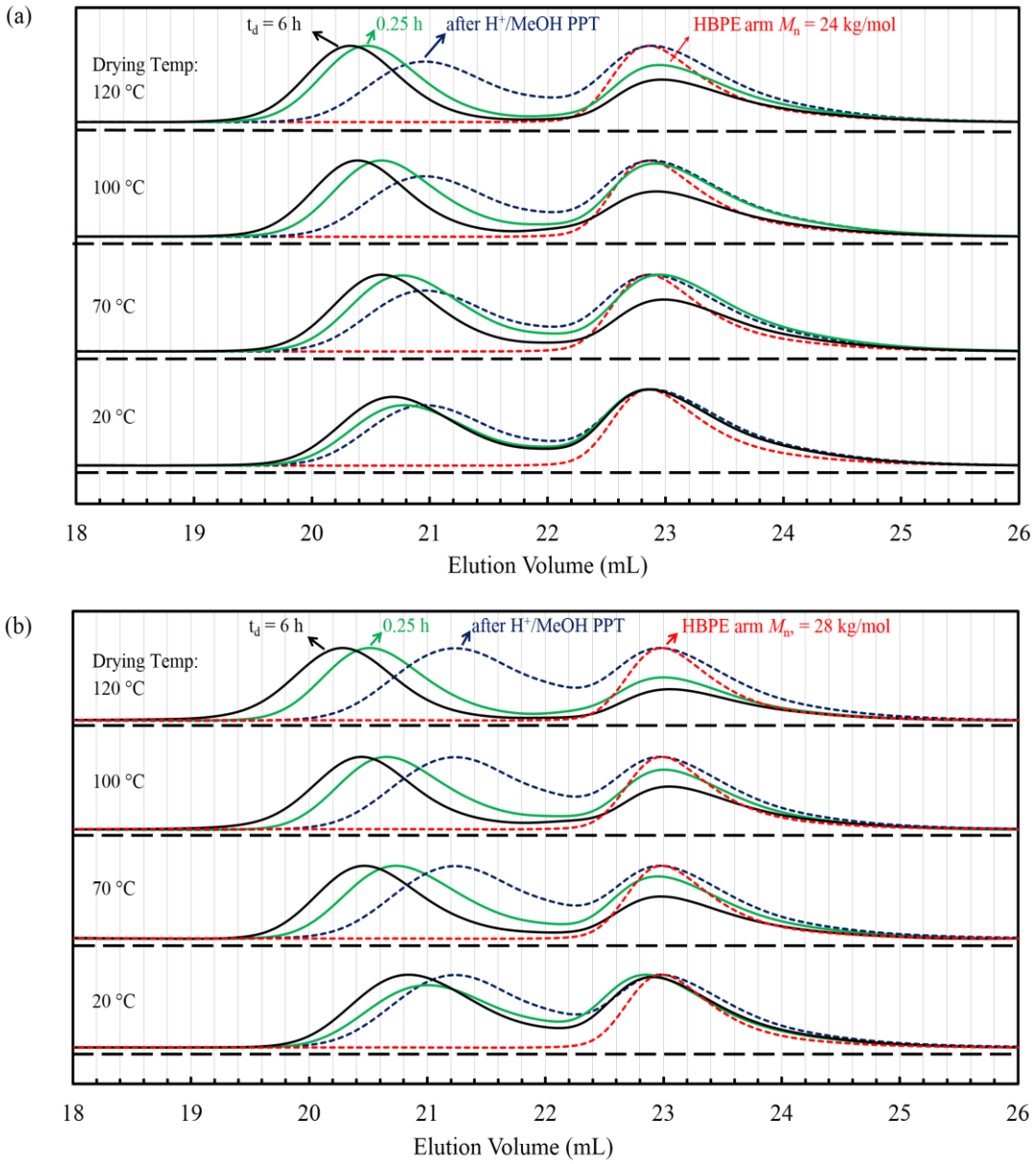

Figure 3.17 GPC elution traces (obtained from DRI detector) of H^+/MeOH precipitated SPE-NPs produced in Run 1 (a) and 2 (b) when dried at different temperatures for t_d = 0.25 h and 6 h.

Figure 3.18 shows the plots of f_n and star yield as function of drying time for SPEs dried at 20, 70, 100, and 120 °C in Runs 1 (a) and 2 (b). The plots from both runs are nearly identical, showing the same increasing trends in f_n and star yield as the drying temperature and time increased. After 6 h of drying at the above drying temperatures, the resulting SPEs reached f_n of 16, 22, 31, and 40 in Run 1 compared to the corresponding values of 12, 24, 32, and 41 in Run 2. Similarly, the star yields are also improved when elevating the drying temperature above 20 °C. In Runs 1 and 2, after drying for 6 h, the star yields obtained increased to 46-57 % and 51-66 %, respectively, when the drying temperature was raised from 20 to 120 °C. The difference in star yield from Run 1 to 2 may be attributable to the higher $[NBD]_0/[\mathbf{1}]_0$ amount added in Run 2.

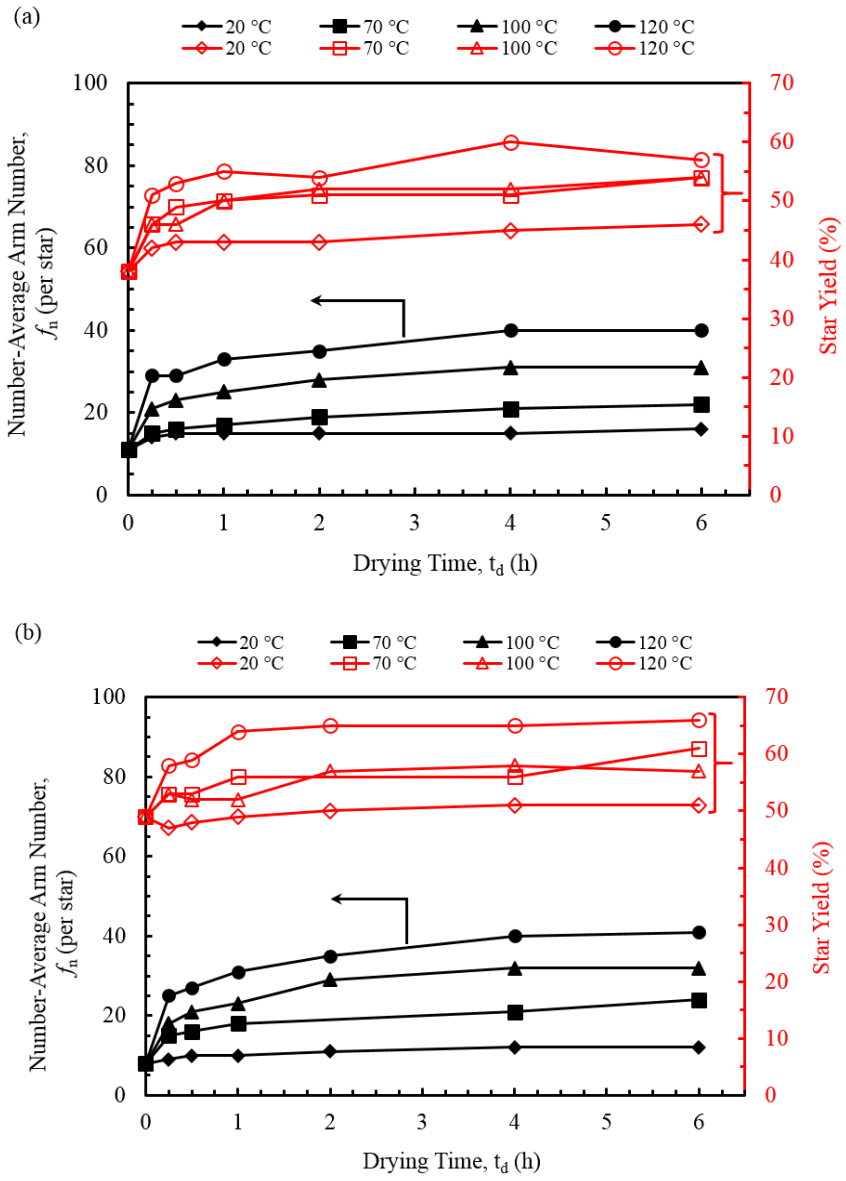

Figure 3.18 Effects of drying temperature and drying time (t_d) on the number-average arm number (f_n) and star yield of the resulting H^+/MeOH precipitated SPE-NPs in Run 1 (a) and 2 (b).

The dilute solution properties for these star polymers were also studied. Despite the different drying temperatures, all resulting SPE-NPs showed very low dependency of their [η] on the molecular weight. This trend is evident in Figure 3.19 which shows the Mark-Houwink plots for star polymers produced in Runs 1 (a) and 2 (b), immediately after

H^+/MeOH precipitation and dried for 6 h at 20, 70, 100, and 120 °C. The $[\eta]_w$ values of these SPE-NPs are only 1.6-1.8 times those of their constituting HBPE arms (see $[\eta]_w$ ratio in Tables 3.10-3.13). These data are indicative of polymer solution behavior with reduced chain entanglements which is characteristic for polymers of highly compact chain confirmations, such as star polymers.[60] In addition, α values of these SPEs are in the range of -0.22 to 0.04, which again are typical values reported for rigid spherical-shaped polymers including star polymers and other SPEs.[43, 45, 47, 74]

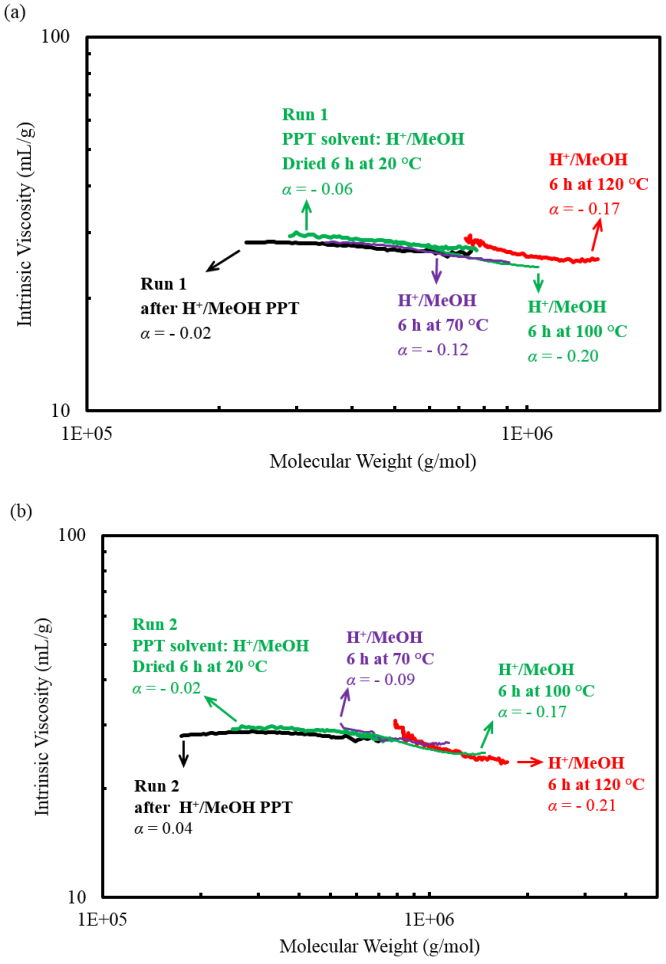

Figure 3.19 Mark-Houwink plots of H^+/MeOH precipitated SPE-NPs dried for 6 h via air blowing at 20 °C and *in vacuo* at 70, 100, and 120 °C in Runs 1 (a) and 2 (b).

Table 3.10. Run 1: Effect of Drying Temperature at 20 and 70 °C on Star Formation at Different Drying Times Following Acidified-Methanol Precipitation [a]

drying temperature (°C)	drying time (h)	GPC results of star polymers							
		star yield [b] (%)	$M_{n,LS}$ (kg/mol)	$M_{w,LS}$ (kg/mol)	$[\eta]_w$ (mL/g)	$[\eta]_w$ [c] ratio	PDI	f_n [d]	α [e]
-	after PPT	42	278	347	27.6	1.7	1.25	12	-0.02
20	0.25	42	278	347	27.6	1.7	1.25	12	-0.02
	0.5	42	352	430	28.5	1.8	1.22	15	-0.03
	1	43	358	441	28.0	1.7	1.23	15	-0.03
	2	43	369	454	28.4	1.8	1.23	15	-0.04
	4	45	378	465	27.5	1.7	1.23	16	-0.02
	6	46	386	477	28.1	1.8	1.24	16	-0.06
70	0.25	46	363	456	26.8	1.7	1.26	15	-0.07
	0.5	49	388	481	26.7	1.7	1.24	16	-0.08
	1	50	396	494	26.5	1.7	1.25	17	-0.08
	2	51	451	547	26.5	1.7	1.21	19	-0.10
	4	51	496	596	25.7	1.6	1.2	21	-0.11
	6	54	516	608	26.0	1.6	1.18	22	-0.12

[a] Run 1 conditions: catalyzed by 0.1 mmol of **1**, 1 atm C_2H_4/15°C in 50 mL of ClBz for t_E = 3 h, addition of $[NBD]_0/[\mathbf{1}]_0$ = 109, t_{NBD} = 2 h, precipitation in H^+/MeOH and drying. Run 1 HBPE arm: M_n, 24 kg/mol; M_w, 27 kg/mol; PDI, 1.11; $[\eta]_w$, 16.1 mL/g. [b] Star yield was calculated from the area percentage of star polymer to overall polymer product by fitting DRI curves using Equation 2.2. [c] $[\eta]_w$ ratio was calculated from $[\eta]_w$ SPE-NP and HBPE arm. [d] Arm number (f_n) was calculated from the M_n of SPE-NP and HBPE arm using Equation 2.3. [e] α is the Mark-Houwink exponent of the SPE-NPs.

Table 3.11. Run 1: Effect of Drying Temperature at 100 and 120 °C on Star Formation at Different Drying Times Following Acidified-Methanol Precipitation [a]

drying temperature (°C)	drying time (h)	GPC results of star polymers							
		star yield [b] (%)	$M_{n,LS}$ (kg/mol)	$M_{w,LS}$ (kg/mol)	$[\eta]_w$ (mL/g)	$[\eta]_w$ [c] ratio	PDI	f_n [d]	α [e]
-	after PPT	42	278	347	27.6	1.7	1.25	12	-0.02
100	0.25	46	497	576	26.3	1.7	1.16	21	-0.12
	0.5	46	534	600	26.1	1.6	1.12	23	-0.12
	1	50	590	655	25.9	1.6	1.11	25	-0.17
	2	52	655	716	25.9	1.6	1.09	28	-0.16
	4	52	723	781	25.5	1.6	1.08	31	-0.19
	6	54	736	789	25.7	1.6	1.07	31	-0.20
120	0.25	51	687	758	27.3	1.7	1.10	29	-0.14
	0.5	53	679	758	26.6	1.7	1.12	29	-0.14
	1	55	776	833	27.0	1.7	1.07	33	-0.14
	2	54	815	876	26.3	1.7	1.07	35	-0.16
	4	60	950	1,003	28.2	1.8	1.06	40	-0.02
	6	57	937	988	26.4	1.7	1.06	40	-0.17

[a] Run 1 conditions: catalyzed by 0.1 mmol of **1**, 1 atm C_2H_4/15°C in 50 mL of ClBz for t_E = 3 h, addition of $[NBD]_0/[\mathbf{1}]_0$ = 109, t_{NBD} = 2 h, precipitation in H^+/MeOH and drying. Run 1 HBPE arm: M_n, 24 kg/mol; M_w, 27 kg/mol; PDI, 1.11; $[\eta]_w$, 16.1 mL/g. [b] Star yield was calculated from the area percentage of star polymer to overall polymer product by fitting DRI curves using Equation 2.2. [c] $[\eta]_w$ ratio was calculated from $[\eta]_w$ SPE-NP and HBPE arm. [d] Arm number (f_n) was calculated from the M_n of SPE-NP and HBPE arm using Equation 2.3. [e] α is the Mark-Houwink exponent of the SPE-NPs.

Table 3.12. Run 2: Effect of Drying Temperature at 20 and 70 °C on Star Formation at Different Drying Times Following Acidified-Methanol Precipitation [a]

drying temperature (°C)	drying time (h)	GPC results of star polymers							
		star yield [b] (%)	$M_{n,LS}$ (kg/mol)	$M_{w,LS}$ (kg/mol)	$[\eta]_w$ (mL/g)	$[\eta]_w$ [c] ratio	PDI	f_n [d]	α [e]
-	after PPT	49	229	294	27.9	1.7	1.29	8	0.04
20	0.25	47	259	329	29.0	1.8	1.27	9	0.02
	0.5	48	272	351	28.8	1.8	1.29	10	0.01
	1	49	274	353	28.7	1.8	1.29	10	0.02
	2	50	294	378	28.7	1.8	1.29	11	-0.01
	4	51	326	414	28.6	1.7	1.27	12	-0.02
	6	51	329	415	28.6	1.7	1.26	12	-0.02
70	0.25	53	409	513	28.1	1.7	1.25	15	-0.06
	0.50	53	439	545	27.9	1.7	1.24	16	-0.08
	1.00	56	502	595	28.0	1.7	1.19	18	-0.11
	4.00	56	589	689	26.8	1.6	1.17	21	-0.11
	6.00	61	654	750	27.7	1.7	1.15	24	-0.09

[a] Run 2 conditions: catalyzed by 0.1 mmol of **1**, 1 atm C_2H_4/15°C in 50 mL of ClBz for t_E = 3 h, addition of $[NBD]_0/[\mathbf{1}]_0$ = 230, t_{NBD} = 2 h, precipitation in H^+/MeOH and drying. Run 2 HBPE arm: M_n, 28 kg/mol; M_w, 30 kg/mol; PDI, 1.06; $[\eta]_w$, 16.4 mL/g. [b] Star yield was calculated from the area percentage of star polymer to overall polymer product by fitting DRI curves using Equation 2.2. [c] $[\eta]_w$ ratio was calculated from $[\eta]_w$ SPE-NP and HBPE arm. [d] Arm number (f_n) was calculated from the M_n of SPE-NP and HBPE arm using Equation 2.3. [e] α is the Mark-Houwink exponent of the SPE-NPs.

Table 3.13. Run 2: Effect of Drying Temperature at 100 and 120 °C on Star Formation at Different Drying Times Following Acidified-Methanol Precipitation [a]

drying temperature (°C)	drying time (h)	GPC results of star polymers							
		star yield [b] (%)	$M_{n,LS}$ (kg/mol)	$M_{w,LS}$ (kg/mol)	$[\eta]_w$ (mL/g)	$[\eta]_w$ [c] ratio	PDI	f_n [d]	α [e]
-	after PPT	49	229	294	27.9	1.7	1.29	8	0.04
100	0.25	53	491	616	27.2	1.7	1.25	18	-0.09
	0.5	52	585	674	27.0	1.7	1.15	21	-0.12
	1	52	648	735	26.2	1.6	1.13	23	-0.10
	2	57	794	868	26.8	1.6	1.09	29	-0.19
	4	58	876	971	27.1	1.7	1.11	32	-0.18
	6	57	887	989	26.5	1.6	1.11	32	-0.17
120	0.25	58	698	772	28.4	1.7	1.11	25	-0.22
	0.5	59	760	847	28.2	1.7	1.11	27	-0.17
	1	64	852	920	27.0	1.7	1.08	31	-0.19
	2	65	959	1,037	26.6	1.6	1.08	35	-0.15
	4	65	1,116	1,194	26.3	1.6	1.07	40	-0.18
	6	66	1,130	1,215	25.4	1.6	1.08	41	-0.21

[a] Run 2 conditions: catalyzed by 0.1 mmol of **1**, 1 atm C_2H_4/15°C in 50 mL of ClBz for t_E = 3 h, addition of $[NBD]_0/[\mathbf{1}]_0$ = 230, t_{NBD} = 2 h, precipitation in H^+/MeOH and drying. Run 2 HBPE arm: M_n, 28 kg/mol; M_w, 30 kg/mol; PDI, 1.06; $[\eta]_w$, 16.4 mL/g. [b] Star yield was calculated from the area percentage of star polymer to overall polymer product by fitting DRI curves using Equation 2.2. [c] $[\eta]_w$ ratio was calculated from $[\eta]_w$ SPE-NP and HBPE arm. [d] Arm number (f_n) was calculated from the M_n of SPE-NP and HBPE arm using Equation 2.3. [e] α is the Mark-Houwink exponent of the SPE-NPs.

3.6 Hydrodynamic Size and Morphology Characterization of Star Polyethylene Nanoparticle

This section aims to further confirm the spherical shape, size, and surface morphology of the SPEs synthesized via this arm-first method. Four different star polymer NPs constructed with topologically different branched PE arms of different lengths were selected for hydrodynamic size characterization and for direct imaging by transmission electron microscopy (TEM), scanning tunneling electron microscopy (STEM), and atomic force microscopy (AFM).

Star polymers bearing HBPE arms of different lengths were synthesized in Runs 17 and 5. Living ethylene polymerizations catalyzed by **1** were carried out at 1 atm C_2H_4/15 °C for t_E = 1 and 3 h, followed by the addition NBD at the $[NBD]_0/[\mathbf{1}]_0$ ratio of 55 and 220, respectively, with t_{NBD} = 2 h. Finally, the polymer products were precipitated in H^+/MeOH and dried *in vacuo* at 120 °C for 6 h to produce the SPEs. Differently, Runs 20 and 21 were carried out at 27 atm/5 °C for t_E = 2 and 3 h, respectively, followed by depressurization of C_2H_4 to 1 atm at 5 °C in order to perform the NBD-step reaction with $[NBD]_0/[\mathbf{1}]_0$ = 330 for t_{NBD} = 2 h and after precipitation/drying steps, producing SPEs with linear arms of different lengths. In all four runs, PE arm and SPE samples were characterized with triple-detection GPC characterization for molecular weight and intrinsic viscosity data and dynamic light scattering (DLS) for hydrodynamic diameter. These data are summarized in Table 3.14.

In Runs 17 and 5, the hydrodynamic diameters (D_h) of the SPEs increased from 29 to 72 nm compared to 6 and 8 nm for their HBPE arms. In contrast, star polymers produced in Runs 20–21 with LBPE arms (D_h's = 8 and 10 nm, respectively) have D_h = 98 and 59 nm, respectively. These different trends in the hydrodynamic size measurements in these two sets of Runs reflects nicely the molecular weight increases (i.e., M_n, M_w) of SPEs synthesized with less bulky linear polymer arms compared to their hyperbranched counterparts of similar size (see Table 3.13, for M_n and D_h data comparison). The particle size distribution curves for the SPEs and their PE arms of these Runs are illustrated in Figure 3.20 as determined by the intensity of scattered light detected in DLS measurements in THF at 25 °C. These results are consistent with a previous report by Sun and Guan where

they synthesized large narrow-distributed dendritic PE-NPs of very high molecular weights having D_h > 100 nm.[81]

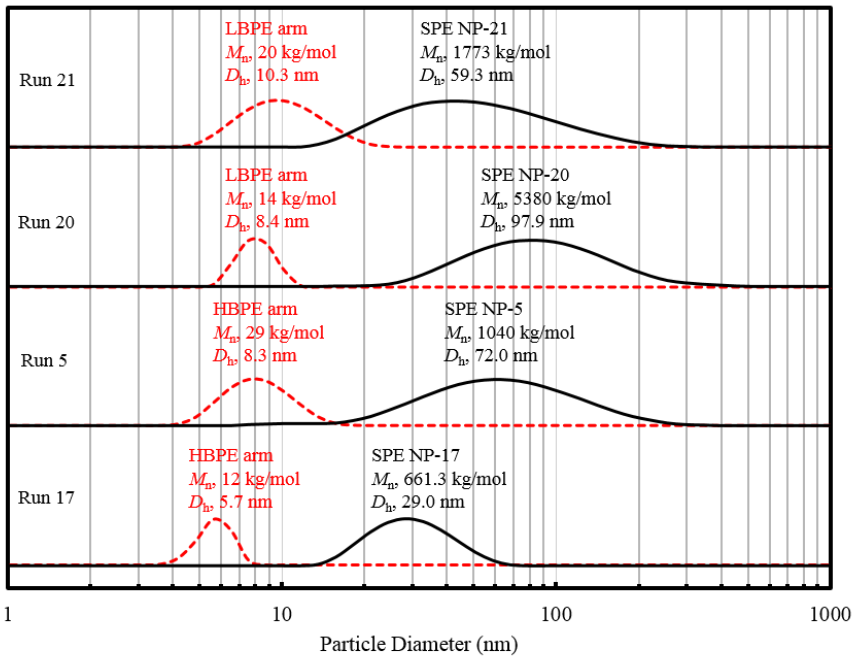

Figure 3.20 Particle size distribution curves of SPE-NPs and their constituting HBPE arms (Runs 17 and 5) and LBPE arms (Runs 20-21) of different lengths obtained from the scattered light intensity detected in DLS characterization using THF as dissolution solvent at 25 °C. See Table 3.14 for reaction conditions, GPC characterization data, and DLS data for SPE-NPs synthesized in these four runs.

The surface morphology of the as-produced SPE-NPs in Runs 17 and 20 bearing hyperbranched and linear arms, respectively, were characterized via direct TEM and AFM imaging. In Figure 3.21, the TEM images clearly show that the SPE-NPs produced in Run 17 (a, b, c) and Run 20 (d, e) are indeed spherical as revealed by the increasing thickness (i.e., darkening) of individual particles from their periphery inward. Similarly, the STEM image (f) of a single SPE-NP synthesized in Run 20 further confirms their globular shape as visualized by centralized increase in thickness (i.e., brightness) from its circumference.

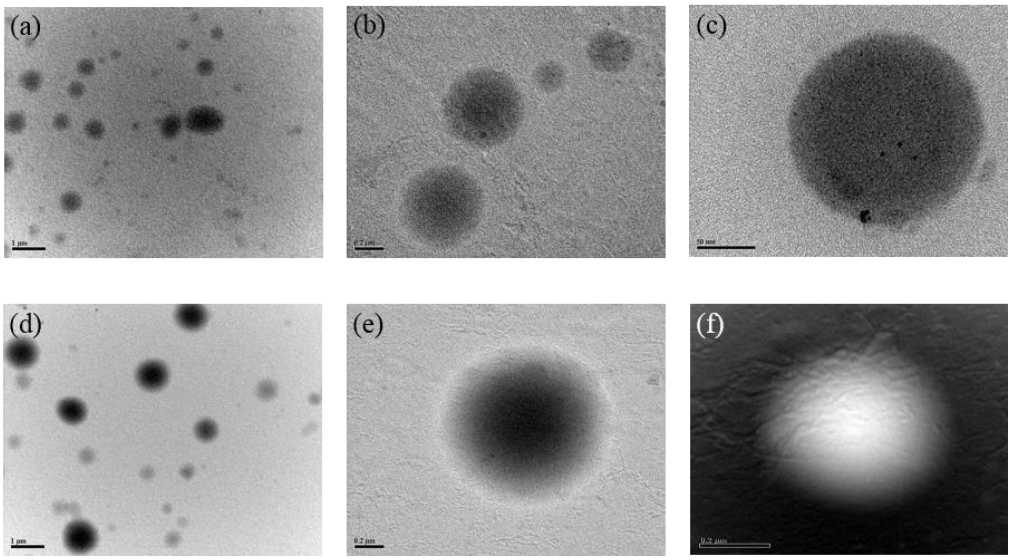

Figure 3.21 TEM images of SPE-NPs constructed with HBPE arms in Run 17 (a-c) and LBPE arms in Run 20 (d-e) at different magnifications along with an STEM image (f) of a single star polymer NP from Run 20. Scale bar: (a) 1 μm, (b) 0.2 μm, (c) 50 nm, (d) 1 μm, (e) 0.2 μm, and (f) 0.2 μm. See Table 3.14 for reaction conditions, GPC characterization data, and DLS data of SPEs synthesized in Run 17 and 20.

Statistical size distributions were conducted in all three runs (17, 5, and 20) by analyzing 100, 210, and 65 particles, respectively, from AFM images (see table (g) in Figure 3.22-24 for averages, min, and max height, area, and diameter). From the height (e) and diameter (f) histograms, SPE-NPs produced in Runs 17, 5, and 20 have average diameters of 101.2, 85.1, and 128.7 nm compared to very low average heights of 2.6-3.2 nm. In addition to these very low height/diameter ratios, 2D (a) and 3D (b, c) height AFM images evidently confirm that these SPE-NPs, with their soft hyperbranched/branched shells, are deformed/flattened into egg-shapes when deposited and dried on hard surfaces, including the TEM grids and mica sheets used herein. This flattening effect thus renders larger diameters (i.e., 85-130 nm) for individual NPs compared to their D_h (i.e., 29-98 nm).

The same deformation phenomenon was observed in several other reports on AFM characterization of dendrimers [107-109] and dendritic PE-NPs.[81]

Table 3.14. Arm-First Pd-Catalyzed Synthesis of SPE-NPs with Cross-Linked PNBD Core [a]

				GPC results of PE arms						GPC results of SPE-NPs							
Run	C_2H_4 (atm)	t_E (h)	$[NBD]_0/[\mathbf{1}]_0$	M_n (kg/mol)	M_w (kg/mol)	$[\eta]_w$ (mL/g)	PDI	D_h[b] (nm)	Star yield [c] (%)	M_n (kg/mol)	M_w (kg/mol)	$[\eta]_w$ (mL/g)	$[\eta]_w$ ratio[d]	PDI	f_n[e]	D_h[b] (nm)	α[f]
17	1	1	55	12	12	11.4	1.01	6	71	661	766	13.5	1.2	1.16	57	29	-0.03
5	1	3	220	29	31	17.6	1.07	8	63	1,040	1,126	27.0	1.5	1.08	36	72	-0.20
20	27	2	329	14	14	20.2	1.03	8	86	5,380	9,720	24.7	1.2	1.81	391	98	0.16
21	27	3	330	20	21	23.8	1.02	10	80	2,106	2,106	29.3	1.2	1.19	88	59	-0.12

[a] SPE-NP reaction conditions: catalyzed by 0.1 mmol of **1**, at 1 atm C_2H_4/15°C or 27 atm/5°C in 50 mL of ClBz, precipitated in H^+/MeOH, and dried 6 h *in vacuo* at 120 °C. [b] D_h of SPE-NP and its PE arm were calculated from the intensity of scattered light at 90° in DLS measurements. [c] Star yield was calculated from the area percentage of star polymer to overall polymer product by fitting DRI curves using Equation 2.2. [d] $[\eta]_w$ ratio was calculated from $[\eta]_w$ SPE-NP and HBPE arm. [e] Arm number (f_n) was calculated from the M_n of SPE-NP and HBPE arm using Equation 2.3. [f] α is the Mark-Houwink exponent of the SPE-NPs.

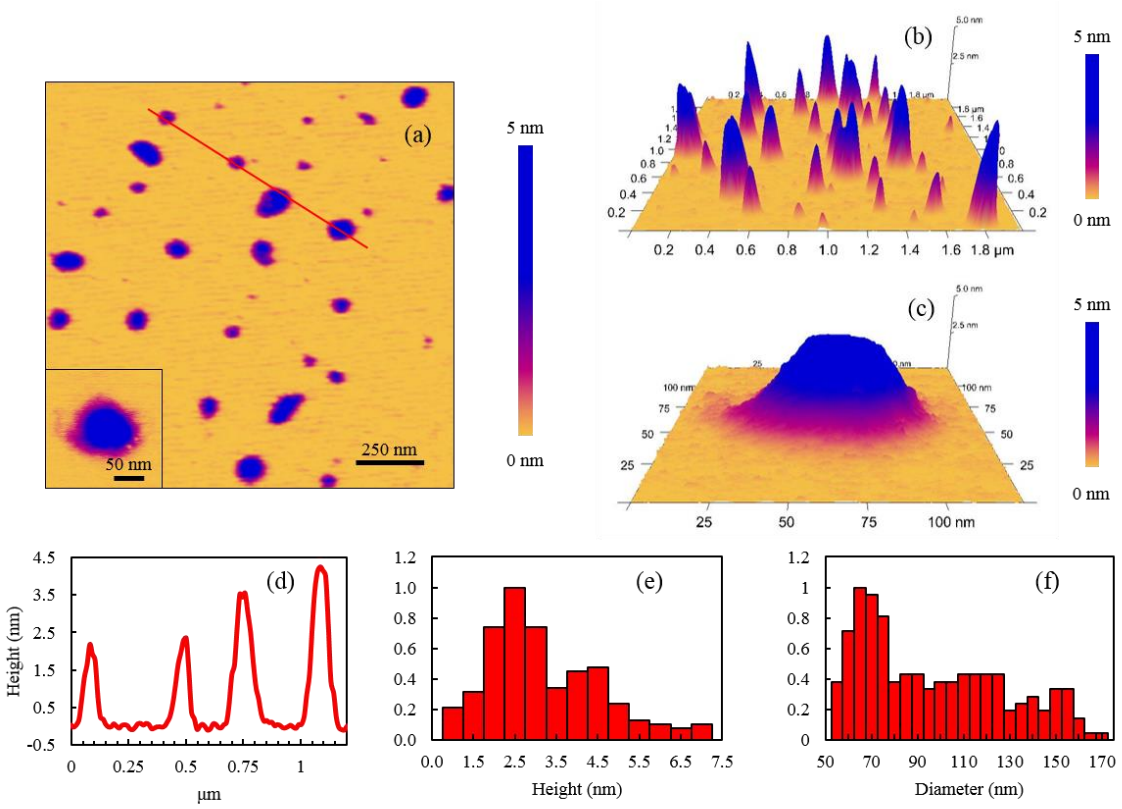

(g)

Parameter	Mean	σ	Min	Max
Total Count	100	–	–	–
Height (nm)	3.1	± 1.5	0.7	7.4
Area (nm^2)	900	± 700	200	4,600
Diameter (nm)	101.2	± 36.8	55.1	242.9

Figure 3.22 Tapping mode AFM imaging and statistical particle analysis of SPE-NPs of Run 17 deposited on a freshly cleaved mica sheet: (a, b, c) 2D and 3D height images with a magnification of a single NP; (d) height distribution of NP along the cross-section (red line) highlighted in image (a); (e, f) particle diameter and height histograms based on statistical analysis of 100 NPs; (g) statistical analysis including height, area, and, diameter of the NPs. See Table 3.14 for reaction conditions, GPC characterization data, and DLS data of SPE-NPs synthesized in Run 17.

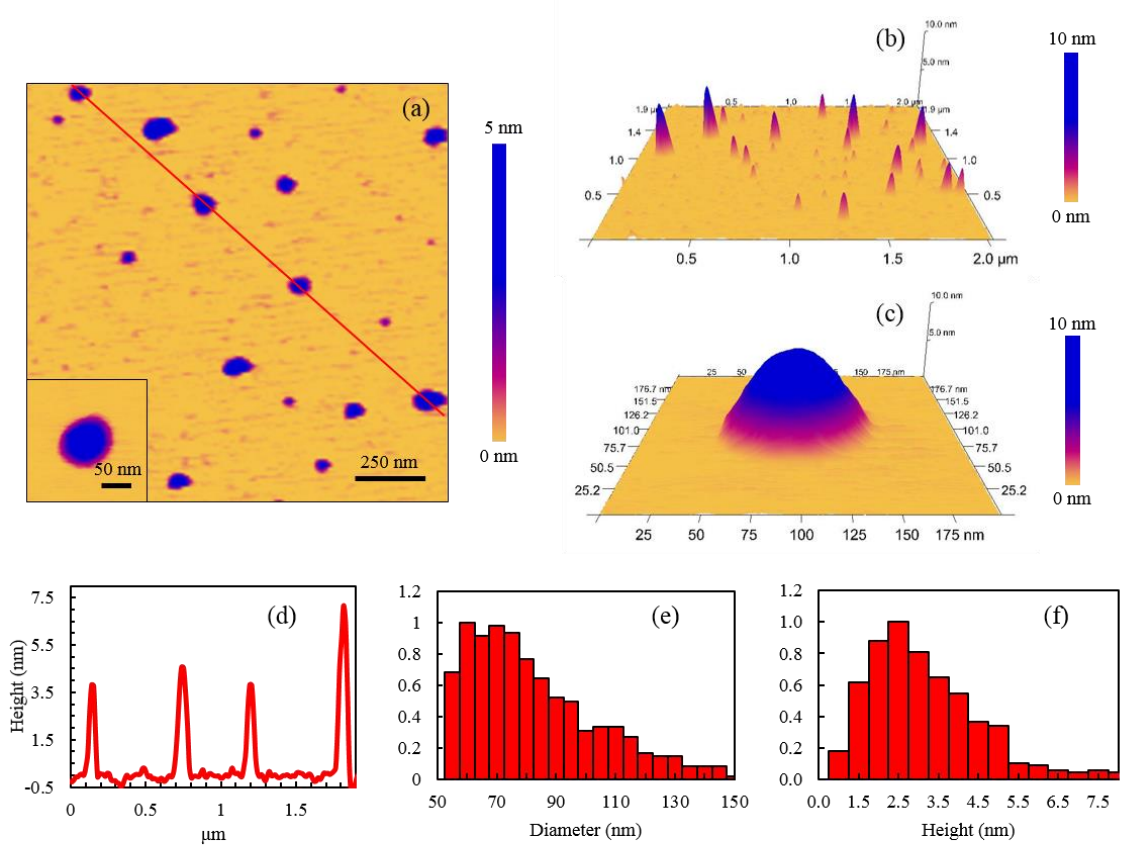

(g)

Parameter	Mean	σ	Min	Max
Total Count	210	–	–	–
Height (nm)	3.2	± 2.0	0.5	17.3
Area (nm^2)	629.8	± 502.8	238.4	4186.6
Diameter (nm)	85.1	± 28.0	55.1	230.9

Figure 3.23 Tapping mode AFM imaging and statistical particle analysis of SPE-NPs of Run 5 deposited on a freshly cleaved mica sheet: (a, b, c) 2D and 3D height images with a magnification of a single NP; (d) height distribution of NP along the cross-section (red line) highlighted in image (a); (e, f) particle diameter and height histograms based on statistical analysis of 210 NPs; (g) statistical analysis including height, area, and, diameter of the NPs. See Table 3.14 for reaction conditions, GPC characterization data, and DLS data of SPE-NPs synthesized in Run 5.

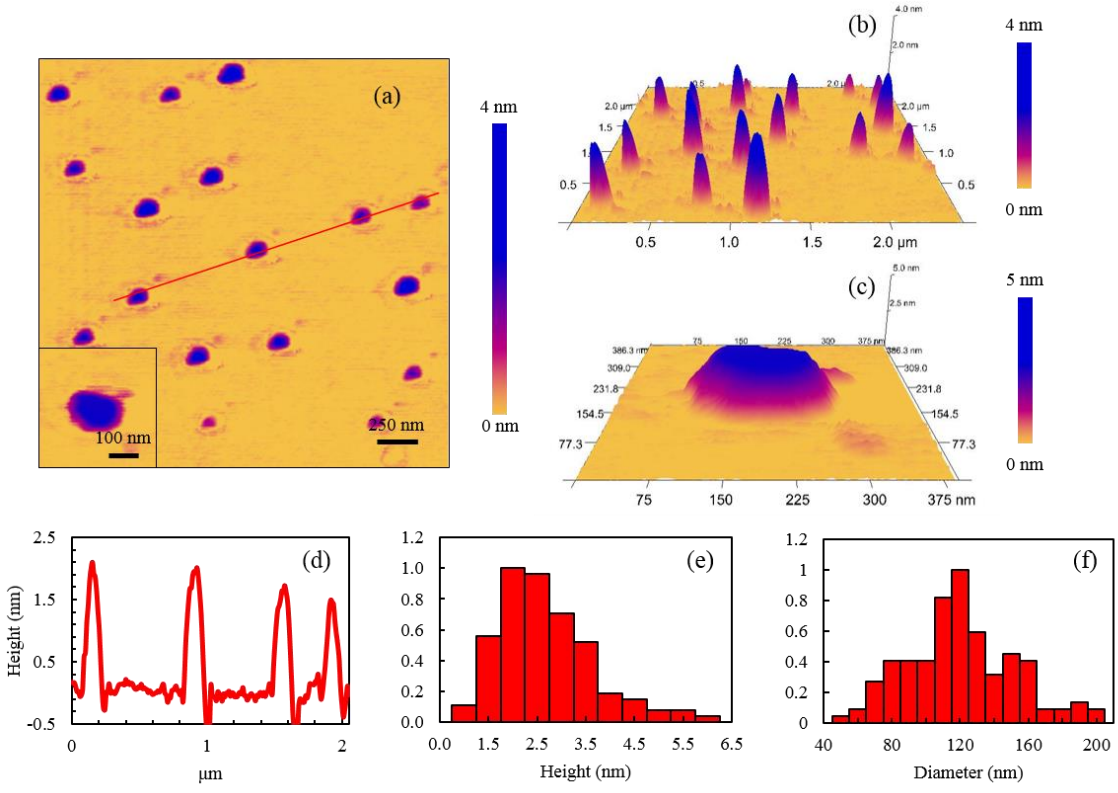

(g)

Parameter	Mean	σ	Min	Max
Total Count	65	–	–	–
Height (nm)	2.6	± 1.2	1.0	8.2
Area (nm^2)	152.1	± 189.0	248.0	1530.0
Diameter (nm)	128.7	± 52.9	56.2	441.3

Figure 3.24 Tapping mode AFM imaging and statistical particle analysis of SPE-NPs of Run 20 deposited on a freshly cleaved mica sheet: (a, b, c) 2D and 3D height images with a magnification of a single NP; (d) height distribution of NP along the cross-section (red line) highlighted in image (a); (e, f) particle diameter and height histograms based on statistical analysis of 65 NPs; (g) statistical analysis including height, area, and, diameter of the NPs. See Table 3.14 for reaction conditions, GPC characterization data, and DLS data of SPE-NPs synthesized in Run 20.

CHAPTER 4: Catalytic Applications of Star Polyethylene Nanoparticles as Vessels for Recyclable Encapsulated Pd(II) Catalysts

In past decades, there has been significant efforts in developing and improving Pd-based catalysts in numerous organic reactions[102-103], including carbon-carbon cross-coupling reactions[104] (e.g., Heck[105-107], Suzuki[108-110], Sonogashira[111], etc.), olefin hydrogenation reactions[112-113], olefin polymerizations[24, 28, 114] and carbon monoxide-olefin copolymerizations[115]. In regards to the chemical industry, the elemental rarity and one-time use of many of these Pd-catalysts poses high costs and environmental pollution issues associated with chemical production and purification/washing.[116] These issues are being addressed through considerable research efforts and significant progress in immobilizing Pd-species onto various supports (e.g., carbon, silica, polymers, dendrimers, etc.) to produce reusable and easily recoverable catalysts with minimal Pd-leaching/loss.[104, 117-118]

In particular, soluble polymer supports offer the additional advantage of conducting organic reactions in homogeneous medium, thus optimizing the Pd-catalysts activity/interaction with the reactants, while maintaining their recyclability in biphasic systems or via nanofiltration or precipitation processes.[117, 119-121] More recently, the use of dendrimers[122-124], hyperbranched polymers[125-126], and star polymers[127-128] have emerged as commendable homogenous supports for Pd-complexes/nanoparticles due to their valuable physicochemical characteristics including controllable size of their unimolecular three-dimensional nanoglobular architecture, tunable core-shell structure, with multiple peripheral and/or central core functionalities, and high stability and solubility in many solvents.

Though dendrimers have been extensively researched as supports for these Pd-catalysis applications, their multi-step synthesis is a major inconvenience for large-scale production. For this reason, hyperbranched polymers and star polymers represent more suitable options with their more simplistic and convenient syntheses, while maintaining the same structural advantages of dendrimers.[125-128] However, encapsulation/immobilization

of the metal catalysts (including Pd-catalysts) onto hyperbranched and star polymer supports is most often achieved during post-polymerization reactions.[33, 63, 117, 125]

To date, there are only few reports on direct encapsulation of metal catalysts during the synthesis of the polymer support.[129] One remarkable advancement (and most relevant to this thesis) is the Pd-diimine catalyzed one-pot synthesis of HBPEs tethered with disulphide functionalities capable of immobilizing the Pd^{2+} species of the diimine catalyst *in situ*.[65] These homogeneous HBPE containing self-supported Pd(II) catalysts have been demonstrated to have high activities for Heck reactions of iodobenzene (IBz) and *n*-butyl acrylate (BA) with minimal Pd-leaching.[65] The work shown in this chapter presents another interesting contribution to this research area with the convenient arm-first Pd-diimine catalyzed synthesis of SPE-NPs encapsulating/trapping Pd^{2+} species *in situ* during the star-forming core cross-linking reaction. The catalytic performance of two different Pd(II) SPE-NP catalysts was investigated in olefin (i.e., 1-octene and 1-hexyne) hydrogenation/isomerization reactions (Section 4.1) and their recyclability was studied in the aforementioned carbon–carbon coupling Heck reaction (Section 4.2). The SPE-NPs were selected according to their highest star yields and high f_n made with topologically different PE arms (hyperbranched versus linear branched).

For the sake of having a sufficient amount of polymer for these catalytic studies, a large batch of SPE-NPs (SPE-NP-52) bearing HBPE arms was synthesized in Run 52 using three times the usual concentration of catalyst **1**. More specifically, living ethylene polymerization was catalyzed by 0.3 mmol of **1** (instead of 0.1 mmol used in all other Runs) dissolved in 50 mL of chlorobenzene under 1 atm C_2H_4 pressure at 15 °C for t_E = 1 h. Triple-detection GPC characterization (LS, viscometer, and DRI detectors) revealed the living HBPE arms have expected M_n = 9.56 kg/mol with PDI = 1.005. NBD-step reaction was initiated by the addition NBD at $[NBD]_0/[\mathbf{1}]_0$ = 147 under 1 atm C_2H_4 at 15 °C for t_{NBD} = 2 h. Star polymer nanoparticles were obtained after H^+/MeOH precipitation and drying *in vacuo* at 120 °C for 6 h. The 78 % star yield in this run is the highest obtained for all SPE-NPs constructed with HBPE arms. It was further purified to 97 % following GPC fractionation in THF at 33 °C (fractionation method described in our previous report).[45] GPC characterization of SPE-NP-52 shows it has high M_n = 758 kg/mol (PDI = 1.33) and

f_n = 79, and also confirms its nanoglobular star-structure (from dilute solution properties and Mark-Houwink relationship).

The Pd(II) encapsulated SPE-NP-catalyst (SPE-NP-20) bearing linear branched arms produced in Run 20 was selected as the second supported catalyst to be tested (reaction conditions and GPC data listed in Table 3.5 in Chapter 3). The star yield is 85%, M_n = 5,380 kg/mol (PDI = 1.81) and f_n = 391. Given the much higher f_n in SPE-NPs produced in Run 20 compared to Run 52, the former is expected to have much higher catalytic performance in both hydrogenation/isomerization and Heck coupling reactions. However, the more densely packed LBPE shell of SPE-NP-20 compared to the more spacious HBPE shell of SPE-NP-52 may slow down the diffusion rate of the reactants to the active Pd(II) species presumably trapped in the cross-linked PNBD core, consequently affecting the catalytic performance.

It should be noted that these catalytic experiments were designed based on an estimated value for the Pd(II) catalysts contained within the SPE-NPs. We assumed that every living PE-*b*-PNBD block copolymer arm incorporated into star polymers donated/trapped its Pd(II)-catalyst within the highly cross-linked PNBD core. This assumption was founded based on the livingness of the ethylene polymerization catalyzed by **1**[40, 43, 45, 47] and the strong coordinative ability of NBD to Pd complexes[87-89]. Thus, the Pd(II) content was calculated from the mass of SPE-NP used in the reactions (typically 0.05–0.08 g in hydrogenation reactions and 0.1 g in Heck reactions) over the PE arm M_n (g/mol) multiplied by the star yield (Equation 2.1). Determination of the actual Pd content in these star polymers was not attempted due to the limited amount of purified star polymers (c.a., 0.2 g of SPE-NP-52), which was predominantly required in these preliminary catalytic experiments.

4.1 Hydrogenation and Isomerization Reactions of 1-Octene and 1-Hexyne Catalyzed by Pd(II)-Encapsulated Star Polyethylene Nanoparticles

Hydrogenation [130-137] and isomerization [32, 138-142] reactions of alkenes and alkynes are well-documented and widely-accepted platforms for catalytic performance studies

employing a wide range of Pd-catalysts including polymer-supported ones[130, 133]. Thus, as a starting point, we chose to investigate our Pd(II)-encapsulated SPE-NPs in the hydrogenation reactions of 1-octene and 1-hexyne using mild conditions (i.e., 1–10 atm H_2, at 20–85 °C) similar to those previously reported.[130, 133, 136-137, 143] Reaction kinetics were studied through a systematic evaluation of the effects of reaction temperature, H_2 pressure, hyperbranched versus linear-but-branched shells of the Pd(II)-SPE-NP-catalysts.

The effect of four different reaction temperatures, ranging from 20–85 °C, were first investigated in Runs 19–22 for the hydrogenation/isomerization of 1-octene catalyzed by the purified SPE-NP-52 (i.e., star yield, 97%) made of hyperbranched arms. The mass of SPE-NP used in each run was 0.05 g, which represents an estimated total Pd(II) content of 5 μmol per reaction (calculated using Equation 2.1). H_2 pressure was fixed to 10 atm and the average initial molar ratio of 1-octene to Pd(II)-catalyst (avg. $[1\text{-octene}]_0/[Pd]_0$) was 266. An equimolar amount of anisole to 1-octene was also added as the internal standard used in the ^{1}H NMR spectra normalization. Hydrogenation reactions were carried out in a 20 mL stainless steel reactor which was temperature controlled by submerged it in an oil bath heated by magnetic stirrer/hotplate.

Throughout the reaction, samples (c.a. 0.2 μL) were collected regularly over 120 h (t_{H_2}) and immediately cooled down in an ice bath to stop the reaction. ^{1}H NMR samples were prepared in $CDCl_3$ and analyzed on a Varian Gemini 2000 NMR spectrometer (200 MHz) operated at 25 °C. Figure 4.1 demonstrates the ^{1}H NMR spectra of samples collected in Run 20 conducted at 10 atm H_2/45 °C over a wide range of t_{H_2} (0–72 h). ^{1}H resonance signals arising from terminal double bond protons, **a** (at 5.7 ppm, 1 H) and **c** (at 4.97–4.91 ppm, 2 H), of 1-octene and internal double bond protons, **b** (at 5.47–5.34 ppm, 2 H), of *n*-octene isomers were used to determine the contents and yields of reactants and products. As t_{H_2} increases, we observed an increase in the relative intensity of peak **b** in comparison to peaks **a** and **c**, thus indicating a progressing isomerization reaction of 1-octene. Based on the integrations of these ^{1}H NMR signals (I_a, I_b, and I_c), the percent contents of 1-octene, *n*-octene isomers, total residual octenes, and octane yields were calculated during the

hydrogenation/isomerization reactions using Equations 2.5–2.9. These results are summarized in Table 4.1 for Runs 19–22.

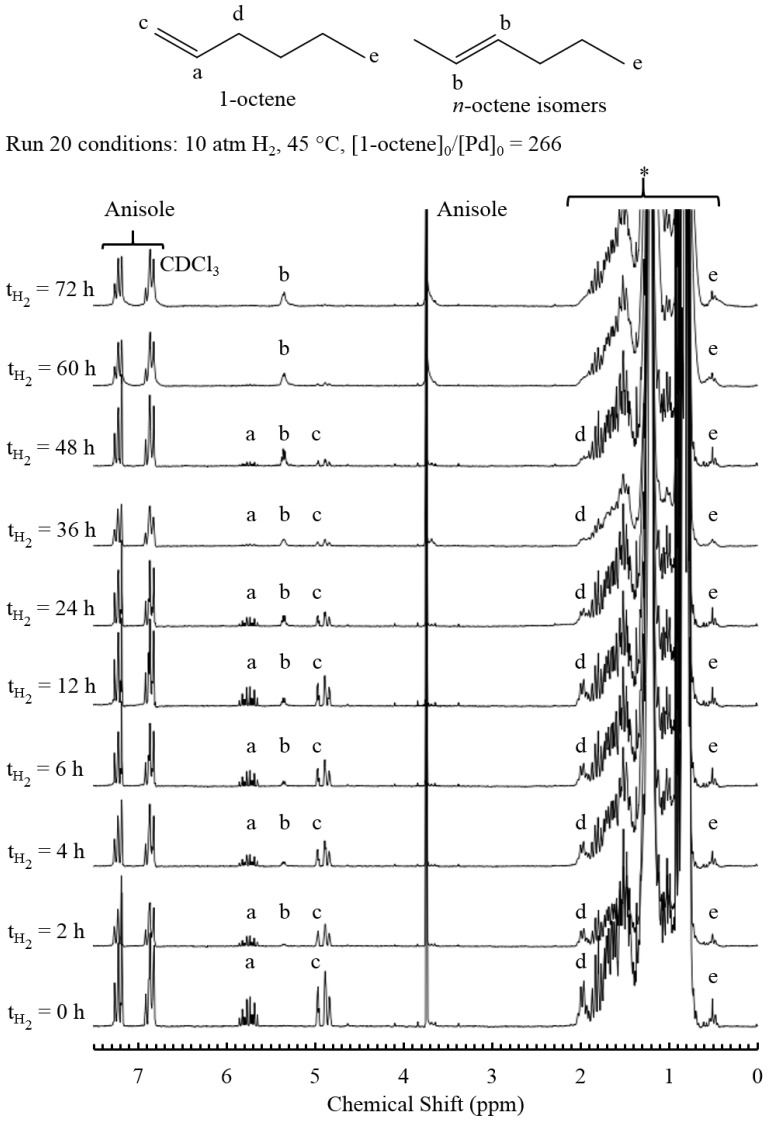

Figure 4.1 ^{1}H NMR spectra of Run 20 at different reaction times (t_{H2}) during 1-octene hydrogenation/isomerization reactions catalyzed Pd(II)-encapsulated SPE-NP-52 carried out under 10 atm H_2 at 45 °C. Other reaction conditions and kinetic results are listed in Table 4.1.

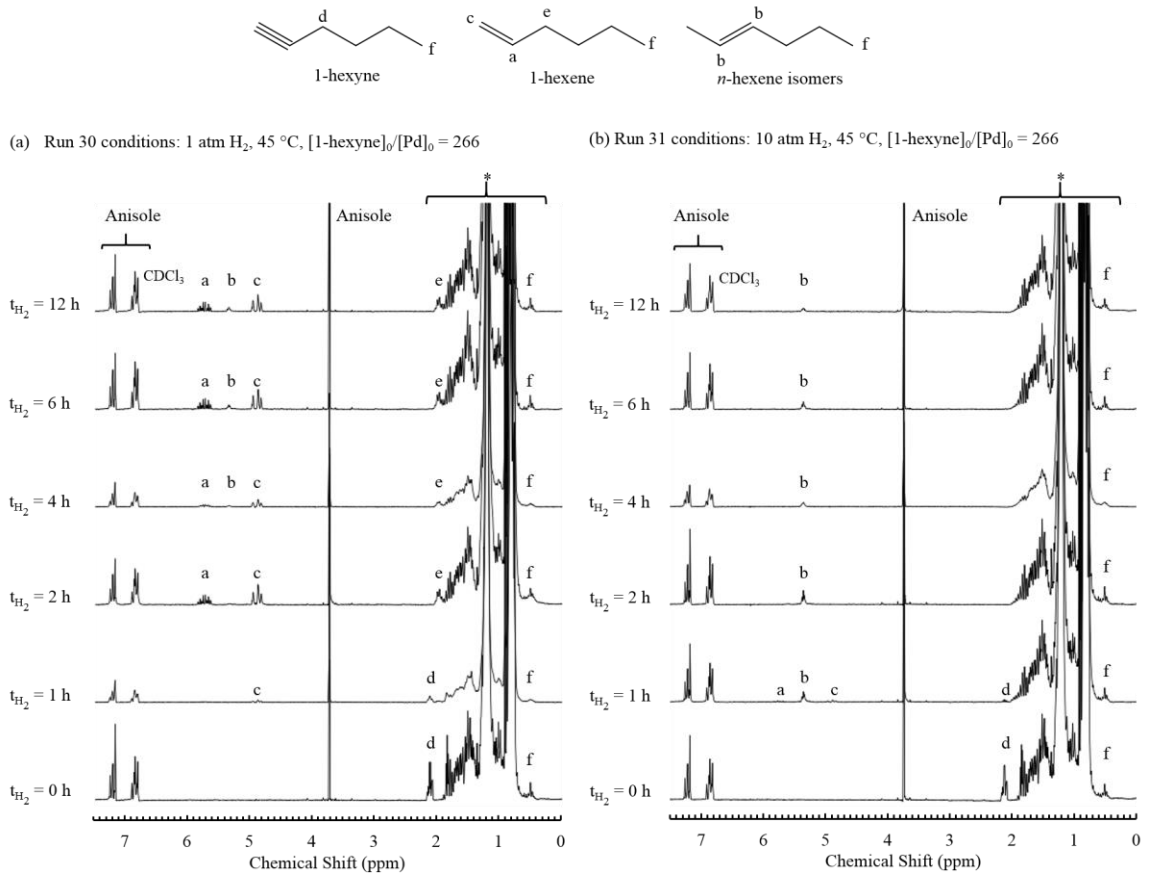

Figure 4.2 ^{1}H NMR spectra of Run 30 (a) and 31 (b) at different reaction times (t_{H2}) during 1-hexyne/1-hexene hydrogenation/isomerization reactions catalyzed Pd(II)-encapsulated SPE-NP-20 carried out at 45 °C at 1 atm and 10 atm H_2, respectively. Other reaction conditions: mass of SPE-NP-20, 0.08 g; estimated Pd amount, 5 μmol; solvent, hexanes; total reaction volume, 5 mL.

To investigate the effect of H_2 pressure, two sets of experiments were carried out using SPE-NP-20 (having the more abundant amount of polymer available at high star yield = 85%) at 1–10 atm H_2 in Runs 26–27 and Runs 30–31 for the hydrogenation/isomerization reactions of 1-octene and 1-hexyne, respectively. Figure 4.2 shows a comparison of the ^{1}H NMR spectra collected for a range of t_{H2} (0–72 h) in Run 30 (a) and 31 (b) for 1-hexyne reaction catalyzed by SPE-NP-20 at 1 and 10 atm H_2, respectively. The ^{1}H NMR resonance signals arise from secondary protons adjacent to the terminal triple bond of 1-hexyne (peak **d** at 2.18 ppm, 2 H), terminal vinyl protons of 1-

hexene (peaks a at 5.8 ppm, 1 H and c at 4.96–4.92 ppm, 2 H), and internal vinyl protons of *n*-hexene isomers (peak **b** at 5.44–5.37 ppm, 2 H). The kinetic parameters including, percent contents/yields of residual 1-hexyne, 1-hexene, *n*-hexene isomer, and hexane, were determined from ^{1}H NMR integration of these signals (I_d, I_a, I_c, and I_b) and calculated using Equations 2.10–2.15 as defined in Chapter 2. These results are also summarized below in Table 4.2 (Runs 26–27 and Runs 30–31).

Table 4.1. Hydrogenation/Isomerization Reactions of 1-Octene Catalyzed by Pd(II)-Encapsulated Star Polyethylene Nanoparticle (SPE-NP-52): Effect of Temperature on the Reaction Kinetics

Run	$[1\text{-octene}]_0/[Pd]_0$	H_2 (atm)	Temp (°C)	Reactants & products	Percent reactants and products (%) [a]												
					t_{H2} (h)												
					0	1	2	4	6	12	24	36	48	60	72	96	120
19	266	10	25	1-octene	100	–	86	74	72	71	41	30	20	16	6	0	0
				n-octene	0	–	4	6	6	8	14	16	21	22	21	18	18
				octane	0	–	10	20	22	21	45	54	59	62	73	82	82
				total octene	100	–	90	80	78	79	55	46	41	38	27	18	18
20	266	10	45	1-octene	100	–	92	84	70	57	16	6	0	0	0	0	0
				n-octene	0	–	4	6	8	12	22	22	23	22	20	14	10
				octane	0	–	4	10	22	31	62	72	77	78	80	86	90
				total octene	100	–	96	90	78	69	38	28	23	22	20	14	10
21	266	10	65	1-octene	100	–	87	75	43	1	0	0	0	0	0	0	0
				n-octene	0	–	5	7	12	22	14	11	9	4	4	2	1
				octane	0	–	8	18	45	77	86	89	91	96	96	98	99
				total octene	100	–	92	82	55	23	14	11	9	4	4	2	1
22	266	10	85	1-octene	100	–	8	0	0	0	0	0	0	0	0	0	0
				n-octene	0	–	26	28	26	20	13	9	7	6	6	4	3
				octane	0	–	66	72	74	80	87	91	93	94	94	96	97
				total octene	100	–	34	28	26	20	13	9	7	6	6	4	3

Other reaction conditions: 1330 μmol of 1-octene was catalyzed by 5 μmol of Pd(II) contained in 50 mg of SPE-NP-52 (calculated with Equation 2.1) in 5 mL of hexanes at 10 atm H_2. [a] Percent amounts of products and residual reactants were determined by ^{1}H NMR integration of resonance signals arising from the vinyl protons of 1-octene and *n*-octene isomers (Equations 2.5-2.9).

Table 4.2. Hydrogenation/Isomerization Reactions of 1-Octene and 1-Hexyne Catalyzed by Pd(II)-Encapsulated Star Polyethylene Nanoparticle (SPE-NP-20): Effect of Hydrogen Pressure on the Reaction Kinetics

Run	Reactant	$[reactant]_0/[Pd]_0$	H_2 (atm)	Temp (°C)	Reactants & products	Percent reactants and products (%) [a]												
						t_{H2} (h)												
						0	1	2	4	6	12	24	36	48	60	72	96	120
26	1-octene	266	1	25	1-octene	100	–	97	92	90	78	51	32	7	n.d.	0	n.d.	0
					n-octene	0	–	2	4	4	6	13	23	30	n.d.	30	n.d.	24
					octane	0	–	1	4	6	16	36	45	63	n.d.	70	n.d.	76
					total octene	100	–	99	96	94	84	64	55	37	n.d.	30	n.d.	24
27	1-octene	266	10	45	1-octene	100	–	49	13	0	0	0	0	0	0	0	0	0
					n-octene	0	–	12	23	23	17	3	0	0	0	0	0	0
					octane	0	–	39	64	77	83	97	100	100	100	100	100	100
					total octene	100	–	61	36	23	17	3	0	0	0	0	0	0
30	1-hexyne	266	1	25	1-hexyne	100	69	0	0	0	0	n.d	–	–	–	–	–	–
					1-hexene	0	25	86	71	70	66	n.d	–	–	–	–	–	–
					n-hexene	0	0	4	13	14	16	n.d	–	–	–	–	–	–
					hexane	0	6	10	16	16	18	n.d	–	–	–	–	–	–
31	1-hexyne	266	10	45	1-hexyne	100	6	0	0	0	0	n.d	–	–	–	–	–	–
					1-hexene	0	10	0	0	0	0	n.d	–	–	–	–	–	–
					n-hexene	0	45	48	36	26	14	n.d	–	–	–	–	–	–
					hexane	0	39	52	64	74	86	n.d	–	–	–	–	–	–

Other reaction conditions: 1330 μmol of reactant was catalyzed by 5 μmol of Pd(II) contained in 80 mg of SPE-NP-20 (calculated with Equation 2.1) in 5 mL of hexanes. [a] Percent amounts of products and residual reactants were determined by ^{1}H NMR integration of resonance signals arising from the vinyl protons of reactant and reactant isomers (Equations 2.5-2.15).

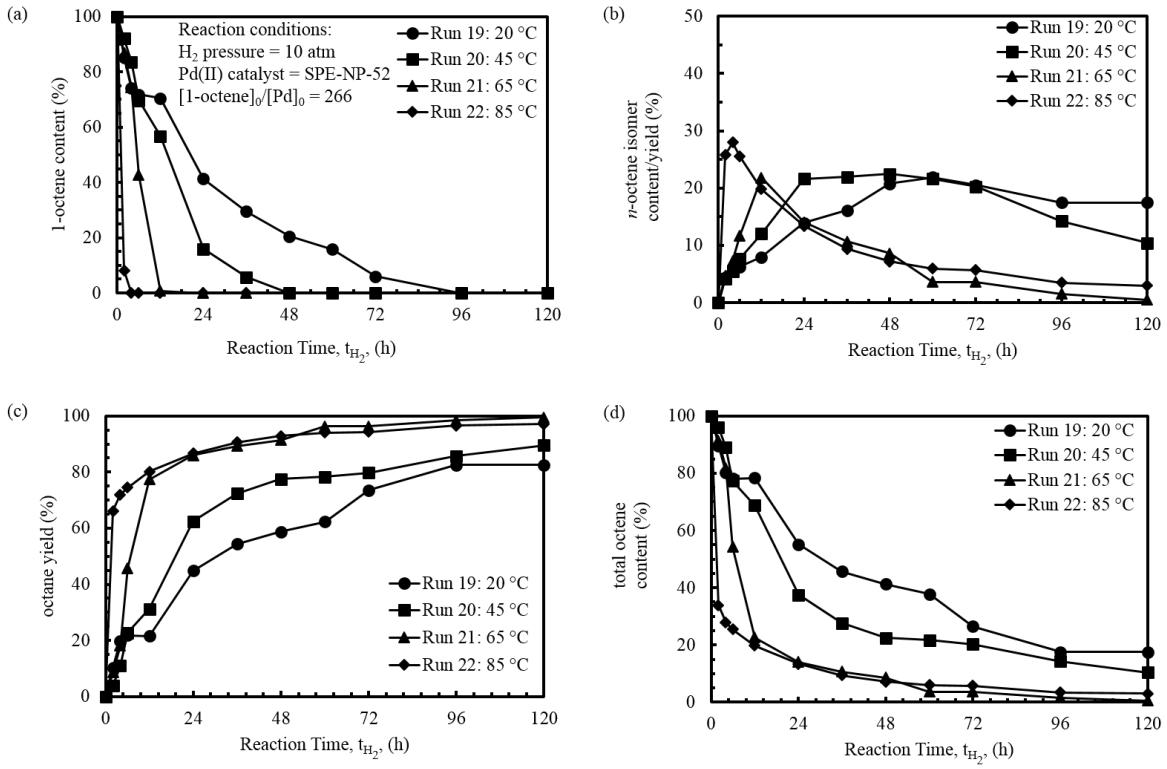

Figure 4.3 Kinetic plots of the hydrogenation/isomerization reactions of 1-octene catalyzed by Pd(II)-encapsulated SPE-NP-52 at 10 atm H_2 demonstrating the effect of reaction temperature on 1-octene content (a), *n*-octene isomer content/yield (b), octane yield (c), and total octene content (d).

Figure 4.3 compares the kinetic plots of Runs 19–22 demonstrating the effect of different reaction temperatures (20, 45, 65, and 85 °C) on the contents/yields of 1-octene (a), *n*-octene isomers (b), octane (c), and total octenes (d). As expected, the hydrogenation (R_{H2}) and isomerization rates (R_{isomer}) are significantly enhanced when reaction temperature is increased, particularly when elevated over 45 °C. This trend is clearly observed in all four plots. At high reaction temperatures of 65 °C and 85 °C, complete conversion of 1-octene was reached at t_{H_2} = 12 h and 4 h, respectively. On the contrary, much longer reaction times, t_{H_2} = 96 h and 48 h, were required to completely convert 1-octene at 20 °C and 45 °C, respectively. Despite these very different reaction times, 1-octene was completely converted into similar contents of residual *n*-octene isomers and octane within

narrow ranges of 18–28 % and 72–82 %, respectively. These results confirm the enhancement in R_{H_2} and R_{isomer} and also indicate that R_{H_2} is relatively higher than R_{isomer}.

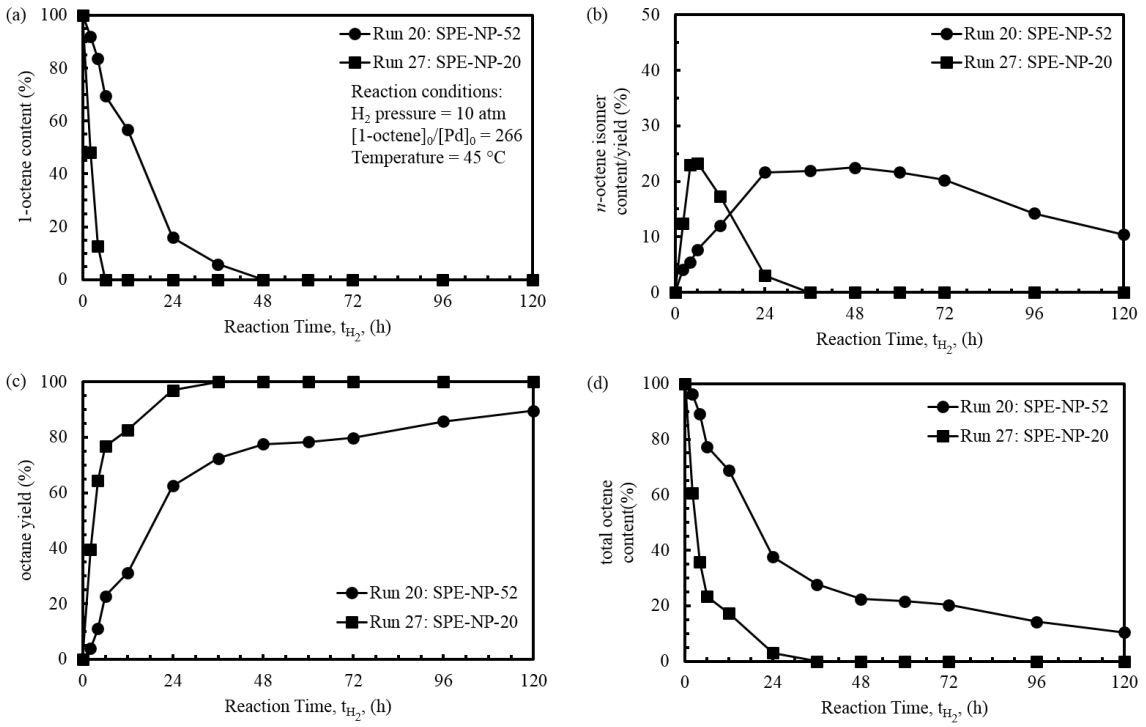

Figure 4.4 Kinetic plots of the hydrogenation/isomerization reactions of 1-octene catalyzed by two different Pd(II)-encapsulated SPE-NP having HBPE arms (Run 20) and LBPE arms (Run 27) under 10 atm H_2 at 45 °C, showing the different effects on 1-octene content (a), *n*-octene isomer content/yield (b), octane yield (c), and total octene content (d).

By comparing 1-octene hydrogenation/isomerization reactions in Runs 20 and 27 carried out at identical conditions (10 atm H_2/45 °C, avg. $[1\text{-octene}]_0/[Pd]_0 = 266$), we can compare the effect of having hyperbranched and densely packed linear-branched PE shells on the activity of Pd(II)-catalysts encapsulated in SPE-NP-52 (i.e., f_n = 79 arms/star) and SPE-NP-20 (i.e., f_n = 391), respectively. Figure 4.4 shows the kinetic plots demonstrating the contents of 1-octene (a), *n*-octene isomers (b), hexane (c), and total octenes (d), for these two runs and compares the use of different SPE-NP-catalysts. From these results, the

catalytic performance of SPE-NP-20 (Run 27) is superior to that of SPE-NP-52 (Run 20) for the hydrogenation of 1-octene and its produced isomers. The relative R_{H_2} and R_{isomer} both seemingly increase in Run 27, as evidence by the complete conversion of 1-octene and max iosmer yield = 23 % after only t_{H_2} = 6 h compared to residual 70 % 1-octene at the same reaction time and max isomer yield = 22–23% reached after t_{H_2} = 24–48 h in Run 20. Though reached at different t_{H_2}, the maximum isomer content (23%) is the same in both runs catalyzed with different SPE-NPs. These results indicate that increasing H_2 pressure has a positive effect on enhancing of both R_{H_2} and R_{isomer} and it also further confirms the higher R_{H_2} compared to $R_{isomser}$.

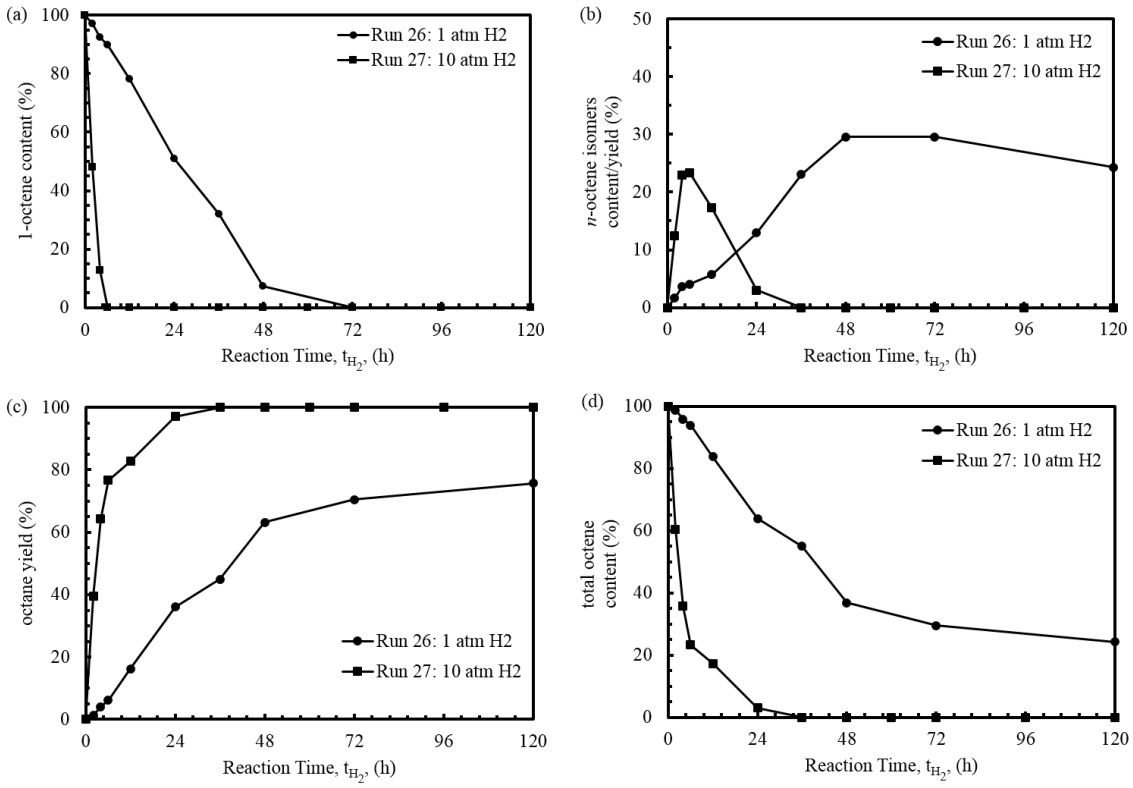

Figure 4. 5 Kinetic plots of the hydrogenation/isomerization reactions of 1-octene catalyzed by Pd(II)-encapsulated SPE-NP having LBPE arms at 45 °C, showing the effect of H_2 pressure on 1-octene content (a), *n*-octene isomer content/yield (b), octane yield (c), and total octene content (d).

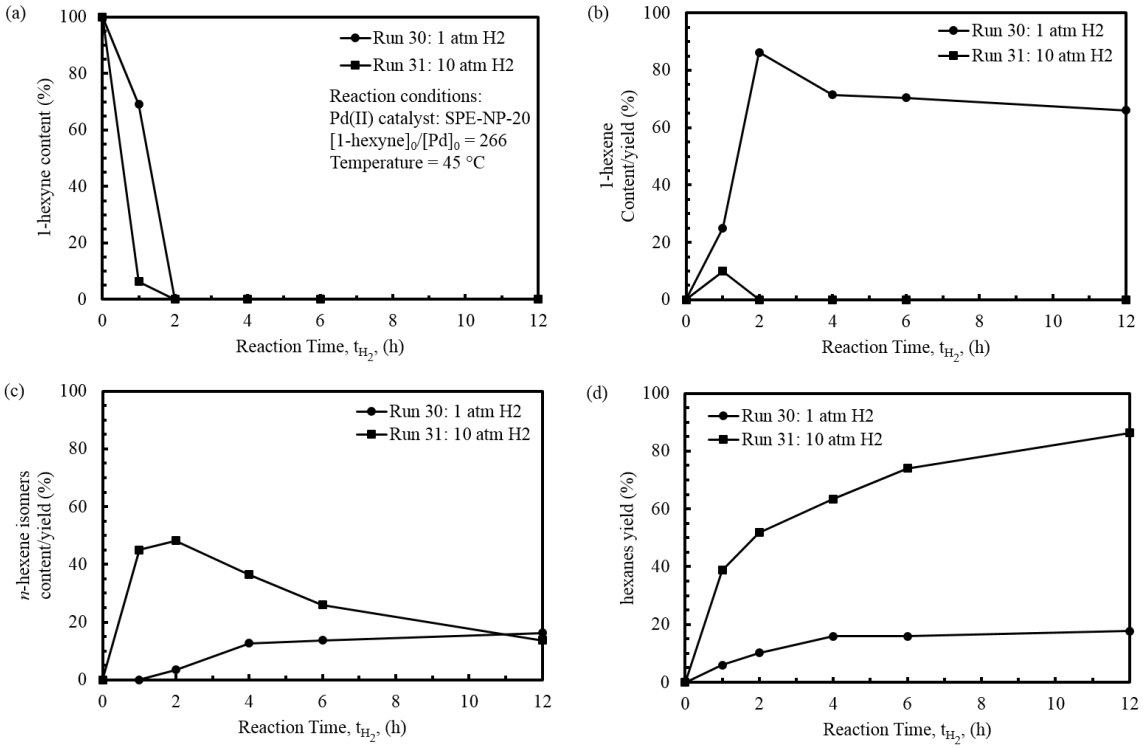

Figure 4. 6 Kinetic plots of the hydrogenation/isomerization reactions of 1-hexyne catalyzed by Pd(II)-encapsulated SPE-NP having LBPE arms at 45 °C, showing the effect of H_2 pressure on 1-hexyne content (a), 1-hexene content/yield (b), *n*-hexene isomer content/yield (c), and hexane (d).

To further control the competition between hydrogenation and isomerization reaction, we aimed to reduce R_{H_2} and improve R_{isomer} by conducting the reactions at lower H_2 pressure (1 atm) and lower reaction temperature (45 °C), thus increasing alkene isomer yields/content. Figure 4.5 shows a comparison of the kinetic plots for 1-octene hydrogenation/isomerization reactions catalyzed by Pd(II)-catalysts encapsulated in SPE-NP-20 carried out at 1 and 10 atm H_2/45°C in Runs 26 and 27, respectively. By first observing the kinetic plots for 1-octene (a), *n*-octene isomers (b), octane (c), and total octenes (d), we can clearly see that higher H_2 pressure (10 atm) in Run 27 resulted enhanced R_{H_2} and R_{isomer} compared to Run 26. This is supported by the fast t_{H_2} = 6 h required in Run

27 to completely convert 1-octene into *n*-octene isomers (23%) and hexane (77%). On the contrary, in Run 26 carried out at lower H_2 pressure (1 atm), it took over 48 h to complete convert 1-octene. However, this reduction in H_2 pressure resulted in more competitive R_{H_2} and R_{isomer}, as shown by the progressive increase and higher isomer content from 0-30 % at t_{H_2} = 0–48 h compared to Run 27.

The effect of H_2 pressure on the kinetics of terminal alkyne (1-hexyne) reaction with Pd(II)-encapsulated SPE-NP-20 were also investigated in Runs 30 and 31 carried out at 1 and 10 atm/45°C, respectively. Figure 4.6 compares the kinetic plots for the contents/yields of 1-hexyne (a), 1-hexene (b), *n*-hexene isomer (c), and hexane (d), for both runs. At both low and high H_2 pressure (1 and 10 atm), we observe from these plots a fast semi-hydrogenation reaction (t_{H_2} = 2 h) of 1-hexyne into 1-hexene followed by fast hydrogenation and isomerization reactions yielding hexane and *n*-hexene isomers, respectively. After t_{H_2} = 2 h at low H_2 pressure, the 1-hexene content in Run 30 is high (86 %) while *n*-hexene isomer and hexane contents are low (4 and 10%, respectively). Differently, at the same reaction time (2 h) but high H_2 pressure, the 1-hexene content is 0 % but interestingly, *n*-hexene isomer yield is 48 % while hexane is 52 %. These results suggest a very fast semi-hydrogenation reaction of 1-hexyne into 1-hexene, which is then quickly hydrogenated or isomerized into hexane and *n*-hexene isomers, respectively.

As observed in the 1-octene reactions of Runs 26 and 27, the R_{H_2} and R_{isomer} are significantly increased when H_2 pressure is increased, thus the yield/contents of hexane and *n*-hexene isomers are higher in Run 31 (carried out at 10 atm H_2) than in Run 30 (1 atm H_2). However, at the same reaction conditions, the relative R_{H_2} and R_{isomer} are lower in 1-octene reactions compared to 1-hexene due to its longer carbon chain that increases the steric hindrance, thus reducing dissolution speed to the active centre.[131-132, 144]

^{13}C NMR was then performed on the 1 h sample of Run 31 containing 1-hexyne (6 %), 1-hexene (10 %) and *n*-hexene isomers (45 %) to verify their contents and determine the types of isomers produced. Figure 4.7 shows the annotated peaks of the ^{13}C NMR spectrum along with their corresponding chemical structures including, anisole internal

standard, 1-hexyne, 1-hexene, *cis*-2-hexene, and *trans*-2-hexene. The ^{13}C resonance signals are as follows: internal standard, anisole peaks: *a* (159.6 ppm), *j* (113.9 ppm), *e* (129.5 ppm), *h* (120.7 ppm), and *m** (55.1 ppm, which was used as the reference peak in chemical shift normalization); 1-hexyne: *l* (68.0 ppm) and *k* (84.7 ppm); 1-hexene: *i* (114.1 ppm) and *b* (139.2 ppm); *trans*-2-hexene: *f* (124.8 ppm) and *c* (131.5 ppm); and *cis*-2-hexene: *g* (123.8 ppm) and *d* (130.6 ppm).

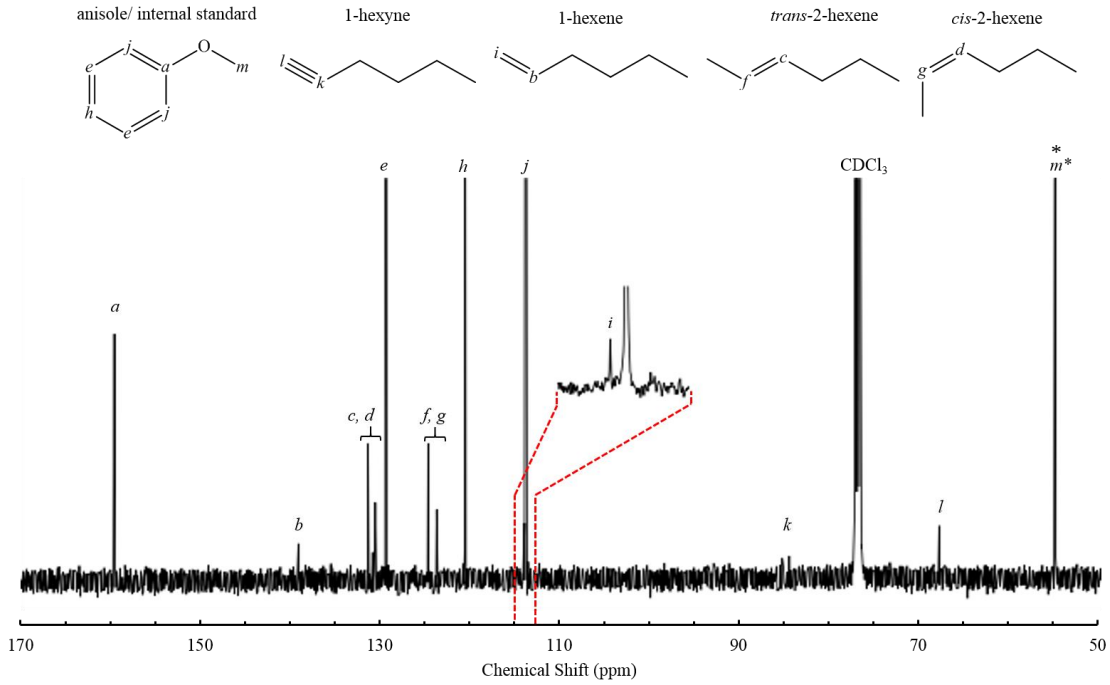

Figure 4. 7 ^{13}C NMR identification of 1-hexyne, 1-hexene, and *n*-hexene isomers present in Run 31's 1 h sample of the hydrogenation reaction of 1-hexyne and consecutive hydrogenation/isomerization reaction of as-produced 1-hexene/*n*-hexene isomers catalyzed by Pd(II)-encapsulated SPE-NP-20 at 10 atm H_2/45°C.

The percent content of the different products and reactants were calculated based on the relative intensity of their ^{13}C resonance peaks. The initial amount of 1-hexyne is the same as the internal standard anisole (added in equimolar amount) thus the integration of

peak ***a*** was used as reference. According to this, the contents of residual 1-hexyne, 1-hexene, and *n*-hexene isomers are 6, 10, and 40 % respectively. These results are nearly the same as those percent yields calculated from ^{1}H NMR results. In addition, the signal intensity for *trans*-2-hexene isomer is twice that of the *cis*-2-hexene isomer and thus, their contents are 27 and 13 %, respectively. This difference in isomers demonstrates the lower steric barriers involved in producing *trans*-isomers. [131-132, 144]

These results indicate a competition between hydrogenation and isomerization reactions[137], whereby the R_{H_2} appears to be faster than the R_{isomer}. We postulate that the Pd(II)-catalyzed mechanisms responsible for the hydrogenation and isomerization reactions herein are similar to those proposed by Spencer et al.[145] and Brookhart et al. [30-35], respectively. Figure 4.8 shows a schematic representation of the proposed mechanism in these reactions.

In the first step of the hydrogenation reaction, the Pd(II) metal centre encapsulated in the SPE-NPs coordinates with the terminal double bond of 1-alkene forming an intermediate π-complex which is then activated by H_2 coordination yielding a dihydrido-Pd-alkene species (complex **18** in Figure 4.8). Fast equilibrium then follows, due to the instability of **18**, by which one of its hydrides (H^-) is rapidly added to the more electron-deficient α-carbon of 1-alkene (i.e., α-hydride addition), thus yielding a more stable monohydrido-Pd-alkyl complex (**19**). This complex will predominantly catalyze the hydrogenation reaction (i.e., faster R_{H2}) by adding the other H^- to the alkene (i.e., β-hydride addition), thus yielding the alkane or it can proceed with the competing isomerization reaction at a mediocre R_{isomer}.

The isomerization reaction is possible when the lifetime of the monohydrido-Pd-alkyl complex (**19**) is sufficiently long to allow fast alkyl bond rotations (fast R_{isomer}) and stabilizations by either γ-hydrogens via coordination to Pd(II) centre which yields intermediates **21**. Upon γ-hydride elimination, naked dihydrido-Pd(II) species are generated and quickly stabilized by either 1-alkene or an alkene isomer following two possible pathways. The first consists of 1-alkene associative exchanges to the Pd(II) metal centres to release *cis*-2- and/or *trans*-2-alkene isomers and regenerate **18**. In the case of

alkene isomer coordination, the formed dihydrido-Pd(II)-alkene-isomer complexes **22** undergo fast β-hydride re-addition (yielding monohydrido-Pd-alkyl complex **23**) followed by fast γ-hydride addition to produce alkanes and finally regenerate the polymer-supported catalyst.

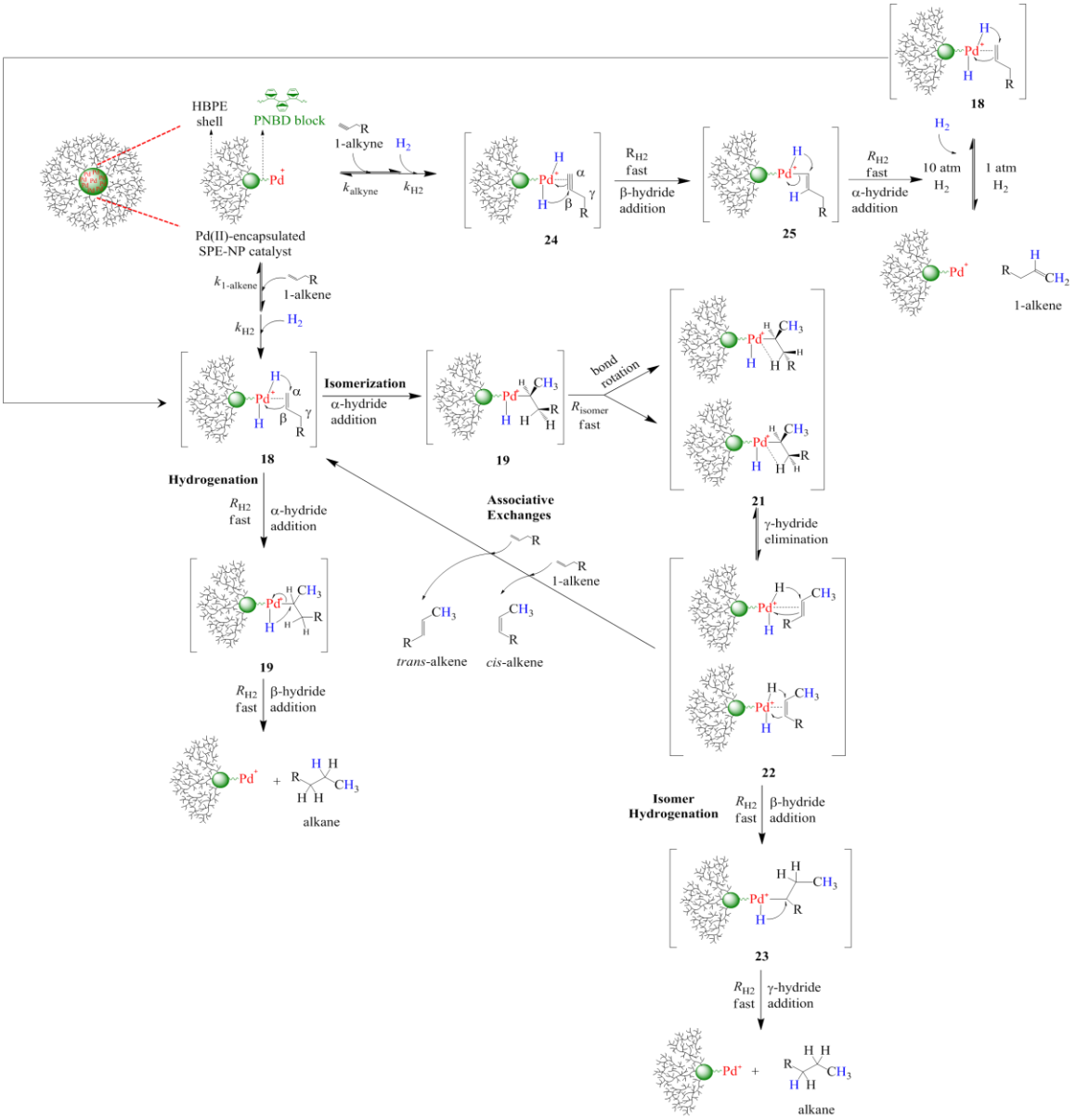

Figure 4.8 Schematic representation of the possible mechanisms for terminal alkyne semi-hydrogenation reaction and alkene hydrogenation/isomerization reactions [30-35, 130-131, 144-145] catalyzed by homogeneous Pd(II)-encapsulated SPE-NPs under H_2 atmosphere. Hydrogens from H_2 gas involved in the hydrogenation reaction are colored in blue.

This isomerization process is very similar to the well-known Pd-diimine catalyzed chain walking ethylene polymerization mechanism, involving β-hydride elimination, bond rotation, and hydride re-addition (scheme represented in Figure 1.4).[30-35] The isomers formed in our reactions are presumed to be released by associative exchanges with terminal alkenes which stabilizes the dihydrido-Pd(II) species, on the basis that the association rate constant of 1-alkene ($k_{1\text{-alkene}}$) should be higher than the isomers' (k_{isomer}) due to the increased steric congestion around the internal double bonds. Previous studies on polymer-supported-Pd(II)-catalyzed hydrogenation of reactions of various olefins (including, terminal and internal olefins of different lengths, cyclic olefins, and cyclic dienes) have shown significant variations in relative reactivity due to the structure and position of the double bond. Longer chain olefins such as, 1-heptene and 1-octene, and internally positioned olefins such as, ethyl oleate and diethyl fumarate, had lower relative reactivity compared to 1-hexene based on the Pd-alkene formation ability of the substrate.[131-132, 144]

The 1-alkyne semi-hydrogenation reaction mechanism is presumed to be similar to that of the 1-alkene hydrogenation. The terminal alkyne and H_2 would coordinate with the star polymer-encapsulated Pd(II) catalysts to produce the active dihydrido-Pd(II)-alkyne complex (**24**). This active species would quickly add a H^- to the more electron deficient β-carbon of the alkyne yielding a monohydrido-Pd(II)-alkene intermediate (**25**) which further adds its other H^- to the α-carbon and thus yields the 1-alkene. At higher H_2 pressure (i.e., 10 atm) the concentration of H_2 around the catalytic centre is higher than at low pressure (i.e., 1 atm), therefore favoring the equilibrium generating the dihydrido-Pd(II)-alkene complex **18**. This complex may preferentially enter either the hydrogenation or isomerization pathways depending on the reaction conditions.

According to our proposed mechanism and the results obtained in Runs 19–22, 26, 27, 30, and 31, the H_2 conditions employed are sufficient to generate the dihydrido-Pd-alkyl complex (**18**) suspected to be catalytically active in both hydrogenation and isomerization reactions. The higher yields of alkanes (i.e., octane and hexane) compared to *n*-alkene isomers (i.e., *n*-octene and *n*-hexene isomers) obtained in all these confirms the R_{H2} to be higher than R_{isomer}. The results obtained in our investigations of temperature and

H_2 pressure on 1-octene hydrogenation/isomerization, indicate that increasing these reaction parameters has a significant enhancement in both R_{H_2} and R_{isomer}.

4.2 Recyclable Star Polymer-Encapsulated Pd-Catalysts for Heck Carbon–Coupling Reaction

Preliminary studies on the use of the two different Pd(II)-encapsulated SPE-NPs (20 and 52) selected above were investigated in the recyclable cross-coupling Heck reaction of iodobenzene (IBz) and *n*-butyl acrylate (BA) carried out in toluene (3 mL) at 100 °C for t_{Heck} = 0–24 h. A typical Heck reaction mixture contained initial molar amounts of IBz, BA, and NEt_3, $[IBz]_0$:$[BA]_0$:$[NEt_3]_0$ = 1:1.5:1.5 with average initial IBz concentrations, $[IBz]_0$ = 0.58 M for Runs catalyzed by SPE-NP-20 and -52, respectively. Figure 4.9 demonstrates the Heck reaction equation investigated in this section. The two star polymer encapsulated catalysts tested were found to be efficient in these Heck reactions.

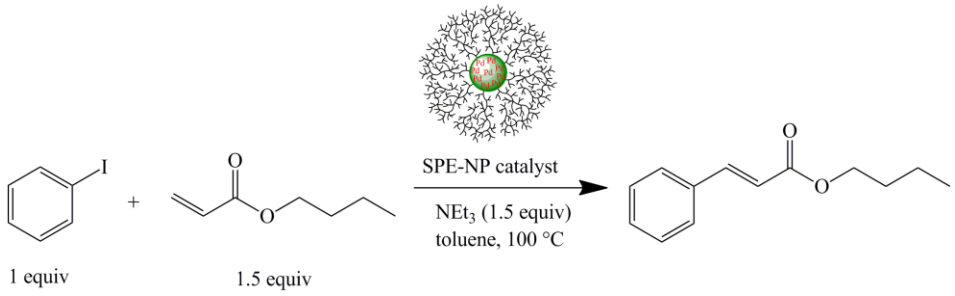

Figure 4.9 Carbon-carbon coupling Heck reaction of iodobenzene and *n*-butyl acrylate catalyzed by Pd(II)-encapsulated SPE-NP catalysts.

Figure 4.10 shows the ^{1}H NMR spectra at t_{Heck} = 16 and 24 h for the Heck reactions catalyzed by SPE-NP-20 (a) and SPE-NP-52 (b). The product yield in these reactions was determined based on ^{1}H NMR integration of the resonance signals A (at 6.18–6.21 ppm, 1 H) and **a** (at 6.22–6.26 ppm, 1 H) arising from analogous vinyl protons of the excess

reactant, BA, and the coupling product, respectively. The peak integrations were normalized by peaks B (at 4.00–4.03 ppm, 2 H) and **b** (at 3.95–3.98 ppm, 2 H). BA conversion was determined by the increase in the integration of the resonance signal arising from the vinyl proton of yielded product (I_a) divided by the combined integration for the resonance peaks of vinyl proton of unreacted BA (I_A) and the final product (I_a). IBz conversion, which corresponds to the product yield, was then calculated using Equation 2.16 simply by multiplying the BA conversion by its molar excess factor of 1.5.

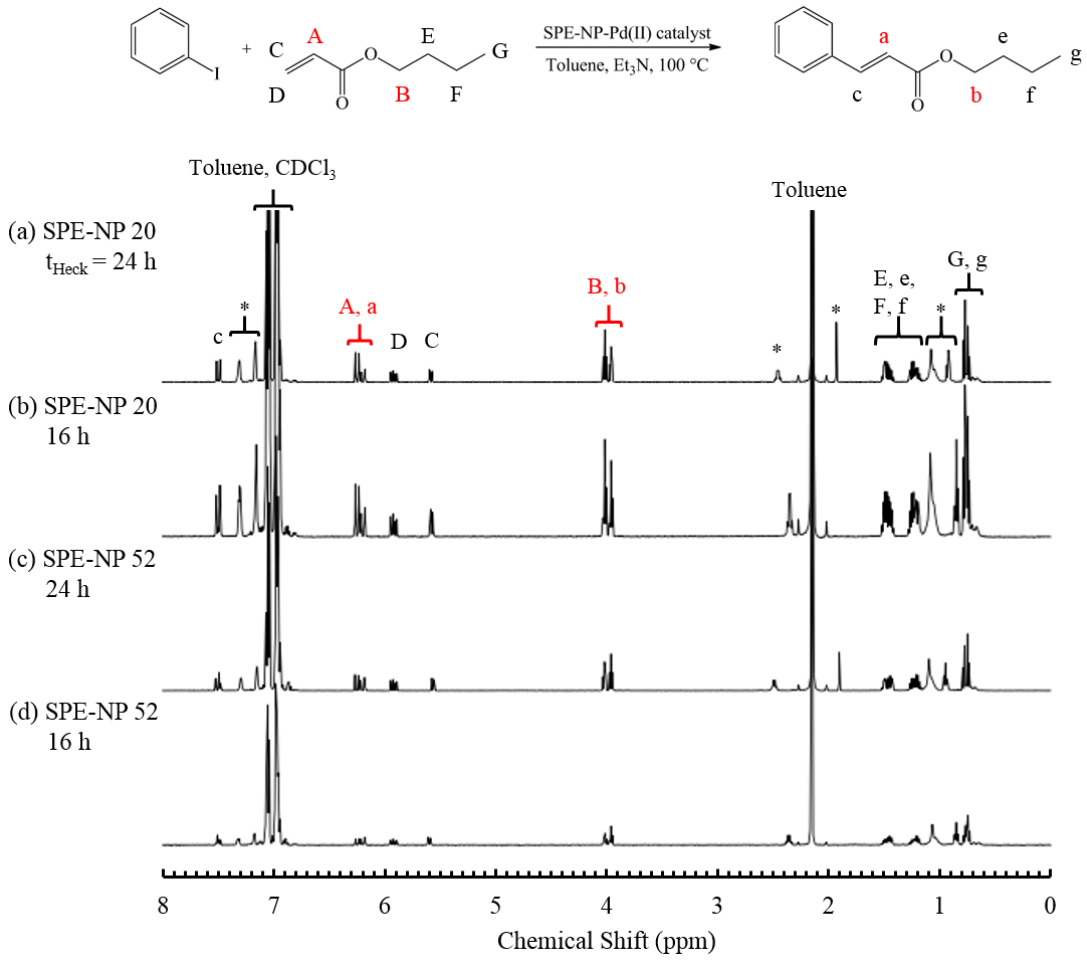

Figure 4.10 ^{1}H NMR analysis of cycle I's carbon-carbon coupling Heck reaction sample of *n*-butyl acrylate and iodobenzene catalyzed by two different Pd(II)-encapsulated star polyethylene nanoparticles, SPE-NP-20 (a, b) and SPE-NP-52 (c, d) at 16 h and 24 h (t_{Heck}), respectively.

Both SPE-NPs tested were found to be efficient recyclable catalysts for this Heck coupling reaction. Figure 4.11 shows the conversion results for IBz (representing product yield) as a function of t_{Heck} for cycles III–VI catalyzed by recycled SPE-NP-20 (a) and SPE-NP-52 (b). ^{1}H NMR data obtained in this recyclability study are summarized in Table 4.3. Even after being recycled six times, both SPE-NP catalysts still converted over 90 % of the initial IBz concentration. There is a slight reduction in catalytic performance as the number of recycles increase. This is probably due to the visible/considerable precipitation of Pd(0) black. This indicates some Pd(II) species leaching out of the cross-linked PNBD cores of the SPE-NPs.

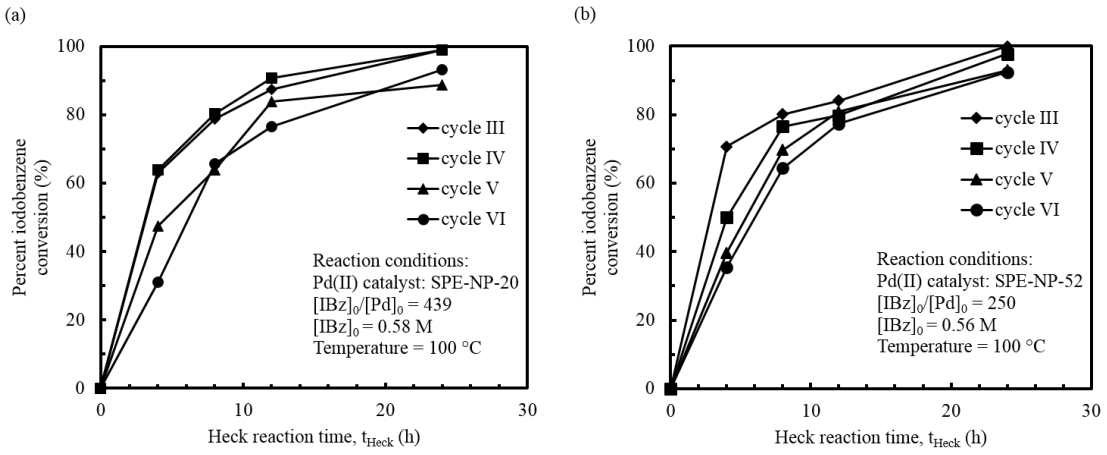

Figure 4.11 Kinetic plots showing the percent iodobenzene conversion results as a function of reaction time for cycles II-V of Heck coupling reaction with *n*-butyl acrylate catalyzed by recycled Pd-encapsulated SPE-NP-20 (a) and SPE-NP-52 (b). Other reaction conditions: initial molar ratios of IBz, *n*-BA, and triethylamine $[IBz]_0:[BA]_0:[NEt_3]_0$ = 1:1.5:1.5; solvent, toluene (3 mL); total volume, 4.344 mL

Interestingly, evidence has emerged reporting that the active Pd(II) species are the ones leached into the reaction mixture.[104, 117, 121, 146-147] Our group recently reported similar results in which disulphide-functionalized HBPEs were used as homogeneous supports for Pd(II) catalysts.[65] We found that high disulfide contents in the HBPEs resulted in lower

Heck reaction activities. However, their recyclability study after five cycles demonstrated good catalytic performance of these supported catalysts with average IBz conversion of 86 % and low Pd(0) leaching ranging from c.a. 7–10 %.[65] Given the preliminary stage of these experiments, the exact amount of Pd(0) leached was not determined but could be investigated by atomic absorption spectroscopy in future work. The results obtained herein are still consistent with literature reports but the visible Pd(0) black leaching from these SPE-NPs is undesirable for recyclability purposes. Nonetheless, with further research and development, these core-cross-linked SPE-NPs have good potential in catalytic applications as homogenous supports for Pd(II) catalysts.

Table 4.3. Carbon–Carbon Cross-Coupling Heck Reaction of Iodobenzene and *n*-Butyl Acrylate Catalyzed by Two Different Pd(II)-Encapsulated Star Polyethylene Nanoparticles: Recyclability Study of Heck Reaction Cycles I–VI

SPE-Pd(II)-catalysts	mass of SPE-NP (g)	Pd(II) content[b] (μmol)	Avg. $[IBz]_0$ (mol/L)	Avg. $[BA]_0/[Pd]_0$ molar ratio	Avg. $[IBz]_0/[Pd]_0$ molar ratio	Temp (°C)	t_{Heck} (h)	Percent product yield (%) [a] Heck reaction cycle I	II	III	IV	V	VI
SPE NP-20	0.1	6	0.58	439	633	100	4	–	–	63	64	47	31
							8	–	–	79	80	64	66
							12	–	–	87	91	84	77
							16	58	86	–	–	–	–
							24	67	92	99	99	89	93
SPE NP-52	0.1	10	0.56	250	379	100	4	–	–	70	50	40	35
							8	–	–	80	77	70	64
							12	–	–	84	80	81	77
							16	86	88	–	–	–	–
							24	91	94	100	98	93	92

Other reaction conditions: initial molar ratios of iodobenzene, *n*–butyl acrylate, and triethylamine, $[IBz]_0:[BA]_0:[NEt_3]_0$ = 1:1.5:1.5; solvent, toluene (3 mL); total volume, 4.344 mL. [a] Product yield determined from the ^{1}H NMR integration signals arising from vinyl protons of the BA reactant (I_A) and Heck coupling product (I_a) calculated using Equation 2.16. [b] Estimated Pd(II) content was calculated by dividing the mass of the SPE-NP (g) used in the Heck reaction by the M_n (g/mol) of its PE arm multiplied by the star yield (Equation 2.1).

CHAPTER 5: Summary, Conclusions, and Future Work

A wide range of narrow-distributed high molecular weight SPE-NPs (i.e., as high as M_n = 11, 900 kg/mol, PDI = 1.81) having average arm numbers (up to f_n = 871) and relatively good yields (up to 85 %) have been conveniently synthesized via arm-first Pd–diimine-catalyzed living ethylene polymerization using NBD as core cross-linking agent. Star formation was found to take place during conventional polymer purification processes, namely, H^+/MeOH precipitation and high temperature drying. We demonstrated control over star parameters including M_n, M_w, f_n, star yield, D_h, PE arm length and topology, through an extensive systematic investigation in every step of the SPE-NP synthesis. This entailed the effects of ethylene polymerization conditions (i.e., C_2H_4 pressure and t_E), NBD-step reaction conditions (i.e., $[NBD]_0/[\mathbf{1}]_0$ and t_{NBD}), precipitation method (i.e., H^+/MeOH vs. MeOH only), and drying conditions (i.e., temperature and t_d) on the formation of star polymer nanoparticles.

NBD was accidentally discovered as a very efficient cross-linker in the formation of SPE-NPs. Given the scarce literature information Pd-diimine catalyzed NBD polymerizations, mechanistic studies were conducted through *in situ* ^{1}H NMR NBD homopolymerizations and NBD-ethylene copolymerizations in order to elucidate NBD's role in this arm-first approach to SPE-NPs. When added to the ethylene polymerization mixture in large molar excess, NBD is quickly coordinated to Pd-diimine catalysts growing the living PE arms and it oligomerized (c.a. 3 repeat units/PE arm) to render PE-*b*-PNBD block copolymer arms. When precipitated in H^+/MeOH, it is proposed that the PNBD core-crosslinking reaction is catalyzed by Pd^{2+} species, which are generated during H^+/MeOH precipitation. Increasing the drying temperature and time (i.e., 120 °C and 6 h) accelerates the star formation process and enhances star parameters.

The applications of the SPE-NPs containing self-encapsulated Pd species were investigated in catalytic olefin hydrogenation/isomerization reactions and carbon-carbon coupling Heck reaction. They were found to be effective in the hydrogenation/isomerization and semi-hydrogenation reaction of 1-octene and 1-hexyne, respectively. At higher H_2 pressure and temperature (i.e., 10 atm H_2/45-85 °C), terminal

double bonds of 1-octene and triple bonds of 1-hexyne were quickly converted (i.e., t_{H_2} = 2-12 h) into octane, *n*-octene isomers, and hexane, 1-hexene, and *n*-hexene isomers, respectively. From ^{13}C NMR analysis, it was determined that the *trans*-2-hexene isomer content is higher than the *cis*-2-hexene. The recyclability and efficiency of the SPE-NPs was also confirmed in preliminary Heck coupling reactions of IBz and BA with over 90% IBz conversion after recycling six times. Further experiments are required to determine the amount of Pd leached after every Heck reaction. The initial/total amount of Pd(II)-encapsulated in the SPE-NP would first be determined via AAS by burning the polymer and dissolving the Pd in acid solution and similarly, the Pd(0) black precipitate obtained after the Heck reaction would be dissolved and analyzed in the same way. From AAS results, the leached Pd could then be calculated.

On the other hand, these SPE-NPs may also serve as suitable nanocontainers in nanomedical applications. Preliminary experiments utilizing a functionalized Pd-diimine catalyst enabled the synthesis of SPE-NPs having multiple PE arms end-capped with 2-bromoisobutyryl group active for ATRP. These star polymers may be used as macro-multifunctional initiators for ATRP of biocompatible, pH responsive, or thermo-responsive polymers, thus producing a two-shell star-structured nanoparticle possessing amphiphilic properties of hydrophilic outer shell and hydrophobic inner shell.

In conclusion, the work presented in this thesis is specialized to the synthesis of architecturally complex PEs and provides a convenient method to synthesize star-structured PE-NPs. Systematic examination of every reaction parameter offers future researchers a well-defined method to easily control/tune SPE characteristics to specific applications. It also gives practical insight into the catalytic potential of these SPE-NPs which encapsulate active Pd(II) species. On a last note, the hallmark of this method is undoubtedly the Pd-diimine catalyst's outstanding polymerization features (which separates it from other late-transition metal catalysts) including its living chain walking ethylene polymerization ability. Furthermore the Pd-diimine catalyst's remarkable resistance to oxophilic poisoning enables facile functionalization of PEs with polar functional groups. Having the Pd-diimine catalysts as part of the polymer chemist's arsenal

of tools, allows unprecedented innovative possibilities that stretch the scope of nanotechnological applications of ethylene based polymers and copolymers.

References

1. Malpass, D.B., *Introduction to Industrial Polyethylene: Properties, Catalysts, and Processes*2010, Scrivener Publishing LCC and John Wiley & Sons, Inc.: USA.

2. Sittig, M. Polyolefin Production Processes, Latest Developments 1976, New Jersey: Noyes Data Corporation.

3. Peacock, A.J. Handbook of Polyethylene Structures, Properties, and Applications 2000, New York, USA: Marcel Dekker, Inc.

4. Carraher, C.E.J. Polymer Chemistry 2003, New York, USA: Marcel Dekker, Inc.

5. Bersted, B.C., S. A. Polyolefin Resins, 2012.

6. Doak, K.W.J., D. E.; Beach, D. L.; Kissin, Y. V.; Coughlan, J. J.; Hug, D. P. Concise Encyclopedia of Polymer Science and Engineering 1990, USA: Wiley-Interscience.

7. Consultants, I. Advanced Polyolefins: The Competitive Position 2000, London: IAL Consultants. 170.

8. Harper, C.A.P., E. M. Plastics Materials and Processes: A Concise Encyclopedia 2003, USA: Wiley-Interscience.

9. Whelan, T., *Polymer Technology Dictionary*1994, Chapman & Hall: London, UK.

10. Ross, J.F.M., J. L., *Polymeric Materials Encyclopedia*1996, CRC Press. p. 5953-5965.

11. Boor, J. Ziegler-Natta Catalysts and Polymerization 1979, New York: Academic Press.

12. Soares, J.B.P.K., J. K.; Rempel. G. L. . Ind. Eng. Chem. Res. 1997, **36**,

13. Mülhaupt, R. Macromol. Chem. Phys. 2003, **204**,

14. Kroschwitz, J.I., *Kirk-Othmer Encyclopedia of Chemical Technology*2007, John Wiley & Sons, Inc.: New Jersey. p. 502-506.

15. Galli, P. and Vecellio, G. *Technology: driving force behind innovation and growth of polyolefins.* Prog. Polym. Sci. 2001, **26**, 1287-1336.

16. Kaminsky, W. *The discovery of metallocene catalysts and their present state of the art.* J. Polym. Sci., Part A: Polym. Chem. 2004, **42**, 3911-3921.

17. Kaminsky, W. Macromol. Chem. Phys. 1996, **197**,

18. Kaminsky, W. J. Polym. Sci. Part A: Polym. Chem. 2004, **42**,

19. Hamielec, A.E.S., J. B. P. Prog. Polym. Sci. 1996, **21**,

20. Chen, E.Y.-X. and Marks, T.J. *Cocatalysts for metal-catalyzed olefin polymerization: activators, activation processes, and structure-activity relationships.* Chem. Rev. (Washington, D. C.) 2000, **100**, 1391-1434.

21. Soares, J.B.P., Kim, J.D., and Rempel, G.L. *Analysis and Control of the Molecular Weight and Chemical Composition Distributions of Polyolefins Made with Metallocene and Ziegler-Natta Catalysts.* Ind. Eng. Chem. Res. 1997, **36**, 1144-1150.

22. Chen, E.Y.X. *Coordination Polymerization of Polar Vinyl Monomers by Single-Site Metal Catalysts.* Chem. Rev. (Washington, DC, U. S.) 2009, **109**, 5157-5214.

23. Gibson, V.C. and Spitzmesser, S.K. *Advances in non-metallocene olefin polymerization catalysis.* Chem. Rev. (Washington, DC, U. S.) 2003, **103**, 283-315.

24. Ittel, S.D., Johnson, L.K., and Brookhart, M. *Late-Metal Catalysts for Ethylene Homo- and Copolymerization.* Chem. Rev. (Washington, D. C.) 2000, **100**, 1169-1203.

25. Nomura, K. *Recent developments in oligomerization of olefins by homogeneous nickel and palladium catalysts.* Recent Res. Dev. Pure Appl. Chem. 1998, **2**, 473-513.

26. Rix, F.C. and Brookhart, M. *Energetics of Migratory Insertion Reactions in Pd(II) Acyl Ethylene, Alkyl Ethylene, and Alkyl Carbonyl Complexes.* J. Am. Chem. Soc. 1995, **117**, 1137-1138.

27. Peuckert, M. and Keim, W. *A new nickel complex for the oligomerization of ethylene.* Organometallics 1983, **2**, 594-597.

28. Johnson, L.K., Killian, C.M., and Brookhart, M. *New Pd(II)- and Ni(II)-Based Catalysts for Polymerization of Ethylene and α-Olefins.* J. Am. Chem. Soc. 1995, **117**, 6414-6415.

29. Deng, L., et al. *The Role of Bulky Substituents in Brookhart-Type Ni(II) Diimine Catalyzed Olefin Polymerization: A Combined Density Functional Theory and Molecular Mechanics Study.* J. Am. Chem. Soc. 1997, **119**, 6177-6186.

30. Mecking, S., et al. *Mechanistic Studies of the Palladium-Catalyzed Copolymerization of Ethylene and α-Olefins with Methyl Acrylate.* J. Am. Chem. Soc. 1998, **120**, 888-899.

31. Tempel, D.J., et al. *Mechanistic studies of Pd(II)-α-diimine-catalyzed olefin polymerizations.* J. Am. Chem. Soc. 2000, **122**, 6686-6700.

32. Shultz, L.H., Tempel, D.J., and Brookhart, M. *Palladium(II) β-Agostic Alkyl Cations and Alkyl Ethylene Complexes: Investigation of Polymer Chain Isomerization Mechanisms.* J. Am. Chem. Soc. 2001, **123**, 11539-11555.

33. Dong, Z. and Ye, Z. *Hyperbranched polyethylenes by chain walking polymerization: synthesis, properties, functionalization, and applications.* Polym. Chem. 2012, **3**, 286-301.

34. Guan, Z., et al. *Chain walking: a new strategy to control polymer topology*. Science (Washington, D. C.) 1999, **283**, 2059-2062.

35. Michalak, A. and Ziegler, T. *Palladium-Catalyzed Polymerization of Propene: DFT Model Studies.* Organometallics 1999, **18**, 3998-4004.

36. Morgan, S., et al. *One-pot synthesis of hyperbranched polyethylenes tethered with pendant acryloyl functionalities by chain walking copolymerizations.* Macromol. Chem. Phys. 2008, **209**, 2232-2240.

37. Zhang, K., et al. *Chain walking ethylene copolymerization with an ATRP inimer for one-pot synthesis of hyperbranched polyethylenes tethered with ATRP initiating sites.* Macromol. Rapid Commun. 2007, **28**, 2185-2191.

38. Wang, J., Ye, Z., and Joly, H. *Synthesis and Characterization of Hyperbranched Polyethylenes Tethered with Polyhedral Oligomeric Silsesquioxane (POSS) Nanoparticles by Chain Walking Ethylene Copolymerization with Acryloisobutyl-POSS.* Macromolecules (Washington, DC, U. S.) 2007, **40**, 6150-6163.

39. Gottfried, A.C. and Brookhart, M. *Living and Block Copolymerization of Ethylene and α-Olefins Using Palladium(II)-α-Diimine Catalysts.* Macromolecules 2003, **36**, 3085-3100.

40. Gottfried, A.C. and Brookhart, M. *Living Polymerization of Ethylene Using Pd(II) α-Diimine Catalysts.* Macromolecules 2001, **34**, 1140-1142.

41. Xiang, P. and Ye, Z. *Alternating, gradient, block, and block-gradient copolymers of ethylene and norbornene by Pd-Diimine-Catalyzed "living" copolymerization.* J. Polym. Sci., Part A: Polym. Chem. 2013, **51**, 672-686.

42. Liu, P., et al. *Synthesis and characterization of PE-b-POEGMA copolymers prepared by linear/hyperbranched telechelic polyethylene-initiated ATRP of oligo(ethylene glycol) methacrylates.* ACS Symp. Ser. 2012, **1101**, 39-64.

43. Liu, P., et al. *"Arm-First" Synthesis of Core-Cross-Linked Multiarm Star Polyethylenes by Coupling Palladium-Catalyzed Ethylene "Living" Polymerization with Atom-Transfer Radical Polymerization.* Macromolecules (Washington, DC, U. S.) 2011, **44**, 4125-4139.

44. Xu, Y., et al. *Hyperbranched-Linear Polyethylene Block Polymers Constructed with Chain Blocks of Hybrid Chain Topologies via One-Pot Stagewise Chain Walking Ethylene "Living" Polymerization.* Macromolecules (Washington, DC, U. S.) 2010, **43**, 8026-8038.

45. Xia, X., et al. *"Core-First" Synthesis of Multiarm Star Polyethylenes with a Hyperbranched Core and Linear Arms via Ethylene Multifunctional "Living" Polymerization with Hyperbranched Polyethylenes Encapsulating Multinuclear Covalently Tethered Pd-Diimine Catalysts.* Macromolecules (Washington, DC, U. S.) 2010, **43**, 4889-4901.

46. Li, S. and Ye, Z. *Synthesis of Narrowly Distributed ω-Telechelic Hyperbranched Polyethylenes by Efficient End-Capping of Pd-Diimine-Catalyzed Ethylene "Living" Polymerization with Styrene Derivatives.* Macromol. Chem. Phys. 2010, **211**, 1917-1924.

47. Zhang, K., Ye, Z., and Subramanian, R. *A Trinuclear Pd-Diimine Catalyst for "Core-First" Synthesis of Three-Arm Star Polyethylenes via Ethylene "Living" Polymerization.* Macromolecules (Washington, DC, U. S.) 2009, **42**, 2313-2316.

48. Zhang, Y. and Ye, Z. *Homogeneous polyhedral oligomeric silsesquioxane (POSS)-supported Pd-diimine complex and synthesis of polyethylenes end-tethered with a POSS nanoparticle via ethylene "living" polymerization.* Chem. Commun. (Cambridge, U. K.) 2008, 1178-1180.

49. Zhang, Y. and Ye, Z. *Covalent Surface Grafting of Branched Polyethylenes on Silica Nanoparticles by Surface-Initiated Ethylene "Living" Polymerization with Immobilized Pd-Diimine Catalysts.* Macromolecules (Washington, DC, U. S.) 2008, **41**, 6331-6338.

50. Zhang, K., Ye, Z., and Subramanian, R. *Synthesis of Block Copolymers of Ethylene with Styrene and n-Butyl Acrylate via a Tandem Strategy Combining Ethylene "Living" Polymerization Catalyzed by a Functionalized Pd-Diimine Catalyst with Atom Transfer Radical Polymerization.* Macromolecules (Washington, DC, U. S.) 2008, **41**, 640-649.

51. Guan, Z. *Recent Progress of Catalytic Polymerization for Controlling Polymer Topology*. Chem.--Asian J. 2010, **5**, 1058-1070.

52. Guan, Z. *Control of polymer topology through late-transition-metal catalysis.* J. Polym. Sci., Part A: Polym. Chem. 2003, **41**, 3680-3692.

53. Popeney, C. and Guan, Z. *Ligand Electronic Effects on Late Transition Metal Polymerization Catalysts.* Organometallics 2005, **24**, 1145-1155.

54. Ye, Z., AlObaidi, F., and Zhu, S. *Melt rheological properties of branched polyethylenes produced with Pd- and Ni-diimine catalysts.* Macromol. Chem. Phys. 2004, **205**, 897-906.

55. Ye, Z. and Zhu, S. *Newtonian Flow Behavior of Hyperbranched High-Molecular-Weight Polyethylenes Produced with a Pd-Diimine Catalyst and Its Dependence on Chain Topology.* Macromolecules 2003, **36**, 2194-2197.

56. Morgan, S., et al. *Higher-molecular-weight hyperbranched polyethylenes containing crosslinking structures as lubricant viscosity-index improvers.* Polym. Eng. Sci. 2010, **50**, 911-918.

57. Zhang, Y. and Ye, Z. *Homogeneous polyhedral oligomeric silsesquioxane (POSS)-supported Pd-diimine complex and synthesis of polyethylenes end-tethered with a POSS nanoparticle via ethylene "living" polymerization.* Chem Commun (Camb) 2008, 1178-1180.

58. Wang, J., Zhang, K., and Ye, Z. *One-Pot Synthesis of Hyperbranched Polyethylenes Tethered with Polymerizable Methacryloyl Groups via Selective Ethylene Copolymerization with Heterobifunctional Comonomers by Chain Walking Pd-Diimine Catalysis.* Macromolecules (Washington, DC, U. S.) 2008, **41**, 2290-2293.

59. Guan, Z. *Control of polymer topology by chain-walking catalysts.* Chem.--Eur. J. 2002, **8**, 3086-3092.

60. Hiemenz, P.C.L., T. P. 2nd ed. ed. Polymer Chemistry 2007, Boca Raton, FL: CRC Press.

61. Cotts, P.M., et al. *Novel Branching Topology in Polyethylenes As Revealed by Light Scattering and 13C NMR.* Macromolecules 2000, **33**, 6945-6952.

62. Wang, J., et al. *Chain-topology-controlled hyperbranched polyethylene as effective polymer processing aid (PPA) for extrusion of a metallocene linear-low-density polyethylene (mLLDPE).* J. Rheol. (Melville, NY, U. S.) 2008, **52**, 243-260.

63. Ye, Z. and Li, S. *Hyperbranched Polyethylenes and Functionalized Polymers by Chain Walking Polymerization with Pd-Diimine Catalysis.* Macromol. React. Eng. 2010, **4**, 319-332.

64. Xu, L., et al. *Noncovalent Nonspecific Functionalization and Solubilization of Multi-Walled Carbon Nanotubes at High Concentrations with a Hyperbranched Polyethylene.* Macromol. Chem. Phys. 2009, **210**, 2194-2202.

65. Liu, P., et al. *Hyperbranched Polyethylenes Encapsulating Self-Supported Palladium(II) Species as Efficient and Recyclable Catalysts for Heck Reaction.* Macromolecules (Washington, DC, U. S.) 2013, **46**, 72-82.

66. Furukawa, T. and Ishizu, K. *Multibranched polymers in solution: stars, dendrimers, and hyperbranched polymers*. 2012. Taylor & Francis.

67. Ishizu, K., Furukawa, T., and Ochi, K. *Architecture of star and hyperbranched polymers: synthesis, solution properties, and structural ordering*. 2006. Nova Science Publishers, Inc.

68. Nakayama, Y. *Hyperbranched Polymeric "Star Vectors" for Effective DNA or siRNA Delivery.* Acc. Chem. Res. 2011, Ahead of Print.

69. Xu, F.J. and Yang, W.T. *Polymer vectors via controlled/living radical polymerization for gene delivery.* Prog. Polym. Sci. 2011, **36**, 1099-1131.

70. Ooya, T., Lee, J., and Park, K. *Effects of ethylene glycol-based graft, star-shaped, and dendritic polymers on solubilization and controlled release of paclitaxel.* J. Controlled Release 2003, **93**, 121-127.

71. Groll, J., et al. *Biofunctionalized, ultrathin coatings of crosslinked star-shaped poly(ethylene oxide) allow reversible folding of immobilized proteins.* J. Am. Chem. Soc. 2004, **126**, 4234-4239.

72. Helms, B., et al. *One-pot reaction cascades using star polymers with core-confined catalysts.* Angew. Chem., Int. Ed. 2005, **44**, 6384-6387.

73. Terashima, T., et al. *Polymer Catalysts from Polymerization Catalysts: Direct Encapsulation of Metal Catalyst into Star Polymer Core during Metal-Catalyzed Living Radical Polymerization.* J. Am. Chem. Soc. 2003, **125**, 5288-5289.

74. Kanaoka, S., et al. *Thermosensitive Gold Nanoclusters Stabilized by Well-Defined Vinyl Ether Star Polymers: Reusable and Durable Catalysts for Aerobic Alcohol Oxidation.* J. Am. Chem. Soc. 2007, **129**, 12060-12061.

75. Chi, Y., Scroggins, S.T., and Frechet, J.M.J. *One-Pot Multi-Component Asymmetric Cascade Reactions Catalyzed by Soluble Star Polymers with Highly Branched Non-Interpenetrating Catalytic Cores.* J. Am. Chem. Soc. 2008, **130**, 6322-6323.

76. Wang, T.-Y., et al. *Preparation and characterization of a star-shaped polystyrene-b-poly(ethylene-co-propylene) block copolymer as a viscosity index improver of lubricant.* J. Appl. Polym. Sci. 2001, **79**, 1838-1846.

77. Chen, Q., et al. *pH-responsive high internal phase emulsions stabilized by core cross-linked star (CCS) polymers.* Polym. Chem. 2013, **4**, 4092-4102.

78. Qiu, Q., Liu, G., and An, Z. *Efficient and versatile synthesis of star polymers in water and their use as emulsifiers.* Chem. Commun. (Cambridge, U. K.) 2011, **47**, 12685-12687.

79. Gao, H. and Matyjaszewski, K. *Synthesis of functional polymers with controlled architecture by CRP of monomers in the presence of cross-linkers: From stars to gels.* Prog. Polym. Sci. 2009, **34**, 317-350.

80. Blencowe, A., et al. *Core crosslinked star polymers via controlled radical polymerization.* Polymer 2009, **50**, 5-32.

81. Sun, G. and Guan, Z. *Cascade Chain-Walking Polymerization to Generate Large Dendritic Nanoparticles.* Macromolecules (Washington, DC, U. S.) 2010, **43**, 4829-4832.

82. Huang, H.-M., Liu, I.C., and Tsiang, R.C.-C. *Studies of hydrodynamic properties for characterizing star-shaped poly(ethylene-co-propylene).* Polymer 2005, **46**, 955-963.

83. Schappacher, M. and Deffieux, A. *New Polymer Chain Architecture: Synthesis and Characterization of Star Polymers with Comb Polystyrene Branches.* Macromolecules 2000, **33**, 7371-7377.

84. Ishizu, K., Ono, T., and Uchida, S. *Geometrical structure of star polymers in solution.* Macromol. Chem. Phys. 1997, **198**, 3255-3265.

85. Gao, H. and Matyjaszewski, K. *Arm-First Method As a Simple and General Method for Synthesis of Miktoarm Star Copolymers.* J. Am. Chem. Soc. 2007, **129**, 11828-11834.

86. Gao, H., Ohno, S., and Matyjaszewski, K. *Low Polydispersity Star Polymers via Cross-Linking Macromonomers by ATRP.* J. Am. Chem. Soc. 2006, **128**, 15111-15113.

87. Kluwer, A.M., et al. *Zero-valent palladium complexes with monodentate nitrogen σ-donor ligands.* Angew. Chem., Int. Ed. 2003, **42**, 3501-3504.

88. Groen, J.H., et al. *Kinetic Study of the Insertion of Norbornadiene into Palladium-Carbon Bonds of Complexes Containing the Rigid Bidentate Nitrogen Ligand Bis(arylimino)acenaphthene.* Organometallics 1997, **16**, 68-77.

89. van, A.R., et al. *Rigid bidentate nitrogen ligands in organometallic chemistry and homogeneous catalysis. 3. Insertion of carbon monoxide and alkenes into palladium-carbon bonds of complexes containing rigid bidentate nitrogen ligands: the first example of isolated complexes in stepwise successive insertion reactions on the way to polyketones.* J. Am. Chem. Soc. 1994, **116**, 977-985.

90. Groen, J.H., et al. *Insertion reactions into palladium-carbon bonds of complexes containing new rigid bidentate nitrogen ligands.* J. Organomet. Chem. 1998, **551**, 67-79.

91. Tsuji, J. and Hosaka, S. *Organic synthesis by means of noble metal compounds. XI. Copolymerization of carbon monoxide and norbornadiene.* J. Polym. Sci., Part B: Polym. Lett. 1965, **3**, 703-707.

92. Sen, A. and Lai, T.W. *Novel palladium(II)-catalyzed copolymerization of carbon monoxide with olefins.* J. Am. Chem. Soc. 1982, **104**, 3520-3522.

93. Kawaguchi, T., et al. *Reaction of carbon monoxide with strained alkenes catalyzed by a cationic palladium(II) complex.* J. Mol. Catal. A: Chem. 1999, **143**, 253-262.

94. Radhakrishnan, K. and Sivaram, S. *Copolymerization of ethylene with 2,5-norbornadiene using a homogeneous metallocene/MAO catalyst system.* Macromol. Chem. Phys. 1999, **200**, 858-862.

95. Blank, F.J., C. *Metal catalysts for the vinyl/addition polymerization of norbornene.* Coord. Chem. Rev. 2009, 827-861.

96. Alexander, R.A.B., N. C.; Carpenter, C.; Doyle, J. R. *Metal-Olefin Compounds. I. The Preparation and Molecular Structure of Some Metal-Olefin Compounds Containing Norbornadiene (Bicyclo[2.2.1.]hepta-2,5-diene).* J. Am. Chem. Soc. 1960, 535-538.

97. Held, D. and Muller, A.H.E. *Synthesis and solution properties of star-shaped poly(tert-butyl acrylate).* Macromol. Symp. 2000, **157**, 225-237.

98. Gauthier, M., Li, W., and Tichagwa, L. *Hard sphere behavior of arborescent polystyrenes: viscosity and differential scanning calorimetry studies.* Polymer 1997, **38**, 6363-6370.

99. Aharoni, S.M., Crosby, C.R., III, and Walsh, E.K. *Size and solution properties of globular tert-butyloxycarbonyl-poly(α,ε-L-lysine).* Macromolecules 1982, **15**, 1093-1098.

100. Aloorkar, N.H., et al. *Star polymers: an overview.* Int. J. Pharm. Sci. Nanotechnol. 2012, **5**, 1675-1684, 1610 pp.

101. Zhang, X., Xia, J., and Matyjaszewski, K. *End-Functional Poly(tert-butyl acrylate) Star Polymers by Controlled Radical Polymerization.* Macromolecules 2000, **33**, 2340-2345.

102. Tsuji, J., *Palladium Reagents and Catalysts: Innovations in Organic Synthesis* 1995: Wiley. 560 pp.

103. Negishi, E.-i. and Editor, *Handbook of Organopalladium Chemistry for Organic Synthesis* 2002, New York: John Wiley & Sons, Inc. 1669 pp.

104. Yin, L. and Liebscher, J. *Carbon-carbon coupling reactions catalyzed by heterogeneous palladium catalysts.* Chem. Rev. (Washington, DC, U. S.) 2007, **107**, 133-173.

105. Heck, R.F. and Nolley, J.P., Jr. *Palladium-catalyzed vinylic hydrogen substitution reactions with aryl, benzyl, and styryl halides.* J. Org. Chem. 1972, **37**, 2320-2322.

106. Mizoroki, T., Mori, K., and Ozaki, A. *Arylation of olefin with aryl iodide catalyzed by palladium.* Bull. Chem. Soc. Jap. 1971, **44**, 581.

107. Beletskaya, I.P. and Cheprakov, A.V. *The Heck Reaction as a Sharpening Stone of Palladium Catalysis.* Chem. Rev. (Washington, D. C.) 2000, **100**, 3009-3066.

108. Suzuki, A. *Recent advances in the cross-coupling reactions of organoboron derivatives with organic electrophiles, 1995-1998.* J. Organomet. Chem. 1999, **576**, 147-168.

109. Miyaura, N. and Suzuki, A. *Palladium-Catalyzed Cross-Coupling Reactions of Organoboron Compounds.* Chem. Rev. (Washington, D. C.) 1995, **95**, 2457-2483.

110. Miyaura, N. and Suzuki, A. *Stereoselective synthesis of arylated (E)-alkenes by the reaction of alk-1-enylboranes with aryl halides in the presence of palladium catalyst.* J. Chem. Soc., Chem. Commun. 1979, 866-867.

111. Kollhofer, A. and Plenio, H. *Homogeneous catalysts supported on soluble polymers: Biphasic Sonogashira coupling of aryl halides and acetylenes using MeOPEG-bound phosphine-palladium catalysts for efficient catalyst recycling.* Chem. - Eur. J. 2003, **9**, 1416-1425.

112. Prechtl, M.H.G., Scholten, J.D., and Dupont, J., *Palladium nanoscale catalysts in ionic liquids: coupling and hydrogenation reactions* 2011: InTech. 393-414.

113. Vries, J.G.d., *Palladium and platinum*, in *Handbook of Homogeneous Hydrogenation*, J.G. De Vries and C.J. Elsevier, Editors. 2007, Wiley-VCH. p. 71-91.

114. Johnson, L.K., Mecking, S., and Brookhart, M. *Copolymerization of Ethylene and Propylene with Functionalized Vinyl Monomers by Palladium(II) Catalysts.* J. Am. Chem. Soc. 1996, **118**, 267-268.

115. Drent, E. and Budzelaar, P.H.M. *Palladium-Catalyzed Alternating Copolymerization of Alkenes and Carbon Monoxide.* Chem. Rev. (Washington, D. C.) 1996, **96**, 663-681.

116. Beller, M. and Zapf, A. *Palladium-catalyzed coupling reactions for industrial fine chemical syntheses*. 2002. John Wiley & Sons, Inc.

117. Molnar, A. *Efficient, Selective, and Recyclable Palladium Catalysts in Carbon-Carbon Coupling Reactions.* Chem. Rev. (Washington, DC, U. S.) 2011, **111**, 2251-2320.

118. van, d.C.R., Klein, G.R.J.M., and van, K.G. *Soluble organic supports for the non-covalent immobilization of homogeneous catalysts; modular approaches towards sustainable catalysts.* Prog. Polym. Sci. 2005, **30**, 474-490.

119. Bergbreiter, D.E., Tian, J., and Hongfa, C. *Using Soluble Polymer Supports To Facilitate Homogeneous Catalysis.* Chem. Rev. (Washington, DC, U. S.) 2009, **109**, 530-582.

120. Lu, J. and Toy, P.H. *Organic Polymer Supports for Synthesis and for Reagent and Catalyst Immobilization.* Chem. Rev. (Washington, DC, U. S.) 2009, **109**, 815-838.

121. Uozumi, Y. *Recent progress in polymeric palladium catalysts for organic synthesis.* Top. Curr. Chem. 2004, **242**, 77-112.

122. de, J.E. and Flores, J.C. *Dendrimers: Solutions For Catalyst Separation and Recycling.* Ind. Eng. Chem. Res. 2008, **47**, 7968-7981.

123. Andres, R., De, J.E., and Flores, J.C. *Catalysts based on palladium dendrimers.* New J. Chem. 2007, **31**, 1161-1191.

124. Scott, R.W.J., et al. *Synthesis, Characterization, and Stability of Dendrimer-Encapsulated Palladium Nanoparticles.* Chem. Mater. 2003, **15**, 3873-3878.

125. Irfan, M. and Seiler, M. *Encapsulation Using Hyperbranched Polymers: From Research and Technologies to Emerging Applications.* Ind. Eng. Chem. Res. 2010, **49**, 1169-1196.

126. Hajji, C. and Haag, R. *Hyperbranched polymers as platforms for catalysts.* Top. Organomet. Chem. 2006, **20**, 149-176.

127. Gao, H. *Development of Star Polymers as Unimolecular Containers for Nanomaterials.* Macromol. Rapid Commun. 2012, **33**, 722-734.

128. Terashima, T. and Sawamoto, M. *Microgel-core star polymers as functional compartments for catalysis and molecular recognition.* ACS Symp. Ser. 2012, **1101**, 65-80.

129. Terashima, T., et al. *Polymer Catalysts from Polymerization Catalysts: Direct Encapsulation of Metal Catalyst into Star Polymer Core during Metal-Catalyzed Living Radical Polymerization.* J. Am. Chem. Soc. 2003, **125**, 5288-5289.

130. Sadanand, D.T., et al. *Kinetics of hydrogenation of some terminal olefins catalyzed by anchored montmorillonitebipyridinepalladium(II) acetate.* J. Indian Chem. Soc. 2001, **78**, 464-467.

131. Ramesh, B., et al. *Hydrogenation of 1-alkenes catalysed by anchored montmorillonite palladium(II) complexes: a kinetic study.* Transition Met. Chem. (Dordrecht, Neth.) 2000, **25**, 639-643.

132. Swamy, K.V., et al. *Hydrogenation kinetics and mechanism of stilbene, cinnamaldehyde and cinnamic acid by anchored montmorillonite-bipyridinepalladium(II) acetate.* Indian J. Chem., Sect. A: Inorg., Bio-inorg., Phys., Theor. Anal. Chem. 1997, **36A**, 98-101.

133. Dalal, M.K. and Ram, R.N. *Hydrogenation of 1-hexene using polymer supported Pd(II) complex catalyst.* Eur. Polym. J. 1997, **33**, 1495-1498.

134. Mathew, J. and Mahadevan, V. *Transition metal ions supported on hydrogels as hydrogenation catalysts.* J. Mol. Catal. 1990, **60**, 189-207.

135. Lopez-Serrano, J., Lledos, A., and Duckett, S.B. *A DFT Study on the Mechanism of Palladium-Catalyzed Alkyne Hydrogenation: Neutral versus Cationic Pathways.* Organometallics 2008, **27**, 43-52.

136. Lopez-Serrano, J., et al. *A para-Hydrogen Investigation of Palladium-Catalyzed Alkyne Hydrogenation.* J. Am. Chem. Soc. 2007, **129**, 6513-6527.

137. Kluwer, A.M., et al. *Kinetic and Spectroscopic Studies of the [Palladium(Arbian)]-Catalyzed Semi-Hydrogenation of 4-Octyne.* J. Am. Chem. Soc. 2005, **127**, 15470-15480.

138. Leatherman, M.D., et al. *Mechanistic Studies of Nickel(II) Alkyl Agostic Cations and Alkyl Ethylene Complexes: Investigations of Chain Propagation and*

Isomerization in (α-diimine)Ni(II)-Catalyzed Ethylene Polymerization. J. Am. Chem. Soc. 2003, **125**, 3068-3081.

139. Shultz, L.H. and Brookhart, M. *Measurement of the Barrier to β-Hydride Elimination in a β-Agostic Palladium-Ethyl Complex: A Model for the Energetics of Chain-Walking in (α-Diimine)PdR+ Olefin Polymerization Catalysts.* Organometallics 2001, **20**, 3975-3982.

140. Yagyu, T., Osakada, K., and Brookhart, M. *Single and Multiple Insertion of Carbon-Carbon Triple Bonds into the Palladium-Aryl Bond of Cationic and Neutral Arylpalladium Complexes with a 2,2'-Bipyridine Ligand.* Organometallics 2000, **19**, 2125-2129.

141. Huff, R.L., Tempel, D.J., and Brookhart, M. *Mechanistic investigations of palladium(II)-catalyzed polymerizations of olefins*. 1998. American Chemical Society.

142. LaPointe, A.M. and Brookhart, M. *Reactions of Cationic Palladium(II) Methyl and Vinyl Complexes with Alkynes.* Organometallics 1998, **17**, 1530-1537.

143. Molero, H., Bartlett, B.F., and Tysoe, W.T. *The hydrogenation of acetylene catalyzed by palladium: hydrogen pressure dependence.* J. Catal. 1999, **181**, 49-56.

144. Velu, U., et al. *Hydrogenation of Olefins Catalyzed by Polymer-Supported Palladium-Imidazole.* Chinese Journal of Catalysis 2011, **32**, 280-285.

145. Yu, J. and Spencer, J.B. *First Evidence That the Mechanism of Catalytic Hydrogenation with Homogeneous Palladium and Rhodium Catalysts Is Strongly Influenced by Substrate Polarity.* J. Am. Chem. Soc. 1997, **119**, 5257-5258.

146. Fihri, A., et al. *Nanocatalysts for Suzuki cross-coupling reactions.* Chem. Soc. Rev. 2011, **40**, 5181-5203.

147. Polshettiwar, V., Len, C., and Fihri, A. *Silica-supported palladium: Sustainable catalysts for cross-coupling reactions.* Coord. Chem. Rev. 2009, **253**, 2599-2626.